Removal of Fluoride, Iron and Arsenic from Drinking Water using a Combination of Electrocoagulation and Microfiltration

Thesis submitted in partial fulfillment of the

requirements for the Degree

of

DOCTOR OF PHILOSOPHY

by

Debasis Ghosh

Department of Chemical Engineering

Indian Institute of Technology Guwahati

Guwahati – 781039, India

Removal of Fluoride, Iron and Arsenic from Drinking Water using a Combination of Electrocoagulation and Microfiltration

Thesis submitted in partial fulfillment of the

requirements for the Degree

of

DOCTOR OF PHILOSOPHY

by

Debasis Ghosh

Department of Chemical Engineering
Indian Institute of Technology Guwahati
Guwahati – 781039, India
July, 2009

CONTENTS

Dedication

To My beloved Grand Father

for whom I have become what I am today.

Department of Chemical Engineering
Indian Institute of Technology Guwahati
Guwahati 781039, India
http://www.iitg.ac.in/chemical

CERTIFICATE

This is to certify that the thesis entitled "**Removal of Fluoride, Iron and Arsenic from Drinking Water using a Combination of Electrocoagulation and Microfiltration"**, being submitted by Debasis Ghosh for the award of PhD degree, is a record of bonafide research carried out by him at the Chemical Engineering Department, Indian Institute of Technology Guwahati, under my guidance and supervision. The work documented in this thesis has not been submitted to any other University or Institute for the award of any degree or diploma.

Date:

(Dr. Mihir Kumar Purkait)
Associate Professor
Department of Chemical Engineering
Indian Institute of Technology Guwahati
Guwahati 781039

Acknowledgement

I take this opportunity to express my deep sense of respect and gratitude to my thesis supervisor, Dr. Mihir Kumar Purkait for providing inspiring and valuable guidance throughout the course of this investigation. I am indebted to him for his constant suggestions and encouragement. The experience of working with him, I strongly believe, will have far-reaching influence in my future life.

I express my gratitude and indebtedness to Dr. P. Saha, Head, Chemical Engineering Department, and Dr. A.K. Ghosal, Ex-Head, Chemical Engineering Department, for providing me with the necessary laboratory and Departmental facilities.

I would like to thank Dr. V.S. Moholkar and Dr. A. Verma of Chemical Engineering Department and Dr. A. Ramesh of the Biotechnology Department for their supports and suggestions as members of my Doctoral Scrutiny Committee. I am also thankful to all the faculty members of Chemical Engineering Department for their useful suggestions and help at various stages of this work.

I am thankful to Mr. B. K. Nandi, Mr. H.K. Solanki, Mr. C. R. Medhi and Mr. Vijay Kumar for their sincere assistance and help in my experimental work. I am also thankful to all other staff members of the Chemical Engineering Department for their sincere help and cooperation during this work.

Finally, I express my humble regards for my grandparents, parents, and all the other family members of mine for their constant moral support. With their selfless love and affection they have always encouraged me throughout this work.

Indian Institute of Technology Guwahati **Debasis Ghosh**

July, 2009

Abstract

Drinking water contamination has been a major issue due to the presence of various organic, inorganic and pathogenic ingredients. Inorganic ingredients particularly fluoride, iron and arsenic contamination is a serious problem in several parts of India as well as in different parts of the world associated with its adequate presence in the drinking water causes serious damage to health. Different techniques like adsorption, precipitation, membrane separation, ion-exchange, hybrid techniques were reported for the removal of fluoride, iron and arsenic from drinking water.

In this work, Electrocoagulation was investigated for the effective removal of fluoride, iron and arsenic from drinking water. Several parameters like initial fluoride, iron and arsenic concentration, current density, electrode connection (monopolar and bipolar), pH, interelectrode distance were found to be dominating in order to remove the above mentioned contaminants from drinking water. Aluminum electrode was considered for the batch mode of electrocoagulation operation. The corrosion of electrodes as well as the sludge formed during the process was estimated. By-products obtained from the electrocoagulation bath were analyzed using SEM, EDAX, FTIR and XRD and explained. Comparative cost estimation for both electrode connections was adopted and presented well. It was found that the drinking water contamination caused by the significant presence of fluoride, iron and arsenic was successfully monitored by the bi-polar electrocoagulation for 45 minutes at 625 A m^{-2} current density and an interelectrode distance of 0.005 m. Electrocoagulation performance was estimated in terms of

percentage removal of fluoride, iron and arsenic. Upto 93.2% of fluoride, 99.74% of iron and 95.65% of arsenic removal was achieved

However, electrocoagulated solution was not suitable for the drinking purpose as the solution pH was alkaline along with the agglomerated suspended sludge with size range 10 - 100 µm. In order to make electrocoagulated solution drinkable, electrocoagulation followed by microfiltration was investigated.

In recent times, ceramic microfiltration membranes are being widely used for their better mechanical, thermal and chemical strength compared to the commercial flat-sheet type polymeric membranes. The porous structure of the microporous membranes, mainly composed of ceramic is formed by the process called sintering. In this study ceramic microfiltration membranes were prepared by paste and uni-axial methods. Solid circular ceramic discs of diameter 50 mm and height of 5 mm were prepared and sintered at different temperatures. Five different sintering temperatures were selected (750 °C, 800 °C, 850 °C, 900 °C and 950 °C). The effects of sintering temperature on the structural changes such as porosity, pore-size distribution, average pore radius etc were investigated. All the membranes were characterized using SEM and water permeation test. It was observed that ceramic membranes prepared by both the methods and sintered at 950 °C had sharp pore size distribution. On the other hand, better consolidated micro-ceramic structure was produced by uni-axial cold pressing method. The preparation cost of the ceramic microfiltraton membranes prepared by paste and uni-axial cold pressing methods were 110.62 $/m^2 and 135.75 $/m^2, respectively.

It was found that ceramic microfiltration membranes prepared at 950 °C had a sharp pore size distribution with surface porosity of 0.43 and average pore radius of 0.56 μm estimated from the water permeation test. This ceramic membrane was considered for the microfiltration experiment in batch mode. Electrocoagulated solution was treated in the microfiltration cell in order to separate suspended agglomerate at different transmembrane pressures. Permeate flux and permeate quality was measured and analyzed. It was observed that the prepared microfiltration membrane was efficient in retaining the suspended particulates formed during the EC process. In addition to this, the retained particulates over the ceramic membrane surface were characterized using SEM, XRD and EDX. It was observed that the hybrid technique can successfully remove fluoride, iron and arsenic from the contaminated drinking water.

List of tables

List of figures

Chapter 1

Introduction

This chapter discusses the background of the problem undertaken in this work i.e. the problem associated with drinking water and different treatment technologies. A brief overview of electrocoagulation and membrane based separation processes are also reported. The chapter subsequently presents detailed literature review on different techniques for the removal of fluoride, iron and arsenic from drinking water. The objectives of the present work are also highlighted in this chapter.

1.1 Background

Industrialization along with the urbanization results in rapid deterioration of water quality. The scientific evidences prove that the effluents released from various process industries viz. textile, leather, paint etc. comprise of different hazardous and toxic compounds, some of which are known carcinogens and others probable carcinogens. The emergence of industrial centers without a corresponding growth in civic amenities and pollution control mechanisms results in a gradual decay of water quality.

Water is an essential natural resource for sustaining life and environment that we have always thought to be available in abundance and free gift of nature. However, chemical composition of surface or subsurface is one of the prime factors on which the suitability of water for domestic, industrial or agricultural purpose depends. Fresh water occurs as surface water and groundwater. Though groundwater contributes only 0.6% of the total water resources on earth, it is the major and the preferred source of drinking water in rural as well as urban areas, particularly in the developing countries like India, because

treatment of the same, including disinfection is often not required. It caters to 80% of the total drinking water requirement and 50% of the agricultural requirement in rural India. But in the era of economical growth, groundwater is getting polluted due to urbanization and industrialization.

Over the past few decades, the ever-growing population, urbanization, industrialization and unskilled utilization of water resources have led to degradation of water quality and reduction in per capita availability in various developing countries. Due to various ecological factors either natural or anthropogenic, the groundwater is getting polluted because of deep percolation from intensively cultivated fields, disposal of hazardous wastes, liquid and solid wastes from industries, sewage disposal, surface impoundments etc. During its complex flow history, groundwater passes through various geological formations leading to consequent contamination in shallow aquifers [1].

Presence of various hazardous contaminants like fluoride, arsenic, nitrate, sulfate, pesticides, other heavy metals etc in underground water has been reported from different parts of India. In many cases, the water sources have been rendered unsafe not only for human consumption but also for other activities such as irrigation and industrial needs [2, 3]. Therefore, now there is a need to focus greater attention on the future impact of water resources planning and development taking into consideration all the related issues. In India, fluoride, iron and arsenic are the major inorganic pollutant of natural origin found in groundwater. In this work, electrocoagulation followed by microfiltration is adopted to remove fluoride, iron and arsenic from drinking water. Detail discussions on electrocoagulation, preparation of inorganic microfiltration membrane and its application in the separation of electrocoagulated byproducts have been discussed.

1.2 Sources of fluoride, iron and arsenic in drinking water and their toxicity

Fluoride

Fluorine is highly reactive and is found naturally as CaF_2. It is an essential constituent in minerals like topaz, fluorite, fluorapatite, cryolite, phosphorite, theorapatite, etc. [4]. The fluoride is found in the atmosphere, soil and water. It enters the soil through weathering of rocks, precipitation or waste run off. Surface waters generally do not contain more than 0.3 mg L^{-1} of fluoride unless they are polluted from external sources. Though drinking water is the major contributor (75–90% of daily intake), other sources of fluoride poisoning are food, industrial exposure, drugs, cosmetics, etc. [5]. The fluoride content of some major food products is given in Table 1.1.

Table 1.1: Fluoride concentration in agricultural crops and other edible items [6]

Food item	**Fluoride concentration (mg Kg)$^{-1}$**	**Food item**	**Fluoride concentration (mg Kg^{-1})**
Cereals:		**Nuts and oil seeds:**	
Wheat	4.6	Almond	4.0
Rice	5.9	Coconut	4.4
Maize:		Mustard seeds	5.7
Pulses and legumes	5.6	Groundnut	5.1
Green gram dal	2.5	**Beverages:**	
Red gram dal	3.7	Tea	60–112

Soyabean	4.0	Aerated drinks	0.77–1.44
Vegetables:		**Spices and condiments:**	
Cabbage	3.3	Corriander	2.3
Tomato	3.4	Garlic	5.0
Cucumber	4.1	Turmeric	3.3
Lady finger	4.0	**Food from animal sources:**	
Spinach	2.0	Mutton	3.0–3.5
Lettuce	5.7	Beef	4.0–5.0
Mint	4.8	Pork	3.0–4.5
Potato	2.8	Fishes	1.0–6.5
Carrot	4.1	**Others:**	
Fruits:		Rock salts	200.0–250.0
Mango	3.7	Areca but (supari)	3.8–12.0
Apple	5.7	Beetle leaf (pan)	7.8–12.0
Guava	5.1	Tobacco	3.2–38

Fluoride in minute quantity is an essential component for normal mineralization of bones and formation of dental enamel [7]. However, its excessive intake may result in slow, progressive crippling scourge known as fluorosis. There are more than 20 developed and developing nations that are endemic for fluorosis. These are Argentina, USA, Morocco, Algeria, Libya, Egypt, Jordan, Turkey, Iran, Iraq, Kenya, Tanzania, S. Africa, China, Australia, New Zealand, Japan, Thailand, Canada, Saudi Arabia, Persian Gulf, Sri Lanka,

Syria, India, etc. [8]. In India, it was first detected in Nellore district of Andhra Pradesh in 1937 [9]. Since then considerable work has been done in different parts of India to explore the fluoride laden water sources and their impacts on human as well on animals. At present, it has been estimated that fluorosis is prevalent in 17 states of India. Following table gives fluoride concentrations in different states of India (Table 1.2)

Table 1.2: Fluoride concentrations in different states of India [10]

States	**Districts**	**Range of fluoride concentration** (mg L^{-1})
Assam	Karbianglong, Nagaon	0.2-18.1
Andhra Pradesh	All districts except Adilabad, Nizamabad, West Godhavari, Visakhapattnam, Vijzianagaram, Srikakulam	0.11-20.0
Bihar	Palamu, Daltonganj, Gridh, Gaya, Rohtas, Gopalganj, Paschim, Champaran	0.6-8.0
Delhi	Kanjhwala, Najafgarh, Alipur	0.4-10.0
Gujarat	All districts except Dang	1.58-31.0
Haryana	Rewari, Faridabad, Karnal, Sonipat, Jind, Gurgaon, Mohindergarh, Rohtak, Kurukshetra, Kaithal,Bhiwani, Sirsa, Hisar	0.17-24.7
Jammu and Kashmir	Doda	0.05-4.2

Karnataka	Dharwad, Gadag, Bellary, Belgam, Raichur, Bijapur, Gulbarga, Chitradurga, Tumkur, Chikmagalur,Manya, Banglore, Mysore	0.2-18.0
Kerala	Palghat, Allepy, Vamanapuram, Alappuzha	0.2-2.5
Maharashtra	Chandrapur, Bhandara, Nagpur, Jalgaon, Bulduna, Amravati, Akola, Yavatmal, Nanded, Sholapur	0.11-10.2
Madhya Pradesh	Shivpuri, Jabua, Mandla, Dindori, Chhindwara, Dhar, Vidhisha, Seoni, Sehore, Raisen and Bhopal	0.08-4.2
Orrissa	Phulbani, Koraput, Dhenkanal	0.6-5.7
Punjab	Mansa, Faridcot, Bhatinda, Muktsar, Moga, Sangrur, Ferozpur, Ludhiana, Amritsar, Patila, Ropar,Jallandhar, Fatehgarh sahib	0.44-6.0
Rajasthan	All the 32 districts	0.2-37.0
Tamilnadu	Salem, Periyar, Dharampuri, Coimbatore, Tiruchirapalli, Vellore, Madurai, Virudunagar	1.5-5.0
Uttar Pradesh	Unnao, Agra, Meerut, Mathura, Aligarh, Raibareli, Allahabad	0.12-8.9
West Bengal	Birbhum, Bhardaman, Bankura	1.5-13.0

Iron

Iron is one of the most abundant metals of the Earth's crust. It occurs naturally in water in soluble form as the ferrous iron (bivalent iron in dissolved form Fe(II) or Fe(OH)+) or complexed form like the ferric iron (trivalent iron: Fe(III) met in the precipity $Fe(OH)_3$) or bacterial form, too. The occurrence of iron in water can also have an industrial origin; mining, iron and steel industry, metals corrosion, etc. There are many industrial situations where iron or impurities must be removed from solutions. This is usually induced by the precipitation of iron oxide/oxyhydroxides and often involves the co-removal of inorganic and organic impurities because of the strong adsorptive capacity of iron oxyhydroxides. Such processes are commercially significant. Iron precipitates are notoriously gelatinous, metastable, and difficult to settle and filter. This can make the process bottleneck [11]. The iron concentration in rivers has been reported to be 0.7 mg L^{-1}. In anaerobic groundwater where iron is in the form of iron(II), concentrations will usually be 0.5–10 mg L^{-1}, but concentrations up to 50 mg L^{-1} can sometimes be found. Concentrations of iron in drinking-water are normally less than 0.3 mg L^{-1} but may be higher in countries where various iron salts are used as coagulating agents in water-treatment plants and where cast iron, steel, and galvanized iron pipes are used for water distribution. Iron occurs as a natural constituent in plants and animals. Liver, kidney, fish, and green vegetables contain 20–150 mg Kg^{-1}, whereas red meats and egg yolks contain 10–20 mg/kg. Rice and many fruits and vegetables have low iron contents (1–10 mg Kg^{-1}). Reported daily intakes of iron in food ranging from 10 to 14 mg [12]. Drinking-water containing 0.3 mg L^{-1} would contribute about 0.6 mg to the daily intake. Concentrations

of fluoride, iron and other ingredients found in tube well water of Guwahati city are shown in Table 1.3:

Table 1.3: Concentration of fluoride, iron and other impurities in selected places of Guwahati [13], India.

Sample location	**Fe^{+2} (mg L^{-1})**	**F^- (mg L^{-1})**	**Sample location**	**Fe^{+2} (mg L^{-1})**	**F^- (mg L^{-1})**
Chandmari colony (HT)	0.15	2.67	Sixmile (HT)	0.18	2.20
Hatigarh Chariali (DTW)	1.48	1.13	Sixmile (DTW)	0.17	4.31
Narengi (DTW)	0.05	1.07	Birkuchi (HT)	4.23	1.11
Birkuchi (HT)	0.32	6.88	Birkuchi (DTW)	0.75	1.50
Narengi (HT)	0.78	4.67	Saatgaon (DTW)	0.17	2.50
Saatgaon (HT)	2.16	2.75	Saatgaon (HT)	1.49	4.40
Saatgaon (DTW)	0.12	2.25	Bagharbari (DTW)	0.04	1.50
Kalyan kuchi (HT)	3.09	2.00	Rukminigaon (HT)	1.70	1.65
Kalapahar (HT)	0.37	0.35	Hatigaon (HT)	0.01	1.13
Lalganesh (HT)	0.49	0.90	Hatigaon (DTW)	0.02	1.08
Saukuchi (DTW)	0.16	3.75	Dipar Bil (Lake)	0.72	0.42
Beltola Chariali(HT)	3.16	1.00	Brahmaputra (River)	0.25	0.18
WHO guideline	**0.30**	**1.50**		**0.30**	**1.50**

HT: Hand tube well, DTW: Deep tube well

Arsenic

Arsenic is found to exist within the shallowzones of groundwater of many countries like Argentina, Bangladesh, India, Pakistan, Mexico, Mongolia, Germany, Thailand, China, Chile, USA, Canada, Hungary, Romania, Vietnam, Nepal, Myanmar, Cambodia, etc. in various concentrations. In some places in Bangladesh its concentration is as high as 1000 μg L^{-1} [14]. The contaminants like iron, calcium, magnesium, bicarbonate, chloride and sulfate are found to be associated with arsenic in the ground water of these countries. Surface water is also found to be contaminated with arsenic by the anthropogenic sources to various degrees.

Arsenic belongs to the metalloid group of elements that shows many metallic properties and co-exists in nature with other metals like Fe, Cu, Ni, Zn, etc., as sulfide or oxide ores. Arsenic cannot be destroyed it can only be converted from one form to other form. The predominant form of inorganic arsenic in aqueous oxic environments is arsenate [As(V) as H_3AsO_4, $H_2AsO_4^{-1,}$ $HAsO_4^{-2}$ and AsO_4^{-3}], whereas, arsenite [As(III) as H_3AsO_3 and $H_2AsO_3^-$] is more prevalent in anoxic environments [15]. Arsenic naturally occurs in over 200 different mineral forms of which approximately 60% are arsenates, 20% sulfides and sulfosalts; the remaining 20% includes arsenides, arsenites, oxides, silicates and elemental arsenic (As). As^0 and As^{3-} are rare in aquatic environments. Organic arsenic species available in contaminated surface and ground water are mono methyl arsenate (MMA) and dimethyl arsenate (DMA) [16]. The sources of arsenic contamination in ground water are:

(A) ***Natural*** [17]**:**

Through dissolution of arsenic compounds adsorbed onto the pyrite ores in to the water by geothermal, geo hydrological and bio geo chemical factors.

(B) ***Anthropogenic*** [17, 18]:

(i) From processing of varieties of ores like Cu, Au, Ni, Pb, and Zn.

(ii) From ingredients of many insecticides and herbicides .

(iii) From cotton and wool processing.

(iv) From arsenic based wood preservative.

(v) From feed additives in various metal alloys and in mining.

(vi) From seepages from hazardous waste sit.

(vii) From areas near cemeteries where burials were conducted from about 1880 to 1910 when arsenic was used as an embalming fluid.

(viii) From power generation by the burning of arsenic contaminated coal.

(ix) From semiconductor and glass manufacturing units.

It has been found that when river water, which is a primary source of drinking water, is polluted by industrial or mining effluent or by geothermal waste the arsenic concentration increases. The highest reported arsenic concentration so far is 850,000μg/l from an acid seep in the Richmond mine at Iron Mountain, California [19]. The arsenic concentration in ground water depends on various factors like presence of thick clay barriers surrounding the aquifer, depth of tube well, etc. It is a proven fact that the presence of elevated concentrations of phosphate or silicate may enhance the sub-surface mobility of As(V) in soils contaminated with arsenate. Different adsorptive affinities of both arsenate

and arsenite to various common mineral surfaces (i.e., ferrihydrite, alumina, etc.) are considered to affect this arsenic mobilization in the aqueous phase [20].

1.3 Maximum contamination level (MCL) and health effects of fluoride, iron and arsenic

Fluoride

Maximum contamination level (MCL) of fluoride in drinking water is 1.5 mg L^{-1} [21]. The endemic fluorosis in India is largely of hydrogeochemical origin. It has been observed that low calcium and high bicarbonate alkalinity favor high fluoride content in groundwater. Water with high fluoride content is generally soft, has high pH and contains large amount of silica. In groundwater, the natural concentration of fluoride depends on the geological, chemical and physical characteristics of the aquifer, the porosity and acidity of the soil and rocks, temperature, the action of other chemicals and the depth of wells. Due to large number of variables, the fluoride concentrations in groundwater range from well under 1.0 mg L^{-1} to more than 35.0 mg L^{-1}. As the amount of water consumed and consequently the amount of fluoride ingested is influenced primarily by air temperature, USPHS [22] has set a range of concentrations for maximum allowable fluoride in drinking water for communities based on the climatic conditions as shown in Table 1.4.

Fluorine being a highly electronegative element has extraordinary tendency to get attracted by positively charged ions like calcium. Hence the effect of fluoride on mineralized tissues like bone and teeth leading to developmental alternations is of clinical

significance as they have highest amount of calcium and thus attract the maximum amount of fluoride that gets deposited as calcium–fluorapatite crystals. Tooth enamel is composed principally of crystalline hydroxylapatite. Under normal conditions, when fluoride is present in water supply, most of the ingested fluoride ions get incorporated into the apatite crystal lattice of calciferous tissue enamel during its formation.

Table 1.4: USPHS recommendations for maximum allowable fluoride in drinking water

Annual average of maximum daily air temperature (◦C)	**Recommended fluoride concentration (mg L^{-1})**			**Maximum allowable fluoride concentration (mg L^{-1})**
	Lower	**Optimum**	**Upper**	
10 – 12	0.9	1.2	1.7	2.4
12.1 - 14.6	0.8	1.1	1.5	2.2
14.7 - 17.7	0.8	1.0	1.3	2.0
17.8 - 21.4	0.7	0.9	1.2	1.8
21.5 - 26.2	0.7	0.8	1.0	1.6
26.3 - 32.5	0.6	0.7	0.8	1.4

The hydroxyl ion gets substituted by fluoride ion since fluorapatite is more stable than hydroxylapatite. Thus, a large amount of fluoride gets bound in these tissues and only a

small amount is excretedthrough sweat, urine and stool. The intensity of fluorosis is not merely dependent on the fluoride content in water, but also on the fluoride from other sources, physical activity and dietary habits. The various forms of fluorosis arising due to excessive intake of fluoride are briefly presented in Table 1.5 [23].

Table 1.5: Effects of fluoride in water on human health

Fluoride concentration (mg L^{-1}**)**	**Effects**
<1.5	Safe limit
1.5 – 3.0	Dental fluorosis (discoloration, mottling and pitting of teeth)
3.0 – 4.0	Stiffened and brittle bones and joints
4.0 – 6.0 and above	Deformities in knee and hip bones and finally paralysis making the person unable to walk or stand in straight posture, crippling fluorosis

Dental fluorosis

Due to excessive fluoride intake, enamel loses its lustre. In its mild form, dental fluorosis is characterized by white, opaque areas on the tooth surface and in severe form, it is manifestated as yellowish brown to black stains and severe pitting of the teeth. This discoloration may be in the form of spots or horizontal streaks.

Skeletal fluorosis

Skeletal fluorosis affects children as well as adults. It does not easily manifest until the disease attains an advanced stage. Fluoride mainly gets deposited in the joints of neck, knee, pelvic and shoulder bones and makes it difficult to move or walk. The symptoms of

skeletal fluorosis are similar to spondylitis or arthritis. Besides skeletal and dental fluorosis, excessive consumption of fluoride may lead to muscle fibre degeneration, low hemoglobin.

Iron

Groundwater easily gets contaminated with iron usually in it's (+2) valence state. Although iron is an essential mineral for human, its presence in groundwater above a certain level make the water unusable mainly for aesthetic considerations such as discoloration, metallic taste, odor, turbidity, staining of laundry and plumbing fixtures. Moreover, iron oxides, which are formed in reservoirs upon aerial oxidation of dissolved iron promotes growth of micro-organism in water. Considering the aesthetic impairment that may arise from the excessive iron in water supplies the revised Indian standard (IS: 10500-91) prescribes desirable and permissible limit of iron in drinking water as 0.3 mg L^{-1} and 1.0 mg L^{-1}, respectively.

Iron is an essential element in human nutrition. Estimates of the minimum daily requirement for iron depend on age, sex, physiological status, and iron bioavailability and range from about 10 to 50 mg day^{-1}. The average lethal dose of iron is 200–250 mg Kg^{-1} of body weight, but death has occurred following the ingestion of doses as low as 40 mg Kg^{-1} of body weight. Autopsies have shown hemorrhagic necrosis and sloughing of areas of mucosa in the stomach with extension into the submucosa. Chronic iron overload results primarily from a genetic disorder (hemochromatosis) characterized by increased iron absorption and from diseases that require frequent transfusions [24]. Adults have often taken iron supplements for extended periods without deleterious effects, and an

intake of 0.4–1 mg Kg^{-1} of body weight per day is unlikely to cause adverse effects in healthy persons [25].

Arsenic

Considering the lethal impact of arsenic on human health, environmental authorities of different countries have taken a more stringent attitude towards the presence of arsenic in water. Table 1.6 summarizes the maximum contamination level of arsenic in different countries.

The toxicity scale of arsenic decreases in the following order: arsine > inorganic arsenic(III) > organic arsenic(III) > inorganic arsenic(V) > organic arsenic(V) > arsonium compounds and elemental arsenic. The carcinogenic and mutagenic effects of arsenic have been established.

Health effects of arsenic on human are classified as acute and sub acute which are typically reversible and chronic effects. Acute and sub acute poisoning results from ingestion of large quantities of arsenic with lower exposure time whereas, chronic poisoning occurs due to consumption of arsenic contaminated water for a long time period. Arsenocosis is caused by drinking arsenic-tainted groundwater.

The disease causes many problems including vomiting and diarrhea; abdominal pain; muscular pain; skin rashes; and swelling of the eyelids, feet and hands. Arsenocosis ultimately affects the heart, lungs, and kidneys and can be fatal. Hematological effects including anemia and leukaemia; and peripheral neuropathy might occur after weeks or month of exposure to high doses of arsenic (0.04 mg Kg^{-1} day^{-1} or higher) [29].

Consumption of large arsenic at a time may also cause stomach pain, nausea, vomiting or diarrhoea, which may lead to shock, coma, and even death. It has also been reported by many researchers that chronic arsenic poisoning causes hypertension, peripheral vascular diseases, cardiac vascular diseases, respiratory diseases, diabetes mellitus, malignancies including cancer of the lungs, bladder, kidney, liver, uterus and skin. The skin is quite sensitive to arsenic and skin lesion (hyperkeratosis and dyspigmentation) has been observed even at the exposure levels in the range of 5–10 μg L^{-1} arsenic in drinking water [29].

Table 1.6: World scenario of arsenic poisoning from drinking water

Country name	**Permissible national limit (μg L^{-1})**	**Reference**
Bangladesh	50	[14]
India	50	[26]
Pakistan	50	[27]
Taiwan	50	[26]
China/Mongolia	50	[26]
USA	10	[26]
Germany	25	[26]
Vietnam	50	[28]
Japan	10	[26]

1.4 Existing processes for the separation of fluoride, iron and arsenic from drinking water.

Fluoride

Defluoridation is the process of removal of fluoride ion from drinking water. The different methods tried so far for the removal of excess fluoride from water can be broadly classified into four categories:

A) Adsorption methods,

B) Ion exchange methods,

C) Precipitation methods, and

D) Membrane separation (reverse osmosis)

Adsorption process using different adsorbents such as trimetal oxide [30], waste carbon slurry [31] and many low-cost materials [32] are investigated for the removal of fluoride from aqueous medium. Membrane separation techniques are investigated for the effective separation of fluoride using electrodialysis [33] , Donnan dialysis [34], nanofiltration [35] and anion-exchange membrane [36]. Garmes et al. (2002) [37] has performed defluoridation of ground water by a hybrid process combining adsorption and Donnan dialysis. Fluoride distribution in electrocoagulation defluoridation process is investigated by Zhu et al. (2007) [38]. The kinetics was developed empirically in the removal process of fluoride using monopolar electrode connection [30, 39]. Advantages and disadvantages of different fluoride removal techniques are summarized in Table 1.7.

Iron

There are many industrial situations where iron or impurities must be removed from solutions. This is usually induced by the precipitation of iron oxide/ oxyhydroxides and often involves the co-removal of inorganic and organic impurities because of the strong adsorptive capacity of iron oxyhydroxides. Such processes are commercially significant. Iron precipitates are notoriously gelatinous, metastable, and difficult to settle and filter. This can make the process bottleneck. World Health Organization (WHO) has set a guideline value of 0.3 mg L^{-1}, of iron in drinking water [21]. There are several methods for removal of iron from drinking water like Ion exchange and water softening [40], activated carbon and other filtration materials [41], supercritical fluid extraction [42], bioremediation [43] and limestone treatment [44], Oxidation by aeration, chlorination, ozonation followed by filtration [45], by ash [46], by aerated granular filter [47] and by adsorption [48]. Aeration and separation is the most common method for removal of iron from groundwater in public water supply systems, which is however not so popular at domestic level. Table 1.8 lists treatment considerations for the various forms of iron

Table 1.7: Advantages and disadvantages of different fluoride removal techniques

Technique	**Adsorption**	**Ion Exchange**	**Coagulation- Precipitation**	**Membrane Process**
Remarks	**Adsorbents:** Activated alumina, activated carbon, calcite, activated saw dust, activated coconut shell carbon and activated fly ash, groundnut shell, coffee husk, rice husk, bone charcoal, activated soil sorbent, etc.	strongly basic anion-exchange resin containing quaternary ammonium functional groups is used	**Nalgonda technique:** In first step, precipitation occurs by lime dosing which is followed by a second step in which alum is added to cause coagulation.	NF and RO is generally used for fluoride removal
Advantage	The process can remove fluoride up to 90%. Treatment is cost-effective	Removes fluoride up to 90–95%. Retains the taste and colour of water intact.	The two-step process has been claimed as the most effective technique by NEERI Under **Rajiv Gandhi Drinking Water Mission**, several fill and draw (F&D) type and	The process is highly effective for fluoride removal. Membranes also provide an effective barrier to suspended solids, all inorganic pollutants, organic

			hand pump attached (HPA) plants based on Nalgonda technique have come up in rural areas for which design and technology has been developed by NEERI.	micropollutants, pesticides No chemicals are required It works under wide pH range. No interference by other ions is observed.
Disadvantage	The process is highly dependent on pH Presence of sulfate, phosphate or carbonate results in ionic competition	Efficiency is reduced in presence of other ions. The technique is expensive because of the cost of resin,	The process removes only a smaller portion of fluoride (18–33%) in the form of precipitates and converts a greater portion of ionic fluoride (67–82%) into soluble aluminum fluoride complex ion, and therefore this technology is erroneous. Silicates have adverse effect on defluoridation by Nalgonda Technique	The process is expensive in comparison to other options

Table 1.8: Treatment considerations for various forms of Iron.

Characteristic	**Known As**	**Treatment Methods**	**Considerations**
Drawn tap water is clear and colorless. When allowed to stand, reddish brown particles appear and settle to bottom.	Soluble Clear Water (Fe^{+2}) Ferrous Dissolved	Aeration/Filtration	May require lengthy contact time. Temperature dependent.
		Water softener	Hardness must be calculated. System must be airtight. All water must be treated.
		Chlorination/Filtration Chlorine	Chlorine liquid or pellets. Frequent monitoring. Proper water pressure.
		Manganese greensand / Filtration	Adequate pressure.
		Catalytic filtration “BIRM”	Dissolved oxygen, organic matter, chlorination, polyphosphate, emperature limitations.
		Ozonation	Used by some municipal systems. Expense.
		Sequestering	May not prevent staining. May need to remove sequestering agents and iron. Test for agents before choosing another treatment device.
Drawn tap water appears rusty or has a red or yellow color. When allowed	Insoluble Red Water Fe+3 Ferric Oxidized	Manganese greensand/ Filtration	Adequate pressure.
		Catalytic filtration “BIRM”	Dissolved oxygen, alkalinity, organic matter, chlorination, polyphosphate, temperature limitations.

to stand particles settle to bottom.		Chlorination/Filtration	Chlorine liquid or pellets. Frequent monitoring. Proper water pressure.
Water tank/toilet tank/plumbing have reddish brown or yellow gelatinous slime or sludge present. May have objectionable odor or oily sheen.	Bacterial Creno-thrix Leptothrix Gallionella	Shock chlorination and consider following with continuous chlorination. Bactericides.	Shock chlorination should include; cleaning the well thoroughly, cleaning pump and riser pipe, and complete chlorination and flushing of distribution system. Make sure bactericides can be used in drinking water. Bactericides need long contact time for adequate treatment.
High color content (yellow or brown) or colorless. enerally groundwater from shallow well or surface water.	Organic Hemme Tannin	Water softener	First step is to treat for organics. Hardness must be calculated. System must be airtight. Treat all water.
		Manganese greensand/ Filtration	First step it to treat for organics. Adequate pressure.
		Ozonation	Used by some municipal systems. Expense.

Arsenic

Various treatment technologies have been developed for arsenic removal from drinking water. The commonly used technologies include coagulation and precipitation with iron and aluminum salts [49] adsorption onto activated alumina, activated carbon and activated bauxite [50], ion exchange and reverse osmosis [51]. Some recent treatment technologies based on oxidation and adsorption are green sand filtration [52], iron oxide coated sand [53], manganese dioxide coated sand [54], ferruginous manganese ore [55], ferrihydrite [56], clay minerals [57] and zero-valent iron [58]. Coagulation, precipitation and other adsorption techniques such as, activated alumina, and activated carbon, have been found to be not as efficient for As(III) removal as for As(V) removal. Therefore for efficient arsenic removal oxidation of As(III) to As(V) has been suggested. The use of external oxidizing agents tends to bring down the water quality. Despite the fact that a variety of treatment methods are available, the efficiency of these processes is not completely known [59]. Many of them have been reported to be capable of removing arsenic to levels lower than 50 $\mu g\, L^{-1}$, but with the impending of revision of the permissible levels to 10 $\mu g\, L^{-1}$ or lower, it is necessary to investigate the treatment approaches that would consistently provide drinking water with arsenic less than 10 $\mu g\, L^{-1}$ levels.

Studies on arsenic indicate that hydrous metal oxides, such as ferric hydroxides, ferrihydrite, and goethite strongly adsorb arsenic [60]. Recently arsenic removal by zero-valent iron has also been reported [61]. In this method, iron oxide produced due to corrosion of iron filings removed both As(III) and As(V) from the contaminated drinking

water. In view of previous discussion, it is clear that As(III) removal is favored by oxidation to As(V) followed by adsorption on to adsorbent.

These conventional techniques have some limitations i.e. (i) use of chemicals, its handling and impact on water quality; (ii) production of large volume of high arsenic contaminated sludge; (iii) need of secondary treatment in some cases (iv) interference of sulfates and other ions on removal efficiency and (v) high installation and operation cost and lower efficiency in many cases. A comparison among some conventional processes of typical cases is summarized in Table 1.9.

Table 1.9: The comparison amongst the conventional processes [62]

Process	**Removal efficiency (%)**	**Advantages**	**Disadvantages**
Precipitation with alum	20 – 90%	Well established; suitable for home use	Use of chemicals; high arsenic contaminated sludge; dose of oxidizing chemicals highly influence the removal efficiency
Precipitation with iron	60 – 90%	Proven and reliable	Use of chemical; high arsenic contaminated sludge; dose of oxidizing chemicals highly influence the removal efficiency
Precipitation with Fe/Mn	40 – 90%	Proven and reliable	Higher and lower pH reduces efficiency; use of chemical; high arsenic contaminated sludge; dose of oxidizing chemicals highly influence the removal efficiency

Lime softening	0 – 90%	Proven and reliable; reduces corrosion	Sulfate ions influence efficiency; secondary treatment is required; use of chemicals
Reverse osmosis	≥ 90%	Highest water quality; treats wide range of dissolved salts, minerals; turbidity	Expensive to install and operation; frequent membrane monitoring; pH, temperature and pressure control to meet membrane tolerance
Electro dialysis	≥ 95%,	Pure quality water	Less proven; costly; needs oxidizing agents
Ion exchanges	≥90%	Can produce treated water with As concentration less than 2 μg L^{-1}	Efficiency affected by sulfate, nitrates, fluorides ions, TDS, selenium, etc
Adsorption in activated alumina	≥ 90%	Well established; suitable for home use; typically inexpensive with simple replacement requirements; improves test and odour	Careful monitoring; effectiveness is based on contaminant type; concentration and rate of water usage; bacteria may grow on alumina surface
Adsorption on activated carbon	30 – 90%	Typically inexpensive with simple replacement requirements; improves test and odour	Efficiency depends on the ash content in the carbon and on the metal concentration; not proven

1.5 Electrocoagulation

1.5.1 Applications of electrocoagulation

Electrocoagulation uses an electrochemical cell to treat polluted water. Sacrificial anodes corrode to release active coagulant cation, usually aluminium or iron, to solution. Accompanying electrochemical reactions are dependent on species present and usually evolve electrolytic gases. The coagulant's delivery and its nature influence the coagulation and separation processes. In recent years, however, smaller scale electrocoagulation processes have advanced to the point where they are seen as a reliable and effective technology. Numerous examples of water treatment systems have been reported in the recent literatures [Table 1.10].

Table 1.10 presents pollutants removed by electrocoagulation and associated references. The pollutant's physicochemical properties influence its interactions within the system and eventual removal path. For example, ions are most likely electro-precipitated whilst charged suspended solids are adsorbed onto the charged coagulant. Electrocoagulation's ability to remove a wide range of pollutants is the reason for its ongoing industrial attraction.

Table 1.10: Various pollutants removed by different electrocoagulation arrangements

Reference	Pollutant	Current/cell voltage	Electrodes anode/cathode	Reference
	Suspended solids			
Abuzaid *et al.* (1998)	Bentonite	0.2, 0.5, 1 A	Stainless steel	**[63]**
Belongia *et al.* (1999)	Silica (SiO_2) and alumina	2.5 to 10.0 V/cm	304 stainless steel	**[64]**
Matteson *et al.* (1995)	Kaolinite	0.01 A m^{-2}	Stainless steel	**[65]**
	Color			
Do and Chen (1994)	Dye	0.1 A	Fe and Al	**[66]**
Ibanez *et al.* (1998)	Dye	9 V	Fe	**[67]**
M. Kashefialasl et al (2006)	Dye	127.8 A m^{-2}	Fe	**[68]**
A.K. Golder et al (2005)	Dye	1.5KWh	Fe	**[69]**
N. Daneshvar et al (2006)	Dye	60-80 A m^{-2}	Fe	**[70]**
	Organics			
Baklan and Kolesnikova (1996)	Sewage	120 A m^{-2}	Fe and Al	**[71]**
Pouet and Grasmick (1995)	Urban waste water	3.9 A	Al/Al	**[72]**
Pouet and Grasmick (1994)	Municipal wastewater	4 -10 A	Al/Al	**[73]**
Vik *et al.* (1984)	Aquatic	6-12 V	Al/Al	**[74]**

	humus			
M. Kobya et al.(2006)	Potato chips waste water	20-300 A m^{-2}	Al/Fe	**[75]**
	Fats, oils			
Balmer and Foulds, (1986)	Oil	200-781 mA	Fe/Pt	**[76]**
Rubach and Saur (1997)	Oil, salt and chemicals	40-220 A	Al	**[77]**
Woytowich *et al.* (1993)	Hydrocarbons		Al and steel tubes	**[78]**
	Ions			
Grechko *et al.* (1982)	Pesticides	150 A m^{-2}	Al/Al	**[79]**
Mameri *et al.* (1998)	Fluorides	75 A m^{-2}	Al/Al	**[80]**
P Ratnakumar et al. (2004)	Arsenic	0.65 to 1.53 mA cm^{-1}	Ai/Fe/Ti	**[81]**

1.5.2 Electrochemistry

Electrocoagulation reactors are electrochemical cells. All such reactors consist of an electrode arrangement in contact with the polluted water, with coagulant production *in situ* being their distinguishing feature. To release the coagulant, an applied potential difference across the electrodes is required. Potential requirements for the electrodes can be deduced from the electrochemical half-cell reactions occurring at each electrode, which will vary according to the operational pH and the species present in the system. Reported electrode designs are numerous, including aluminium pellets in a fluidisedbed

reactor, bipolar aluminium electrodes mesh electrodes, bipolar steel raschig rings as well as simple plate electrodes [Ref: Table 1.10]. Various electrode materials have also been reported including aluminium, iron, stainless steel and platinum. The electrode material used determines the coagulant type. Thus, regardless of the electrode design employed, the electrode material determines the electrochemical reactions occurring, and hence the coagulant cation. For this reason, electrochemistry is one of the foundations for electrocoagulation. Aluminium, the most commonly used anode material, is used here as an example. Equation 1.1 shows the dissolution of aluminium in the anode.

$$Al^{+3} + 3e^{-} \leftrightarrow Al \qquad \ldots\ldots. \ (1.1)$$

Oxygen evolution is also possible at the anode

$$4OH^{-} \longrightarrow O_2 + 2H_2O + 4e^{-} \qquad \ldots.. \ (1.2)$$

Simultaneously, an associated cathodic reaction, usually the evolution of hydrogen, occurs. The reaction occurring at the cathode is dependent on pH. At neutral or alkaline pH, hydrogen is produced via Equation 1.3,

$$2H_2O + 2e^{-} \rightarrow 2OH^{-} + H_2 \qquad \ldots.. \ (1.3)$$

while under acidic conditions, Equation 1.4 best describes hydrogen evolution at the cathode.

$$2H^{+} + 2e^{-} \rightarrow H_2 \qquad \ldots.. \ (1.4)$$

1.5.3. Electrocoagulation and chemical coagulation

Coagulation is a key feature of all electrocoagulation reactors, describing the interaction between the coagulant and any pollutant material. The coagulant's role here is to

destabilise the colloidal suspension by reducing any attractive forces, thereby lowering the energy barrier and enabling particles to aggregate. Depending on the physical and chemical properties of the solution, pollutant and coagulant, a number of coagulation mechanisms (*e.g.* charge neutralisation, double layer compression, bridging and sweep) have been postulated Letterman *et al.* (1999) [82]. For any given electrocoagulation reactor, the dominant coagulation mechanism will vary with the reactor's operating conditions, the pollutant type (and concentration), and the coagulant concentration.

Electrocoagulation has been compared to chemical coagulation to assess its efficiency and advantages. Chemical dosing delivers the coagulant as a salt that dissociates in solution with hydrolysis of the aluminium cation (and associated anions) determining solution speciation and pH. Alum (*i.e.* aluminium sulphate) addition, for example, acidifies the water. By contrast, aluminium added via electrocoagulation does not bring with it any associated salt anions, with the result that the pH typically stabilises in the alkaline range. However, Donini *et al.* (1994) [83] claimed that the coagulation mechanism for electrochemical and chemical dosing are very similar, yet neither author supports their claim with rigorous experimental evidence.

In electrocoagulation, a pollutant's stability is determined by its physicochemical properties. Pollutants composed of similarly charged particles repel each other, with the repulsive forces creating a stable, colloidal system with oppositely charged ions, typically hydroxyl (OH^-) or hydrogen ions (H^+), being attracted to the charged pollutant particles. The attraction of counter ions to a charged pollutant forms an electric double layer - referred to as the Stern and diffuse layers [82] (Letterman et al., 1999;}. Electrostatic repulsion between electric double layers drives particles apart, whilst van der Waals

forces act to bring them together. The energetic is such that attraction dominates at small separations.

However, to reach a small separation, a repulsive energy barrier must first be overcome. The zeta potential is generally used as an experimental measure of the particle's effective charge as it moves through the solution, thus providing a direct indicator of solution stability [82] (Letterman et al., 1999). Hence, zeta potential measurement provides an important characterization for any electrocoagulation system providing an indication of stability and an indication of possible coagulation mechanisms.

1.5.4. Coagulation mechanism for the removal of fluoride, iron and arsenic

The EC process operates on the principle that the cations produced electrolytically from iron and/or aluminum anodes enhance the coagulation of contaminants from an aqueous medium. Electrophoretic motion tends to concentrate negatively charged particles in the region of the anode and positively charged ions in the region of the cathode. The consumable, or sacrificial, metal anodes are used to continuously produce polyvalent metal cations in the vicinity of the anode. These cations neutralize the negative charge of the particles carried toward the anodes by electrophoretic motion, thereby facilitating coagulation. In the following EC techniques, the production of polyvalent cations from the oxidation of the sacrificial anodes (Fe and Al) and the electrolysis gases (H_2 and O_2) works in combination to flocculate the coagulant materials. Even inert electrodes, such as titanium and the passage of an alternating current have also been observed to remove metal ions from solutions and to initiate the coagulation of suspended solids. As mentioned above, gas bubbles produced by the electrolysis carry the pollutant to the top

of the solution where it is concentrated, collected and removed. The removal mechanisms in EC may involve oxidation, reduction, decomposition, deposition, coagulation, absorption, adsorption, precipitation and flotation.

Different electrodes have been reported in the literature like carbon, mild steel, graphite, titanium, iron and Aluminum. But Iron and Aluminum have been reported to be very effective and successful in pollutant removal at favorable operating conditions. The electrode reactions are summarized as follows:

Anode: $Al \Rightarrow Al^{3+} + 3e$ (same as equation 1.1)

Cathode: $3H_2O + 3e \Rightarrow \frac{3}{2}H_2 \uparrow + 3OH^-$ (same as equation 1.3)

During the final stages, coagulated aggregates interact with bubbles and float to the surface or settle to the bottom of the EC bath. Flotation is the dominant pollutant removal path for high operating currents, while sedimentation is dominant at lower currents. The shift is due to the bubble number concentration at low currents is insufficient to remove the aggregated material, allowing sedimentation to dominate. Al (III) and OH^- ions generated by electrode reactions (1.1) and (1.3) react to form various monomeric species such as $Al(OH)^{+2}$, $Al(OH)^{+}_2$, $Al_2(OH)_2^{4+}$, $Al(OH)_4^-$ and polymeric species such as $Al_6(OH)_{15}^{3+}$, $Al_7(OH)_{17}^{4+}$, $Al_8(OH)_{20}^{4+}$, $Al_{13}O_4(OH)^{7+}_{24}$, $Al_{13}(OH)_{34}^{5+}$, which transform finally into $Al(OH)_{3(S)}$ according to complex precipitation kinetics

$$Al^{3+} + 3H_2O \Rightarrow Al(OH)_3 + 3H^+ \qquad \text{……..(1.5)}$$

Freshly formed amorphous $Al(OH)_{3(S)}$ occurs as “sweep flocks” having large surface areas. These flocks are active in rapid adsorption of soluble organic compounds and

trapping of colloidal particles and are easily separated from aqueous medium by sedimentation or H_2 flotation. These flocks polymerizes as $nAl(OH)_3 \Rightarrow Al_n(OH)_{3n}$.

This $Al(OH)_3$ complex is believed to have strong fluoride adsorption capacity as Equation 1.6 [84].

$$Al(OH)_3 + xF^- \Leftrightarrow Al(OH)_{3-x}F_x + xOH^- \quad \text{…….. (1.6)}$$

Iron exists in solution in the ferrous state, it can only remain in solution in the absence of oxygen, and generally when the pH is below 6.5, ferrous ion is oxidized in air according to the following reaction:

$$Fe^{2+} + \frac{1}{4}O_2 + H^+ \Leftrightarrow Fe^{3+} + \frac{1}{2}H_2O \quad \text{…….. (1.7)}$$

Presence of chloride ion may undergo the following reactions

Bulk

$$H_2O \Leftrightarrow H^+ + OH^- \quad \text{……. (1.8)}$$

$$NaCl \Leftrightarrow Na^+ + Cl^- \quad \text{…….. ..(1.9)}$$

$$Fe^{2+} + 2Cl^- \Leftrightarrow FeCl_2 \quad \text{…….. (1.10)}$$

$$FeCl_2 + 3OH^- \Leftrightarrow Fe(OH)_3 \downarrow + 2Cl^- \quad \text{…….. (1.11)}$$

$$H^+ + Cl^- \Leftrightarrow HCl \quad \text{…..…….. (1.12)}$$

Anode

$$2Cl^- \Leftrightarrow Cl_2 \uparrow + 2e \quad \text{…….. (1.13)}$$

The state of iron in water depends mainly on the pH and the redox potential. By increasing the pH, dissolved iron i.e. Fe(II) or Fe(III)) hydrolyzes to form precipitates. The ferrous ion hydrolyzes to produce the array of mononuclear species $FeOH^+$ to

$Fe(OH)_4^{-2}$ between pH 7 and 14. The ferric ion, Fe(III) hydrolyzes much more readily than the ferrous ion, Fe(II). Baes and Mesmer [85] presented diagrams, which show that iron at the range of pH 7–8 is a precipitate. The rates of ferrous ion oxidation by air increase with pH and about 90% conversion may be achieved in a few minutes at a pH of 7 [86]. Precipitation depends on the size and shape of the particle which is formed after coagulation followed by the adsorption on the active surfaces of the coagulants formed during the electrocoagulation process. At the higher pH, removal of iron is achieved mainly by adsorption of iron hydroxide in the form of brown flocks due to the sufficient availability of coagulants in the medium. Therefore the flocks formed were large in size and settled down as a precipitate at the bottom of the container shortly after the completion of the experiment.

The metal cations of As(III) and As(V) react with the OH− ions produced at the cathode during the evolution of hydrogen to yield both soluble and insoluble hydroxides that will react with or adsorb pollutants, respectively, from the solution and also contribute to coagulation by neutralizing the negatively charged colloidal particles that may be present at neutral or alkaline pH. This enables the particles to approach closely and agglomerate under the influence of van der Waals attractive forces.

1.5.5. Floatation

The production of electrolytic gases is an inevitable by-product of electrocoagulation. These gases lift pollutant particles and coagulant aggregates to the surface by a flotation-like process, while encouraging contact between pollutant particles and coagulant by providing a certain amount of mixing action. The main difference between this

"electrolytic flotation" and more conventional flotation techniques is the method of bubble production and resultant bubble size. Expertise from other flotation techniques, including electroflotation, dissolved air flotation and air-lift reactors, can be employed to understand the flotation process in electrocoagulation reactors. Electroflotation describes the production of electrolytic gases for the sole purpose of pollutant removal. One of the main advantages of flotation by electrolytic gases is the small size of the bubbles produced. For a given gas volume, a smaller bubble diameter results in both a greater surface area and more bubbles, thereby increasing the probability of collision and the ability to remove fine pollutant particles [87]. Also, as noted, electrolytic bubbles enhance mixing in the bulk solution via their overall upward momentum flux, increasing the likelihood of effective contact between coagulant and pollutant particles.

Bubble movement within a reactor is a function of the bubble density, bubble path and bubble residence time. Current density determines the production rate of electrolytic gas, and thus the bubble density, while reactor geometry (size, height, electrode positioning, effective electrode surface area to volume ratio) determines the bubble path. The average time a bubble spends in the reactor is referred to as its residence time, which is a function of bubble size and path length. It should be noted that shear forces from any mixing source affect the growth of aggregates. Operation at a low current density produces relatively few bubbles, resulting in gentle agitation - conditions that are idea for aggregate growth and flocculation. As the current density increases, however, bubble density and the net upward momentum flux increases. These increase change the reactor's hydrodynamic behaviour and the degree of mixing. High shear forces induced

by mixing can damage and break flocks apart, reducing the effectiveness of pollutant removal.

Electrochemistry, coagulation and flotation thus form the three foundation stones for electrocoagulation. Each component is a well-studied technology in its own right. However, it is clear from the published literature that what is lacking is a quantitative appreciation of the way in which these technologies interact to provide an electrocoagulation system.

1.6 Application of membrane technology for the treatment of drinking water

Membrane separation process in water treatment has gradually gained popularity because it effectively removes a variety of contaminants from raw waters. While microfiltration (MF) and ultrafiltration (UF) membranes can mainly remove suspended particles, nanofiltration (NF) membranes are an effective technology to remove dissolved organic contaminants with molecular weights (*M*W) of larger than 200 Da and about 70% of monovalent ions by electrostatic repulsion (charge effect), size exclusion (sieving effect) and a combination of the rejection mechanisms [88]. NF membranes offer an attractive approach to meeting multiple objectives of advanced drinking water treatment, such as the removal of disinfection byproduct precursors, natural organic matter (NOM), endocrine disrupting chemicals and pesticides [89]. However, the decrease of permeate flux (i.e., membrane fouling) is a major obstacle to the application of NF membranes to drinking water treatment. Fouling worsens membrane performance and ultimately shortens membrane life, resulting in the increase of operational cost. Efficient control of membrane fouling is, therefore, required to successful application of NF technology.

Since a broad spectrum of constituents in feed waters can cause membrane fouling, it is important to investigate what types of materials (i.e., foulants) should be removed from feed waters by pretreatments prior to NF process. NF membranes are subject to fouling by dissolved and macromolecular organic substances, sparingly soluble inorganic compounds, colloidal and particulate matter, and microorganisms [90 - 92], which are not primarily removed by the pretreatment process, such as coagulation–flocculation. To date conventional pretreatment (coagulation followed by filtration) and MF are usually used in the drinking water treatment [93-94]. NF process could only be applied directly without pretreatment to the groundwaters containing very low turbidity. Since surface waters contain higher turbidity and the water quality characteristics of surface waters vary significantly, the selection of pretreatment processes is one of the most important factors that determine the success or failure of NF process in the drinking water treatment because membrane fouling is caused by a combined effect of the membrane and feed water properties. Better understanding of the properties of tested waters and the efficiency of different pretreatments to remove foulants from feed waters may help us preventing membrane fouling and designing the best pretreatment process for NF membranes. However, there is little information on the effect of pretreatment processes on the NF membrane fouling in the treatment of actual surface water.

1.7 Advantages and disadvantages of membrane process.

Although various conventional techniques of water purification described earlier are being used at present to solve the problem of groundwater pollution, none of them is user-friendly and cost-effective technique due to some or the other limitation and has

either no or very long pay back period. In the recent years, RO membrane process has emerged as a preferred alternative to provide safe drinking water without posing the problems associated with other conventional methods. RO is a physical process in which the contaminants are removed by applying pressure on the feed water to direct it through a semipermeable membrane. The process is the reverse of natural osmosis as a result of the applied pressure to the concentrated side of the membrane, which overcomes the natural osmotic pressure. RO membrane rejects ions based on size and electrical charge. The factors influencing the membrane selection are cost, recovery, rejection, raw water characteristics and pretreatment. Efficiency of the process is governed by different factors such as raw water characteristics, pressure, temperature and regular monitoring and maintenance, etc.

There are two types of membranes that can remove fluoride, iron and arsenic from water: NF and RO. NF is a relatively low pressure process that removes primarily the larger dissolved solids as compared to RO. Conversely, RO operates at higher pressures with greater rejection of all dissolved solids. Fluoride, iron and arsenic removal efficiencies upto 98% by membrane processes have been documented by many researchers.

In the past, the use of membrane technology for water treatment, particularly for drinking water production had been considered uneconomical in comparison with conventional means, but in the recent years the increased demand and contamination of water, rise in water quality standards and the problems associated with other methods have led to reconsideration of membrane technology for water purification. The progressive technical improvements in design and materials of the membranes have made the water treatment process economically competitive and highly reliable. Also, the capital and operational

costs of RO plant go on decreasing with increasing plant capacity [95]. Thus with improved management, this new technology for drinking water production might be the best option. Furthermore, membrane processes present several advantages as compared with other treatment methods [96].

Advantages

- The process is highly effective for fluoride removal. Membranes also provide an effective barrier to suspended solids, all inorganic pollutants, organic micropollutants, pesticides and microorganisms, etc.
- The process permits the treatment and disinfection of water in one step.
- It ensures constant water quality.
- No chemicals are required and very little maintenance is needed.
- Life of membrane is sufficiently long, so problem of regeneration or replacement is encountered less frequently.
- It works under wide pH range.
- No interference by other ions is observed.
- The process works in a simple, reliable automated operating regime with minimal manpower using compact modular model.

Disadvantages

- It removes all the ions present in water, though some minerals are essential for proper growth, remineralization is required after treatment.
- The process is expensive in comparison to other options.

- The water becomes acidic and needs pH correction.
- Lot of water gets wasted as brine.
- Disposal of brine is a problem.

1.8 Ceramic membrane – an overview

Existing and ongoing policies in process industries enforce the replacement of conventional process technology with membrane technology. Some of the aspiring features that membrane technology bestows include compact design, high product quality and lower operating cost. Alumina [97, 98], zirconia [99], titania [100] and silica [101] based ceramic membranes with high chemical, mechanical and thermal stability and longer life time [102] are found to be useful in different membrane based applications. However, the cost of these membranes is very high compared to polymeric membranes. This is primarily due to the higher cost of the inorganic precursors (alumina, zirconia, titania, silica) as well as very high sintering temperature (more than 1100 ^{o}C) [97-101] required for the fabrication of membrane. Due to these two key issues, the economic competitiveness of the inorganic membranes has not been appreciable till date to drive their industrial sustainability.

To circumvent the higher costs of inorganic membranes, existing and ongoing research in the preparation of low cost inorganic membranes is dovetailed towards the usage of low cost inorganic precursors and lower sintering temperatures (below 1000 ^{o}C). However, these variants in ceramic membrane research need to guarantee cheaper membranes that have the inherent ability to provide stable on time performance and life time, in similarity to the existing expensive ceramic membranes.

Recently, much work has been reported for the fabrication of inorganic membranes using cheaper raw materials such as apatite powder [103], fly ash [104], natural raw clay [105], dolomite [106] and kaolin [107, 108]. However, the sintering temperature used in these works was more than 1100 ^{o}C and the average pore size of the membranes was more than 1 μm. In this regard, it is well known that MF membranes with pore size in the submicron range (0.1 to 0.5 μm) are preferable for the industrial application to obtain excellent solute separation efficiency. Presently, surface modification technique is used to prepare submicron size membrane from micron size MF membrane. In this method, various inorganic precursors such as zeolite [109, 110], zirconia, alumina [109] and titania [111] are coated over the membrane surface, separately. However, the fabrication of such multilayer ceramic membranes involve a tedious cycle of sintering processes, which further contributes to the cost of the membrane [109, 110]. Therefore, there exist a necessity to develop alternate formulations using low cost precursors and low sintering temperature for the preparation of submicron range ceramic membrane with average pore size around 100 to 500 nm to further the industrialization of ceramic membranes.

Ceramic membranes are found to suitable in different process applications such as desalinations [105], high temperature membrane reactor [112], membrane bioreactor, food processing, colored effluent treatment, drinking water purification, treatment of industrial waste water [113]. Among all of these, the treatment of waste water using membrane technology in industrial systems appears more relevant and the need of the hour due to stricter and tighter environmental and health legislations.

1.9 Advantages of ceramic membranes over polymeric membranes

The advantages of inorganic membranes have been recognized for a long time. In fact, studies of the use of some inorganic membranes such as platinum and porous glass were evident even in the last century. Thermal and pH resistance characteristics of inorganic and organic membranes are compared in Table 1.11 where approximate ranges of operable temperature and pH are given. Although inorganic polymers have not been used commercially yet, polyphosphazene which is under development is included in the table. It can be seen that thermal stabilities of organic polymers, inorganic polymers and inorganic materials as membrane materials can be conveniently classified as <100-150°C, 100-350 °C and >350 °C, respectively. It should be stressed that the use of pH stability is only a crude indication of the chemical stability of the membrane material. An example is silver which can withstand strong bases and certain strong acids. Although silver is resistant to strong hydrochloric or hydrofluoric acid, it is subjected to be attacked by nitric and sulfuric acids and cyanide solutions. Therefore, the wide operable pH range of silver can not be construed that it is resistant to all acids.

The operable temperature limits of inorganic membranes are obviously much higher than those of organic polymeric membranes. The majority of organic membranes begin to deteriorate structurally around 100°C. Thermal stability of membranes is becoming not only a technical problem but also an economic issue. Inorganic membranes generally can withstand organic solvents, chlorine and other chemicals better than organic membranes. This also permits the use of more effective and yet corrosive cleaning procedures and chemicals. Many organic membranes are susceptible to microbial attack during applications. This is not the case with inorganic types, particularly ceramic membranes.

In addition, inorganic membranes in general do not suffer from the mechanical instability of many organic membranes where the porous support structure can undergo compaction under high pressures and cause decrease in permeability.

Table 1.11: Commonly used membrane materials and their properties [114]

Material	**Application(s)**	**Approximate maximum working temperature (^{o}C)**	**PH range**
Cellulose acetates	RO, UF, MF	50	3-7
Aromatic	RO, UF	60 - 80	3-11
Fluorocarbon	RO, UF, MF	130-150	1-14
Polyimides	RO, UF	40	2-8
Polysulfone	UF, MF	80-100	1-13
Nylons	UF, MF	150-180	--
Polycarbonate	UF, MF	60-70	--
PVDF	UF	130-150	1-13
Alumina (gamma)	UF	300	5-8
Alumina (alpha)	MF	>900	0-14
Glass	RO, UF	700	1-9

Zirconia	UF, MF	400	1-14
Zirconia (hydrous)	RO, UF	80-90	4-11
Silver	MF	370	1-14
Stainless steel (316)	MF	>400	4-11

1.10 Combination of various separation processes

In some studies, better separation was achieved by combining two or more processes. Dhale and Mahajani [115] used an integrated process including nanofiltration and wet oxidation to treat a disperse dye bath waste. The dye bath waste stream was undergone nanofiltration for recovering reusable water from the permeate stream, thus reducing fresh water consumption and minimizing effluent discharge. The concentrate obtained from the membrane unit had a high COD content, which was then treated by wet oxidation (WO) process. In another study [116], a combination of coagulation, adsorption and ultrafiltration was used for the treatment of a primary effluent. Primary effluent contained organic mineral, dissolved and suspended matter (colloids). Microfiltration or ultrafiltration was adequate for producing disinfected clear water suited for different applications. However, direct filtration on membrane was limited by the fouling phenomena, which led to a substantial and continuous decrease of the permeate flux during filtration at constant pressure. On the other hand, coagulation and adsorption made

it possible to remove the colloidal fraction, which played a significant role in membrane fouling. It was observed that coagulation significantly improved the ultrafiltration performances. In the study of Lin et al. [117], treatment of high-strength phenolic wastewater was investigated by a novel two-step method. The two-step treatment method consisted of chemical coagulation of the wastewater by metal chloride followed by further phenol reduction by resin adsorption. The combined treatment was found to be highly efficient in removing the phenol concentration from the aqueous solution and proved to be capable of lowering the initial phenol concentration considerably. The effectiveness of a combined reduction–biological treatment system for the decolorization of non-biodegradable textile dyeing wastewater was investigated by Ghoreishi et al. [118]. In this treatment system, a bisulfite-catalyzed sodium borohydride reduction followed by activated sludge technique was used in order to remove the color at ambient temperature and pressure.

Combination of adsorption and membrane based processes in the treatment of process wastewater were reported in literature. Baudin et al. [119] used a combination of adsorption and ultrafiltration for the treatment of surface water in 12 full-scale drinking water treatment plants in Europe. Later on, Meier et al. [120] used a combination of adsorption and nanofiltration for the treatment of severely contaminated wastewater. Powdered adsorbent was injected into the feed of a nanofiltration unit and removed from the concentrate subsequently by a thickener. The adsorbent in the feed had a positive effect on permeate quality, permeate flux and fouling layer in the nanofiltration unit. In comparison to reverse osmosis, the combination process had higher maximum recovery rate, lower operating pressure and energy consumption, which resulted in lower treatment

costs. In another recent work [121], the combination of adsorption and ultrafiltration was used in the treatment of colored wastewaters. In this process, adsorption was carried out in batch reactors using activated carbon cloths (ACCs). Adsorption was carried out to uptake the low molecular weight compounds (mainly dyes), while ultrafiltration was used for removing the high-sized compounds (macromolecules, colloids and turbidity). The membrane filtration step allowed a great removal of turbidity (about 98%), whereas adsorption onto ACC provided the decolorization of the stream with a high adsorption capacity. The continuous process of adsorption onto ACC and ultrafiltration resulted in successful discoloration with a high permeate flow rate.

During electrocoagulation, dissolution of electrodes in the form of metallic hydroxides creates flocks which in turn increase the alkalinity and turbidity. Therefore further treatment is strongly recommended. In view to this, combination of other techniques such as electroflotation, nanofiltration and reverse-osmosis were investigated along with electrocoagulation for drinking water treatment. Zuoa et al, 2008 [122] has studied a combined electrocoagulation and electroflotation for removal of fluoride from drinking water. Aouni et al., 2009 [123] has studied a hybrid electrocoagulation/nanofiltration process for the treatment of textile wastewater. Removal of silica from brackish water by electrocoagulation followed by reverse osmosis has been studied by Den and Wang, 2008 [124]. Particle size of the flocks generated during electrocoagulation would definitely determine the type of filtration process to be combined with the existing process. It was found that particle size of the electrocoagulated products were in the range of 10 t o 100 m. It was therefore realized that microfiltration may be a suitable process rather than Ultrafiltration, nanofiltration or reverse osmosis. Hence, in the present work,

microfiltration membranes were prepared according to the requirement. Electrocoagulation followed by microfiltration is adopted to remove fluoride, iron and arsenic from drinking water. Detail discussions on electrocoagulation, preparation of inorganic microfiltration membrane and its application in the separation of electrocoagulated byproducts have been discussed.

1.11 Aim of the current research: Treatment of Fluoride, Iron and Arsenic using a combination of electrocoagulation and microfiltration

Many processes are developed for the removal of fluoride, iron and arsenic from drinking water. For implementing any process scheme in industrial application, a detailed parametric study is required along with cost estimation. However, few literatures are available on such detailed experimental study along with cost estimation. Moreover, literatures on the post treatment process of electrocoagulation technique are scant.

Keeping this in mind, in the present work, a combination process is adopted for the removal of fluoride, iron and arsenic from drinking water involving both electrocoagulation and microfiltration. Aqueous synthetic solutions of fluoride, iron and arsenic are selected separately for electrocoagulation study. Later on, the process scheme is applied to the treatment of mixture of fluoride, iron and arsenic.

Ceramic membranes are prepared for microfiltration experiments. Both paste and uniaxial methods are adopted to prepare microfiltration membranes. The treated water after electrocoagulation, is passed through the microfiltration unit, where the unsettled electrocoagulated byproducts are separated and the water from the MF unit can safely be used for drinking purpose.

To summarize, the objectives of this thesis can broadly be categorized as,

- To develop a process involving both electrocoagulation and microfiltration and apply this in the treatment of drinking water with the aim of separating fluoride, iron and arsenic.
- To study the effect of various process parameters in electrocoagulation using aqueous synthetic solution of fluoride, iron and arsenic.
- To prepare low cost ceramic membranes for microfiltration application
- To develop a preliminary cost estimation for electrocoagulation and membrane preparation, essential in designing such processes in industrial level.

1.12 Outline of the dissertation

Keeping in mind the broad objectives of the work, the present thesis is organized as follows.

Chapter 1 gives an overview of the problem undertaken in this work i.e. the problem associated with the presence of fluoride, iron and arsenic in drinking water. A brief overview of electrocoagulation, inorganic membrane and membrane based separation processes is given in this chapter. It also discusses the features of different techniques for the treatment of fluoride, iron and arsenic containing drinking water. The chapter subsequently presents detailed literature review that includes electrocoagulation, preparation and characterization of inorganic membranes and different treatment technologies of contaminated drinking water. The aims of the present work are also highlighted in this chapter.

Chapter 2 gives the complete description of the experimentations involved in electrocoagulation of fluoride, iron and arsenic containing drinking water. The results of electrocoagulation experiments are reported in chapter 3. Effects of different parameters such as applied current density, initial concentration of pollutant, inter electrode distance and mode of electrode connections over the extent of pollutant removal are presented in detail. Performance of the EC process and the operating cost for the removal of fluoride, iron and arsenic are calculated and also discussed in chapter 3. Ceramic membranes are prepared using paste and uniaxial method. Details of preparation and characterization techniques have been elaborated in chapter 4. Chapter 5 discusses the structural and morphological analysis of the prepared membrane. The cost analysis of the prepared membranes is also reported in this chapter to compare the membrane along with other similar membrane available in market. The application of the proposed combination process involving electrocoagulation and followed by microfiltration is represented in chapter 6. Tap water containing the mixture of fluoride, iron and arsenic is used in this study. Finally, a general conclusions and future recommendations drawn from this study are summarized in chapter 7.

Chapter 2

Electrocoagulation: Experimental

This chapter discusses different experimental necessities for electrocoagulation process adopted in this study. In addition to this, it also includes the fine points of the characterization techniques for the electrocoagulated byproducts along with the supportive detail that provide important information of the experimental findings.

2.1 Electrocoagulation bath

Electrocoagulation in batch mode exhibit time-dependent behavior as the coagulant is continuously generated in the reactor due to anodic oxidation. Electrocoagulation bath operating in a batch mode is always best suited to laboratory scale applications. Nonetheless, batch electrocoagulation bath is so difficult to model mathematically due to its inherently dynamic behavior coupled with the interplay between thermodynamic considerations. Electrocoagulation bath operating in batch mode consists of a constant volume where contents are well mixed and internal concentrations change with time. The performance of such bath depends mostly on the reaction time i.e. the time in the reactor. In the present work a perspex made tank of working volume around 2.8 L and dimensions 0.14 m × 0.147 m × 0.137 m was considered for the electrocoagulation bath (Fig. 2.1). The performance of the process depends on the interactions between species which must contact with each other and well-mixed. Mixing is a gross measure and depicts the homogeneity within a reactor. Therefore, mixing strongly influences the performance and effectiveness of electrocoagulation bath. Mixing in an electrocoagulation bath operating

in a batch mode is primarily a function of fluid flow and agitation. A magnetic stirrer is used for stirring purpose.

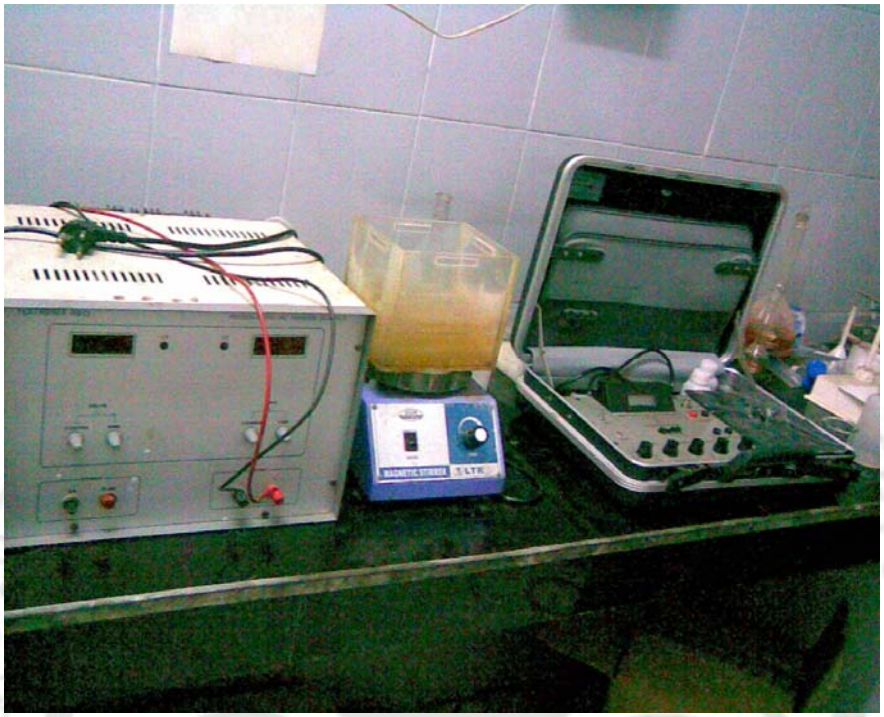

Fig. 2.1: Picture of electrocuagulation setup

2.2 Electrode

In electrocoagulation process, an applied potential generates the coagulant species in situ as the sacrificial metal anode (aluminium or iron) dissolves, while hydrogen is simultaneously evolved at the cathode. Coagulant species aggregate the suspended particles and adsorb the dissolved contaminants. Choice of electrode material depends on various criteria such as low-cost, low-oxidation potential, inertness towards the system under consideration, etc. Different electrodes were reported in the literature like carbon [125], mild steel [69], iron [126], graphite titanium [127] and aluminium [128].

Aluminium was reported to be very effective and successful in pollutant removal at favorable operating conditions [84,11]. In this work, aluminum sheets of 0.15 m × 0.05 m × 0.002 m were used as electrodes and the effective surface area of each electrode was 40 × 10^{-4} m^2. Two types of electrode connection (monopolar and bipolar) were investigated during the EC of fluoride, iron and arsenic present in drinking water.

Monopolar electrode connection

In monopolar electrode connection one end of the electrode was connected to the positive terminal of the power source whereas the other end of the electrode was connected to the negative terminal of the same power source, thus completed the formation of a primary cell which under the application of potential in contact with the contaminant solution initiated the electrocoagulation process.

Bipolar electrode connection

In bipolar connection, more than two electrodes were used to make such arrangement in order to reduce the effective corrosion of the electrode and improve the process performance. Only two end electrodes were connected to the DC power source whereas other two electrodes had no connection to the DC source. In such condition, induced polarization took place when voltage was applied to the end electrodes so that the inner electrodes started acting as a secondary cell. Therefore, the total assembly was bipolarized with a primary and a secondary cell acting together. The entire electrode assembly was fitted on non-conducting wedges and hung from the top of the electrocoagulation tank. The assembly was connected to DC power source (Textronics

36D, Agarwal Electronics, Mumbai, India) to constitute an electrochemical cell with galvanostatic mode for constant current supply. Schematic diagram of monopolar and bipolar electrochemical cell is shown in Fig 2.2. The electrode assembly was placed in the cell and the electrodes were connected to the respective terminals of the DC power supply and a constant current was supplied for a given time.

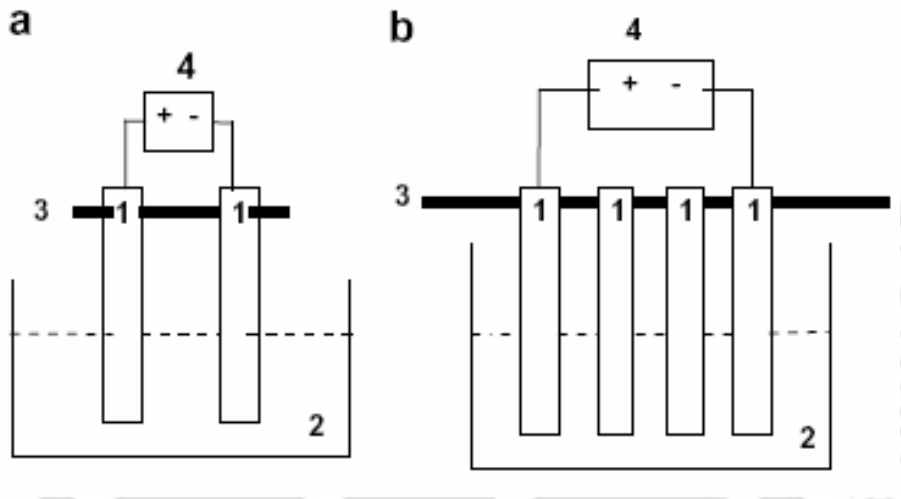

Fig. 2.2 Schematic diagram of electrochemical cell for the EC experiments. (a) Monopolar connection; and (b) bipolar connection. (1) electrodes; (2) fluoride contaminated drinking water; (3) electrode support; and (4) DC power source.

2.3 Solution preparation

Sodium fluoride (NaF, supplied by Aldrich Chemical Company, USA) was used in this study for the preparation of fluoride solution. Ferrous sulfate ($FeSO4 \cdot 7H_2O$, Aldrich Chemical Company, USA) and arsenic tri-oxide (As_2O_3, Merck, India) were used to prepare synthetic iron and arsenic solutions, respectively. In all the cases, a measured

quantity of salts was added in tap water (1 L) for the preparation of fluoride, iron and arsenic contaminated drinking water. Conductivity and pH of tap water was 12 S/m and 7.5, respectively. Initial fluoride concentration varied from 4 to 10 mg L^{-1}, whereas that for iron was 5 to 25 mg L^{-1} and for arsenic was 50 to 200 µg L^{-1}. The range of concentration is selected based on availability of fluoride, iron and arsenic concentration in drinking water.

2.4 Experimental procedure

In each EC Experiment, 1 L water solution was placed into the electrolytic cell (EC bath). The current density was adjusted to a desired value and the operation was started. After the experiment, the power was switched off and the electrodes were dismantled. The treated sample collected at different time interval was filtered before analysis. Before each run, the electrodes were washed with acetone to remove surface grease, and the impurities on the aluminum electrode surfaces were removed by dipping for 5 minutes in acetone solution followed by rubbing with an abrasive paper (C220) in order to ensure the complete removal of impurities before every experiment. After each experiment the used anode and cathode plate was interchanged for effective electrode utilization. All the runs were performed at constant temperature of 25 ^{o}C. The parameters chosen in the present experiments were reported in subsequent section. Fluoride ion meter was used to determine the fluoride concentration whereas AAS (Atomic Absorption Spectrometer) was used to determine the iron as well as arsenic concentration. Conductivity and pH were also measured using conductivity meter and pH meter, respectively.

Fluoride ion meter

Fluoride ion meter (Make: Eutech Instrument, Singapore, Model: ECFOO301BEU) was used to determine the fluoride concentration after calibrating using TISAB (Total Ionic Strength Adjuster Buffer). TISAB is a solution containing CH_3COOH (acetic acid), NaCl (sodium chloride), CDTA (trans 1,2-diaminocyclohexane– N,N,N´,N´ tetra acetic acid monohydrate) and NaOH (sodium hydroxide).

AAS (Atomic Absorption Spectrometer)

Atomic Absorption Spectrometer (Model No.240 FF, Varian, Netherlands) was used to determine iron and arsenic concentration in the sample collected during EC. For determination of iron concentration, the flame (acetylene-air) method was applied with the presence of Fe lamp provided (Varian, 240 FF) for the experiment. VGA mode was applied in presence of reducing agents ($NaBH_4$) and dilute HCl for the determination of arsenic concentration.

pH meter

A pH meter (Make: Century Instruments (P) Ltd., Chandigarh, India) was used to determine the pH of solution. The meter was first calibrated using two different buffers of pH 4 and pH 9.2. Each time the meter was thoroughly washed with de-ionized water before and after the dipping inside the buffer solutions.

Conductivity meter

The conductivity of solution in the EC bath was measured using a digital conductivity meter (Make: Electronics Pvt. Ltd., India, Model: VS1) before and after the treatment to

match with the recommendable limit of 0.2 mmhos [129]. The conductivity meter was also calibrated by matching the known conductivity of 0.1(N) KCl solutions given in the manual supplied by the manufacturer. After the calibration, the conductivity meter was thoroughly washed with de-ionized water and soaked with the tissue paper without touching the coated detector inside the meter.

2.5 Operating conditions

Different important parameters such as initial concentration, interelectrode distance, electrode connection, current density and time of the treatment were investigated to know the sufficient information about the EC process applied mainly for the purification of drinking water contaminated with fluoride, iron and arsenic. All the experimental conditions considered in this study are shown in Tables 2.1 to 2.3.

Table 2.1: Experimental conditions for the removal of fluoride using EC

Parameters	Conditions maintained
Initial concentration (mg L^{-1})	4, 6, 8, 10
Interelectrode distance (m)	0.005, 0.01, 0.015
Current density (A/m^2)	250, 375, 500, 625
Experiment time (min)	45
Temperature (° C)	25
Electrode connection	Monopolar and bipolar

Table 2.2: Experimental conditions for the removal of iron using EC

Parameters	**Conditions maintained**
Initial concentration (mg L^{-1})	5, 10, 15, 20, 25
Current density (A m^{-2})	100, 200, 300 ,400
Interelectrode distance (m)	0.005. 0.01, 0.015, 0.02
Experiment time (minutes)	35
Temperature (° C)	25
Electrode connection	Monopolar

Table 2.3: Experimental conditions for the removal of arsenic using EC

Parameters	**Conditions maintained**	
	Monopolar connection	**Bipolar connection**
Initial concentration (µg/L)	50, 75, 100	50, 100, 200
Interelectrode distance (m)	0.015, 0.01, 0.005	0.015, 0.01, 0.005
Current density (A/m^2)	125, 187.5, 312.5, 625	250, 375, 500, 625
Experiment time (min)	60	60
Temperature (° C)	25	25

2.6 Characterization of byproducts

A whitish precipitate was formed inside the electrocoagulation bath at the end of EC process for the treatment of drinking water contaminated with fluoride and arsenic. On the other hand, a brownish precipitate was formed when the water was contaminated with

iron. The precipitate was taken out after the filtration using a filter paper (HM2, Indiachem, India) and dried inside a hot-air oven for 3–4 hours. It was then grinded to a fine powder and prepared for SEM, EDAX, FTIR and XRD analysis in order to characterize the by-product.

Scanning electron microscopy and elemental analysis (SEM & EDAX)

The morphology of the by-products obtained from the EC bath was analyzed by SEM, whereas elemental information of the by-products were recorded using EDAX. Furthermore, it is mention worthy that before SEM analysis the sample was finely grinded and coated with the Au inside a plasma chamber operated under vacuum for 135 seconds with a leakage current of 4 mA. This was done to ensure the less possibility of charging during the analysis. Sample was analyzed under the application of the probe current of 94 pA and at different magnifications with the primary electron hitting the sample with energy of 10 kV – 15 kV. EDAX is an integrated part of the scanning electron microscopy where energy dispersion according to the element was calibrated with a standard Co (cobalt) sample before the analysis.

X-ray diffraction (XRD)

The phase of the byproducts was recorded using XRD. Powder X-ray diffraction of the by-product was recorded by a diffractometer operating with a Cu Kα radiation source and nanobragg mode. The XRD analysis result is recorded from 5° to 90° with a step increase rate of 0.05^{o} per second. The spectrum of the analyzed by-products showed broad and diffuse peaks. Therefore, the identification of peaks with such broad humps is

a well known confirmed characteristic of phases which are amorphous or poorly crystalline in nature.

Fourier Transform Infrared Spectroscopy (FTIR)

The finely grinded by-product was mixed with potassium bromide properly and pressed under 5 Ton weight for 10 seconds to prepare the pellet necessary for the analysis. Furthermore, the pellet was subjected to the Infrared spectra and scans were recorded with wave numbers ranging from 4000 to 450 cm^{-1}. Different peaks at different wave numbers were leveled and matched with the standard data available for certain identified bond stretching. Some peaks were not been identified due to the lack of standard data related to our work. Nonetheless, the available data well matched with the experimental results presented here.

Chapter 3

Electrocoagulation: Results and Discussion

This chapter discusses the results obtained for the removal of fluoride, iron and arsenic from drinking water using electrocoagulation (EC) technique. By-products obtained from the EC bath were characterized by SEM, EDAX, FTIR and XRD analysis. Operating cost for the removal of fluoride, iron and arsenic were calculated and presented well. In the calculation of the operating cost, only material and energy costs were considered. Other cost items such as labour, maintenance and solid/liquid separation costs were not taken into account. A simplified cost equation was used to evaluate the operating cost of EC for the removal of fluoride, iron and arsenic [11, 84].

3.1 Fluoride removal

In this work, two different electrode connections (monopolar and bipolar) were investigated for choosing the better alternative in order to intensify the performance of the process. Different initial concentration (4 to 10 mg L^{-1}) of fluoride was considered for the experiment that had duration of 45 minutes. Experiments were carried out with different current densities. Corrosion of electrodes as well as the sludge formation during the experiments for both electrode connections was estimated. Variation of film thickness deposited over the electrode surfaces with change in initial fluoride concentrations and current densities were determined.

3.1.1 Effect of initial fluoride concentration

In the fluoride removal process by electrocoagulation, initial fluoride concentration is an important parameter for a particular mode of electrode connection. Figure 3.1 reveals the variation of fluoride concentration in the EC bath during the experiment using monopolar electrode connection. It was observed that after the treatment, final fluoride concentration was not dropped below the recommendable limit suggested by WHO for all the initial fluoride concentrations. It was also observed from Fig. 3.1 that around 35 min was required to attain final fluoride concentration of 1 mg L^{-1} for the initial fluoride concentration of 4 mg L^{-1} and current density of 250 A m^{-2}. Again, for an initial fluoride concentration of 6 mg L^{-1} with monopolar connection, 45 min was needed for the final fluoride concentration to be of 1.4 mg L^{-1}. It was very much clear that with an increase in initial fluoride concentration the treatment time increases to attain the final fluoride concentration at its recommendable limit (1 mg L^{-1}). In EC, initially aluminium cations contribute to charge neutralization of the pollutant particles as the isoelectric point is attained. Here a sorption coagulation mechanism occurs resulting in the formation of loose aggregates. As time progresses, further aluminium cation addition results in amorphous aluminium hydroxide precipitation that promotes pollutant aggregation. As the current density was kept constant so the production of the aluminium cation remained fixed and therefore with an increase in initial fluoride concentration, the complex formation process between the amorphous aluminium hydroxide and fluoride was insufficient at the applied current density mentioned above. This could be the reason so that the drinking water with an initial fluoride concentration of 6 and 8 mg L^{-1} had a final

fluoride concentration of 1.8 and 2.2 mg L^{-1} at the end of 45 min treatment by EC with monopolar electrode connection.

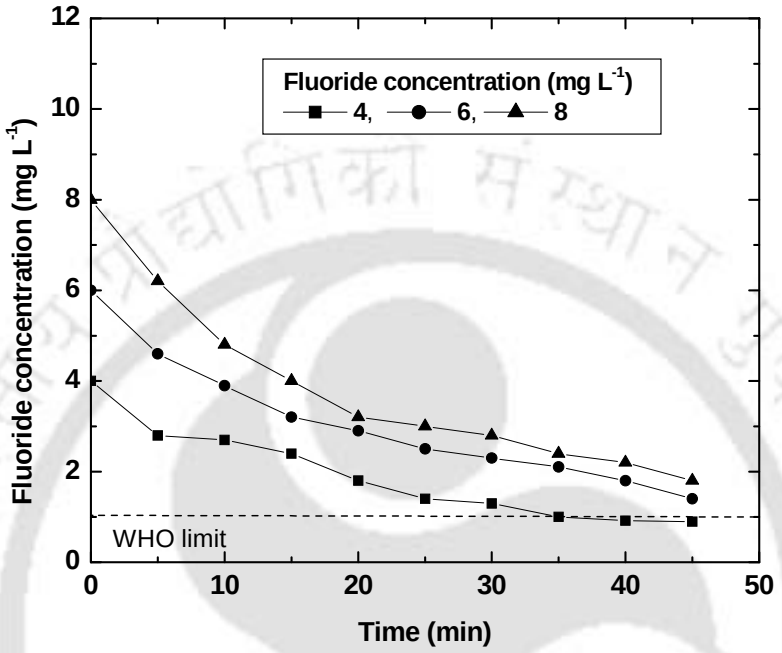

Fig. 3.1: Variation of fluoride concentration in the EC bath with time. Interelectrode distance: 0.005 m; current density: 250 A m^{-2}; temperature: 25 °C, Electrode connection: Monopolar

3.1.2 Effect of bipolar connection of electrodes

In order to improve the fluoride removal from the contaminated drinking water with higher initial fluoride concentration efficiently, electrode connection can have a justified effect on the sludge formation as well as on the corrosion of the electrode. Effect of electrode connections (monopolar and bipolar) for the fluoride removal by EC is shown in the inset of Fig. 3.2. Investigation was performed for the treatment of drinking water

with initial fluoride concentration of 10 mg L^{-1}. Other parameters like current density, interelectrode distance and duration of the experiment were maintained at 250 A m^{-2}, 0.005 m and 45 min, respectively. It was observed that with the passage of time fluoride concentration inside the EC bath was decreased for both electrode connections. It is also seen from Fig. 3.2 that at the end of 45 min in bipolar connection, final fluoride concentration was 1.7 mg L^{-1}, whereas for monopolar connection, the fluoride concentration dropped down to a value of 2.2 mg L^{-1} which was far away from the recommendable limit. It is necessary to mention that in the bipolar connection, two pair of electrodes were used of which only the end electrodes were connected to respective anode and cathode connection of the DC source. In bipolar connection, two electrochemical cells acted together for which higher surface area compared to that of monopolar connection favored the adequate anodic oxidation. As a result, with the same current density applied for both kind of connection, the intensity is higher in the bipolar connection. Therefore, final fluoride concentration in the solution was found lower than that was observed in monopolar electrode connection. However, fluoride concentration in the bath at the end of 45 minute does not attain the permissible limit for both the electrode connections.

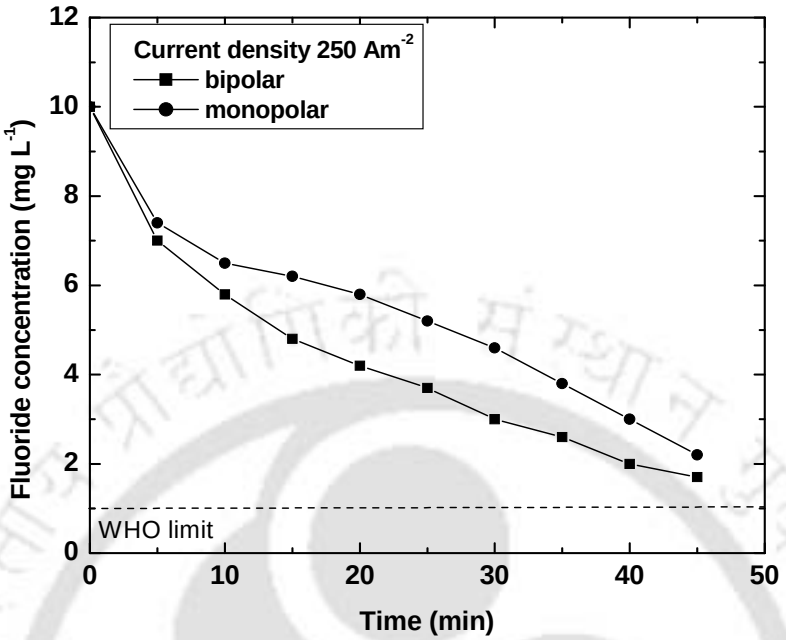

Fig. 3.2: Variation of fluoride concentration in the EC bath with time. Interelectrode distance: 0.005 m; current density: 250 A m^{-2}; temperature: 25 °C, Initial fluoride concentration: 10 mg L^{-1}, Electrode connection: bipolar and monopolar.

3.1.3 Effect of interelectrode distance

The set up of electrode assembly is very important for required effective surface area of electrode and inter electrode distance. Variations of fluoride concentration in the EC bath with inter electrode distance are shown in Fig. 3.3. It was observed from the figure that at any instant fluoride concentration in the EC bath was lower for lower inter electrode distance.

For example, final fluoride concentration in the EC bath decreases from around 3 mg L^{-1} to 0.8 mg L^{-1} when inter electrode distance was decreased from 0.015 m to 0.005 m at the

end of 45 minute by EC for the initial fluoride concentration of 10 mg L^{-1}. It is well known that in the EC bath anodic oxidation is started as the potential is applied to the electrodes initially. Now as the time proceeds a very fine film of metal hydroxides would get formed on the anode generating an extra resistance that even increases with increasing inter-electrode distance. Hence, after some time of the EC current falls down. To maintain a constant current, applied potential has to be increased.

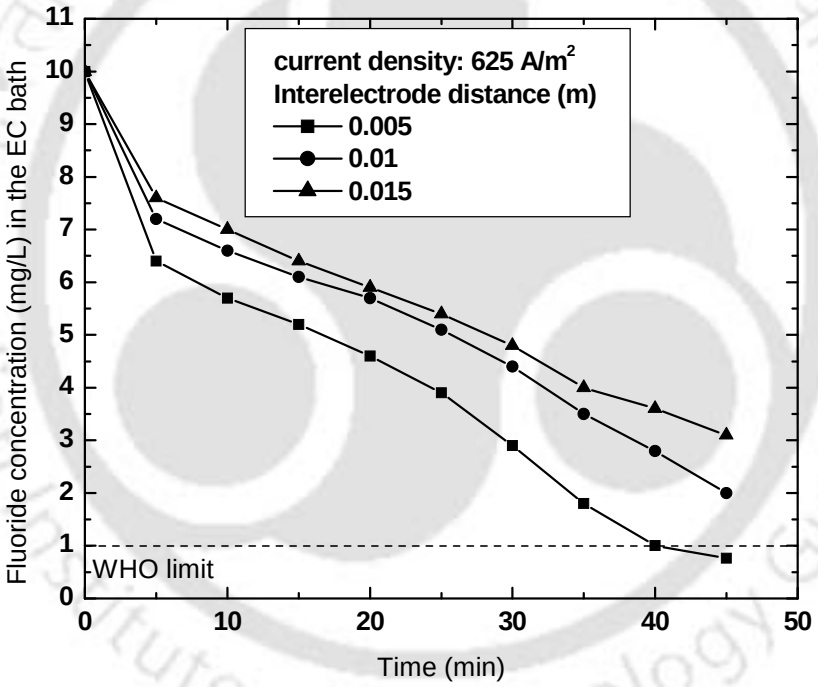

Fig. 3.3: Effects of inter electrode distance on the fluoride concentration in the EC bath with time. Initial fluoride concentration 10 mg L^{-1}, current density: 625 A m^{-2}, inter electrode distance: 0.005 m, temperature: 25°C, electrode connection: monopolar

As the rate of anodic oxidation becomes lower, numbers of cations at anode also decreases. These cations are responsible for the formation of coagulant. Therefore, at higher inter electrode distance, rate of aggregation of suspended particles as well as adsorption of contaminants would be low. This may be reason behind finding the lower removal efficiency at higher inter electrode distance

3.1.4 Fluoride removal with varying current density

Monopolar

In any electrocoagulation process current density (A m^{-2}) and time of electrolysis are important operational parameters setting the ultimate removal and defining the electrical energy and power consumption so eventually the ultimate operating cost for the process. Current density was estimated as the amount of current passing divided by the effective surface area of electrode submerged inside the solution. Sufficient number of electrons passing through the unit area of the electrode surface corresponded to the favorable occurrence of the anodic oxidation. This further enhanced the formation of adequate amount of metal hydroxide species followed by hydrolysis and polymerization. Some investigators reported that in electrocoagulation, current density can influence the treatment efficiency while others pointed out that current density has no significant role on pollutant removal. Therefore, it remained unclear that whether the current density affects the treatment efficiency or not. Choice of electrode material is also vital affecting the cell voltage (different oxidation potential for different electrode materials), responsible to initiate the anodic oxidation. Since the metallic hydroxides can not be formed without anodic oxidation so the formation rate of such species is dependent on the

applied voltage as well as the electrode material. Further, these species take part in the agglomeration of flocks followed by adsorption through which the separation is achieved.

Figure 3.4 shows the removal of fluoride from fluoride-rich water for four different current densities with time. Current density was varied from 250 A m^{-2} to 625 A m^{-2}. It was seen from the figure that for all the current densities, a sharp decrease in fluoride concentration occurred up to 5 minutes of operation. Formation of a thin film of gelatinous aluminium hydroxide on the anode surface inhibits the cation formation rate as well as the agglomeration of the contaminant particles from the solution in the form of flocks. Therefore, after certain period of time (5 minutes in this case), decrease in fluoride concentration became gradual.

It was also observed from the figure that with an increase in current density, defluoridation was improved. Generally with an increase in current density causes the anodic oxidation to take place more readily, which in turn favors the formation of amorphous aluminium hydroxides species adequately in the vicinity of the electrode as well as in the bulk. Formation of such hydroxides at the vicinity of the anode-water interface accumulates as a fine gelatinous film on the electrode surface. It is well known that in the system with co-existing anions, the defluoridation occurs in the bulk of the solution and without co-existing anions it happens on the surface of the anode. Therefore, fluoride ions present in the solution could get the allowance to interact with such species' and form complex. It was found that the final fluoride concentration of 1 mg L^{-1} was

achieved at the end of 40 minutes of EC with an application of 625 A m^{-2} current densities.

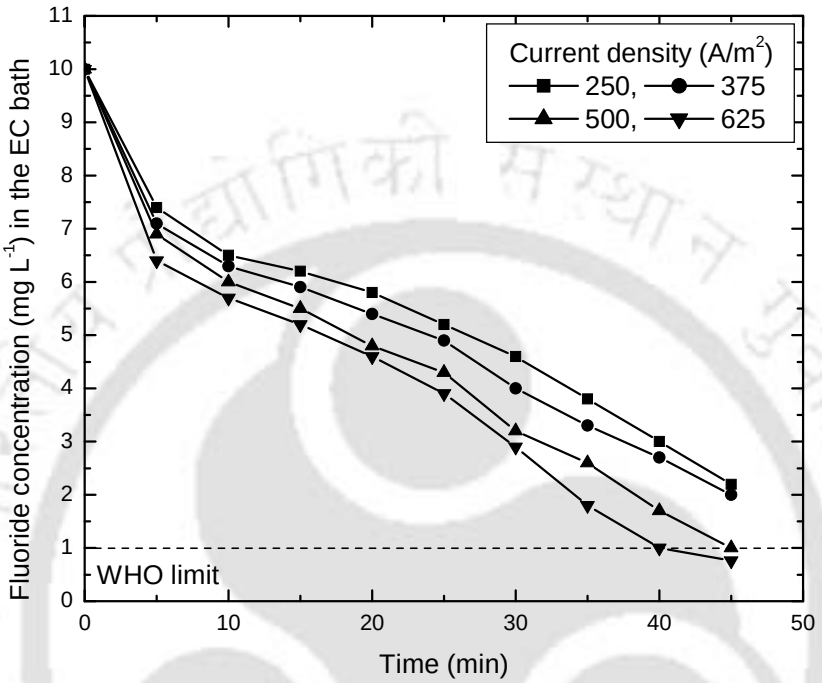

Fig 3.4: Effects of current density on the fluoride concentration in the EC bath with time. Initial fluoride concentration 10 mg L^{-1}, inter electrode distance: 0.005 m, temperature: 25°C, electrode connection: monopolar

Bipolar:

Figure 3.5 represents the effect of current density on the fluoride concentration in the EC bath during the experiment. Current density varied from 375 to 625 A m^{-2} using bipolar electrode connection. It was seen from Fig. 3.5 that the defluoridation was improved with an increase in current density. This is due to the formation of amorphous aluminium hydroxides species adequately in the vicinity of the electrode as discussed for monopolar

case. It was found that the final fluoride concentration of 1 mg L^{-1} was achieved at the end of 30 min of the EC using bipolar connection with an application of 625 A m^{-2}. Furthermore, this was also supported by the fact that with an increase in current density and initial fluoride concentration, the corrosion of the electrodes as well as the sludge formation also increased.

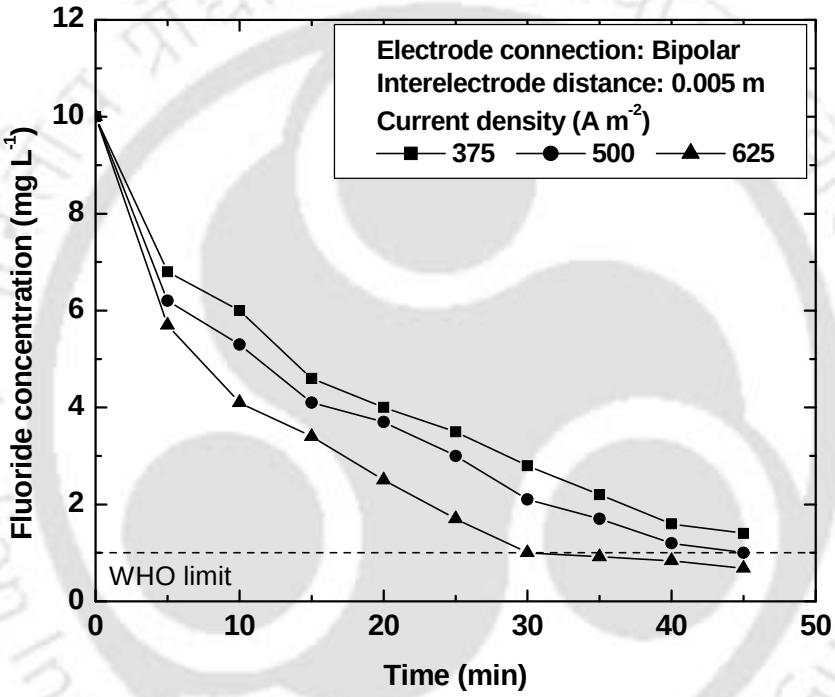

Fig. 3.5: Effect of current density on the fluoride concentration in the EC bath with time. Initial fluoride concentration: 10 mg L^{-1}; interelectrode distance: 0.005 m; electrode connection: bipolar; temperature: 25 °C.

3.1.5 Variation of pH in electrocoagulation bath

Disappearance of fluoride from the EC bath is believed to be a favorable technology due to the formation of more OH^- ions in the electrolysis of water. It was observed that

aluminum electrode produced $Al(OH)_3$ precipitation at slightly basic medium and followed sweep-flock mechanism [131]. Hence, change in pH of the solution in the EC bath would be a measure of $Al(OH)_3$ formation influencing fluoride removal. Duration of the EC was 45 minutes and after every 5 minutes pH of the solution was checked using a digital pH meter (CONSORT, C863, Make: Belgium). Variation of pH in the EC bath is shown in Fig. 3.6 for different current densities (250 A/m^2, 375 A/m^2, 500 A/m^2 and 625 A/m^2) for the initial fluoride concentration of 10 mg/L. For all the cases, initial pH of the solution was taken similar to that of synthetic fluoride containing water and shown in the inset of Fig. 3.6. It was seen that the pH of the solution increases with time for all the current densities.

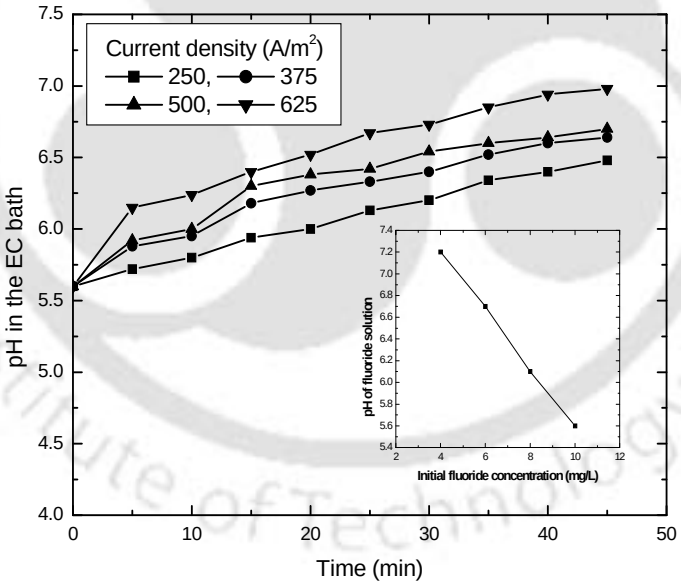

Fig. 3.6: Variation of pH of fluoride containing drinking water in the EC bath with time at different current densities. Inter electrode distance: 0.005 m, initial fluoride concentration: 10 mg L^{-1}, electrode connection: monopolar

At the end of the EC, pH was seen to reach a value of around 6.5, 6.6, 6.7 and 6.9 for the current densities of 250 A m^{-2}, 375 A m^{-2}, 500 A m^{-2} and 625 A m^{-2}, respectively. The increase in pH value with time and current density is due the formation of higher number concentration of OH^- in the EC bath due to electrolysis. This increases the anodic oxidation as well as the formation of aluminum hydroxide complexes. A whitish sludge due to the formation of fluoro-aluminum complexes (as discussed in chapter 2) was observed at the end of experiment. It might be the generation of more aluminum hydroxides which in turn adsorbed fluoride from the solution and remains in the solution as flock.

3.1.6 Variation of electrodes corrosion

Anodic oxidation gives rise to the corrosion of electrode material (aluminium in the present case) by means of aluminium hydroxide formation during EC. The corrosion of electrodes gives an over-view of the life time as well as the experimental cost of the electrode material. Therefore, electrode corrosion during EC can be considered as an important parameter that reflects the viability of the process. Corrosion of the electrodes can be defined as the weight loss (mg) of the electrodes due to anodic oxidation. This loss was calculated by subtracting the weight of the electrodes taken at the end of the experiment from the weight taken before the experiment of the same electrodes. Figure 3.7 describes the extent of electrode corrosion at different current densities with bipolar as well as monopolar electrode connection. The investigation was performed using different initial fluoride concentrations. Parameters like interelectrode distance and

duration of the experiment were kept constant at the values mentioned in Fig. 3.1. It was observed that with an increase in initial fluoride concentration and current density, the electrode corrosion enhanced due to the increased dissolution of electrodes. In addition to this, it was seen that electrode corrosion was greater for bipolar connection. It can be seen from Fig. 3.7 that the electrode corrosion was 14.5 mg with monopolar connection whereas with bipolar connection the corrosion was 22.8 mg at an applied current density of 250 A m^{-2} for the initial fluoride concentration of 4 mg L^{-1}. This was an obvious situation since anodic oxidation in bipolar connection was higher compared to monopolar connection.

Sludge generated in the EC bath was estimated for bipolar and monopolar electrode connections. It was found more sludge formation for the bipolar connection, whereas for both cases it increased with increasing current density. In the treatment of drinking water with initial fluoride concentration of 4 mg L^{-1} by EC at a current density of 250 A m^{-2}, the amount of sludge produced was 68.6 and 42 mg for bipolar and monopolar connections, respectively. It was noticed that the removal of fluoride from the drinking water having initial fluoride concentration of 4 mg L^{-1} using bipolar connection, the amount of sludge generated was equal to 90.2, 148.5 and 190.3 mg at 375, 500 and 625 A m^{-2}, respectively. It was also observed that with an increase in initial fluoride concentration, more sludge was produced. Figure 3.8 represents the pH variation with time in the EC bath during the experiment using bipolar and monopolar connections. The pH increased with time in both cases (varied from 6.4 to 8.1). It was also observed that for bipolar connection, the pH of the solution was marginally higher than the monopolar

connection. For example, at a current density of 625 A m^{-2} and an initial fluoride concentration of 10 mg L^{-1}, the solution pH was always around 8 at the end of all trials. According to the complex precipitation kinetics, most of the charged aluminium species transformed into $Al(OH)_3$ which exist in equilibrium with some of the soluble species [132]. It can be also seen from Fig. 3.8 that after attaining the pH close to 8, it does not increase significantly irrespective of the connection mode.

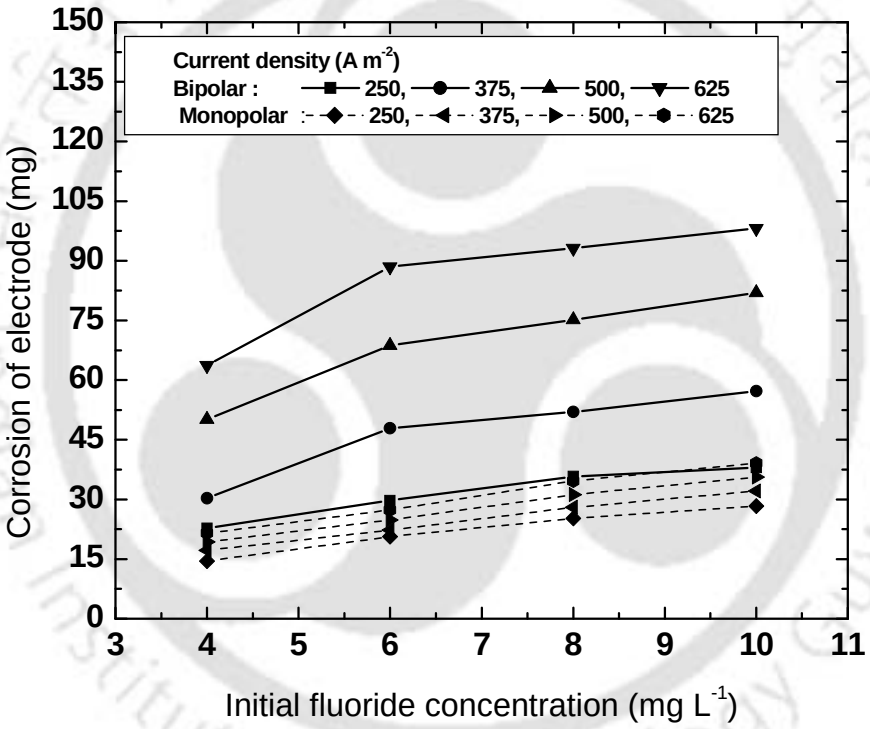

Fig. 3.7: Variation of electrode corrosion with bipolar and monopolar connections at different current densities. Interelectrode distance: 0.005 m; duration of the experiment: 45 min; temperature: 25 °C.

This is probably because of an equilibrium between the $Al(OH)_3$ and the soluble aluminium species at pH about 8 for both electrode connections. The observation also supported the reason behind the electrode dissolution as discussed in section 1.5.4.

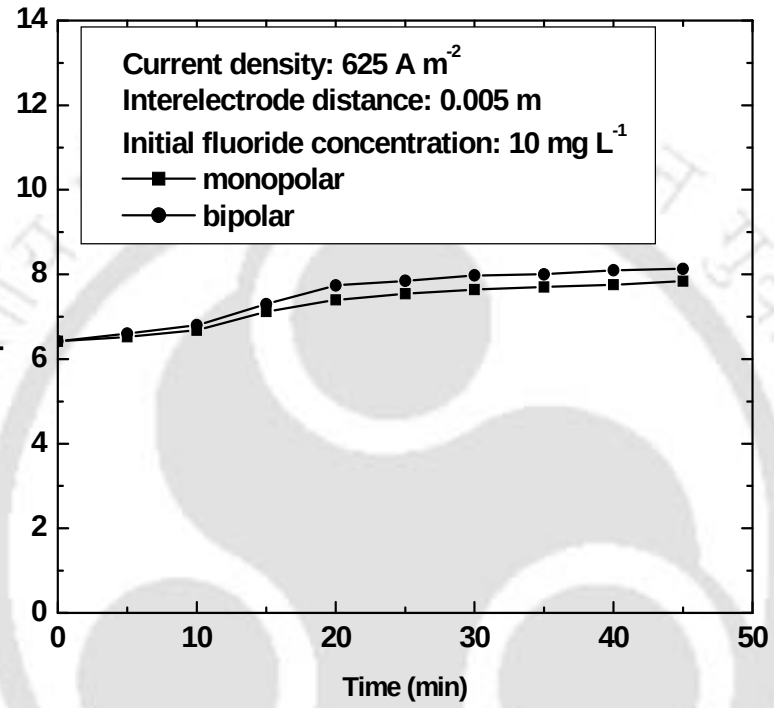

Fig. 3.8: Variation of pH with time in the EC bath for bipolar and monopolar connections. Initial fluoride concentration: 10 mg L^{-1}; interelectrode distance: 0.005 m; duration of the experiment: 45 min; temperature: 25 °C

3.1.7 Variation of film thickness

In EC process, anodic oxidation favors the formation of gelatinous hydroxide species with an interaction between positive metal ions and negative OH^- ions. This gelatinous behavior allows such hydroxide to stick with the electrode surface growing like a film

with the progress of the process. Therefore an extra resistance is created, which in turn affects the performance of the process. Hence, it is very much clear that the film generated during the electrocoagulation process plays a major role in order to operate the technique for the removal of pollutants. The film thickness was calculated using the following simple mass balance equation:

$$\delta \cong \frac{(m_1 - m_2) \times 10^{-6}}{\rho \times A} \qquad (3.1)$$

where δ is the film-thickness (nm), m_1 is the weight of the electrodes (mg) after the experiment without cleaning, m_2 is the weight of the electrodes (mg) after the experiment after cleaning, ρ is the density of the film (g L^{-1}) and A is the area of the electrodes (m^2).

Figure 3.9 depicts the variation of film-thickness over electrode surface with different current densities and initial concentrations of fluoride. It was seen that with an increase in current density and initial fluoride concentration of the drinking water, film-thickness increased for both monopolar (Fig. 3.9) and bipolar connections. It can be observed from Fig. 3.9 that the film thickness increased from around 131 to 470 nm when the initial fluoride concentration increased from 4 to 10 mg L^{-1} at an applied current density of 375 A m^{-2} for bipolar connection. This parameter also increased from 147 to 180 nm when current density was increased from 500 to 625 A m^{-2} for the initial fluoride concentration of 6 mg L^{-1}. Variation of film thickness using monopolar connection has been estimated at the same condition as that of bipolar connection and shown in the inset of Fig. 3.9. It was observed that film formation followed the same trend but it was much lower than in the case of bipolar connection. For example, the film thickness increased from 23.5 to 57 nm when the initial fluoride concentration varied from 4 to 10 mg L^{-1} at an applied

current density of 375 A m^{-2} for 45 min of operation. Furthermore, it was also found that with the increase in current density from 500 to 625 A m^{-2}, the film-thickness increased from 69 to 76.4 nm for an initial fluoride concentration of 10 mg L^{-1}.

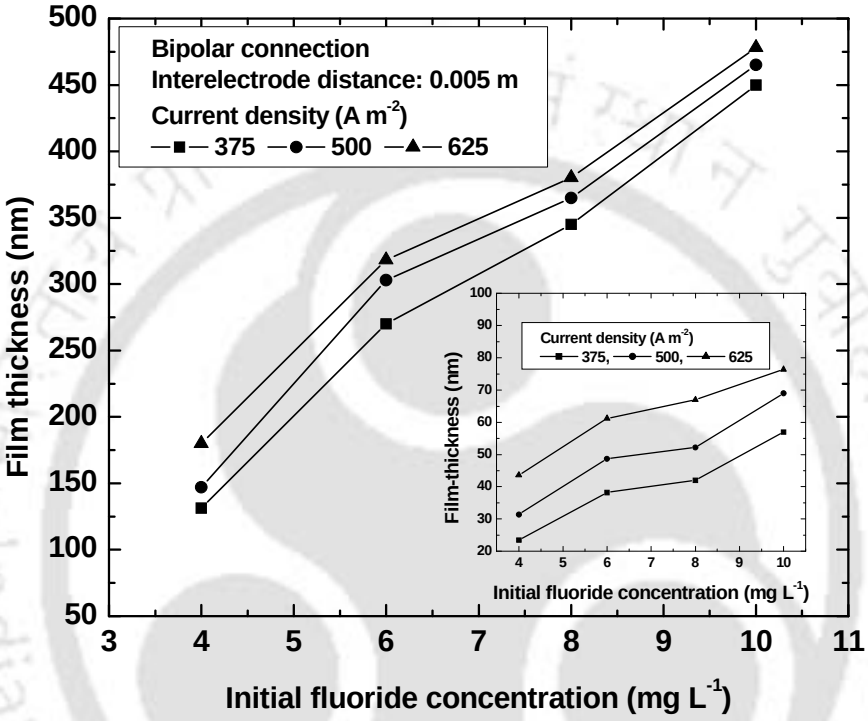

Fig. 3.9: Variation of film thickness over electrode surface with different current densities and initial fluoride ion concentrations. Current density: 375 A m^{-2}; interelectrode distance: 0.005 m; duration of the experiment: 45 min; electrode connection: bipolar; temperature: 25 °C. **Inset:** Film thickness variation over electrode surface with different current densities and initial fluoride ion concentrations for monopolar electrode connection.

An enhancement in the current density favored the anodic oxidation and hence, it increased the possibility of the formation of more metal ions as well as the interactions between the metal hydroxides and the fluoride ions. Therefore, the generation of the film formed during the experiment became thicker.

3.1.8 Variation of conductivity of treated water

In order to examine the treated water quality by electrocoagulation, conductivity measurement was made so that it could be permissible for the drinking purpose. Before each experiment using bipolar electrode connection, the conductivity of the contaminated water was measured as 0.4, 0.6 and 0.9 mmhos for the initial fluoride concentration of 6, 8 and 10 mg L^{-1}, respectively. After the treatment, the sludge was filtered out and the clear solution was collected. The conductivity of treated water was around 0.2 mmhos for all cases, that is, in the range of permissible limit of drinking water [129].

3.1.9 Estimation of operating costs

In any electrical process, cost is incurred due to electrical energy demand, which affects the operating cost. For EC process the operating cost includes material, mainly electrodes, and electrical energy costs, as well as labour, maintenance, sludge dewatering and disposal, and fixed costs. In this preliminary economic investigation, energy and electrode material costs were taken into account as major cost items in the calculation of the operating cost (US$ m^{-3} of fluoride solution) in the form:

$$\textbf{Operating cost} = \mathbf{a}\, C_{\text{energy}} + \mathbf{b}\, C_{\text{electrode}} \qquad (3.2)$$

where C_{energy} and $C_{electrode}$ (kg Al m^{-3} of fluoride solution) are consumption quantities for the fluoride removal, which are obtained experimentally. “a” and “b” given for Indian market in February 2008, are as follows: “a” electrical energy price 0.0065 US$ kWh^{-1}; “b” electrode material price 0.3 US$ kg Al^{-1}. Cost due to electrical energy was calculated from the expression:

$$C_{energy} = \frac{U \times I \times t_{EC}}{V} \qquad (3.3)$$

where U is the cell voltage (V), I is the current (A), t_{EC} is the time of electrolysis (s) and V is the volume (m^3) of fluoride solution. Cost for electrode was calculated from the Faraday’s law:

$$C_{electrode} = \frac{I \times t \times M_w}{z \times F \times V} \qquad (3.4)$$

where I is the current (A), t is the time of electrolysis (s), M_W is the molecular mass of aluminium (26.98 g mol^{-1}), z is the number of electron transferred (z =3), F is the Faraday’s constant (96487 C mol^{-1}) and V is the volume (m^3) of fluoride solution [70]. Total operating costs for the treatment of different initial fluoride concentration using monopolar and bipolar electrode connections were calculated and shown in Fig. 3.10. It was seen from Fig. 3.10 that operating cost was increased with initial fluoride concentration. This is due to the increase in electrode cost as dissolution of electrodes increases with initial fluoride concentration as described in section 4.1.4. Figure 3.10 shows that theoretical electrode cost varied from 0.075 to 0.12 US$ m^{-3} and from 0.15 to 0.38 US$ m^{-3} for monopolar and bipolar electrode connections, respectively. Similarly, energy cost increased from 0.07 to 0.19 US$ m^{-3} and from 0.09 to 0.24 US$ m^{-3} for

monopolar and bipolar connections, respectively, while initial fluoride concentration varied from 4 to 10 mg L^{-1}. In addition to this, it would be necessary to mention that though energy cost was 21% higher for bipolar connection but electrode cost dominates more over the energy cost due to the higher dissolution of electrodes compared to the monopolar connection.

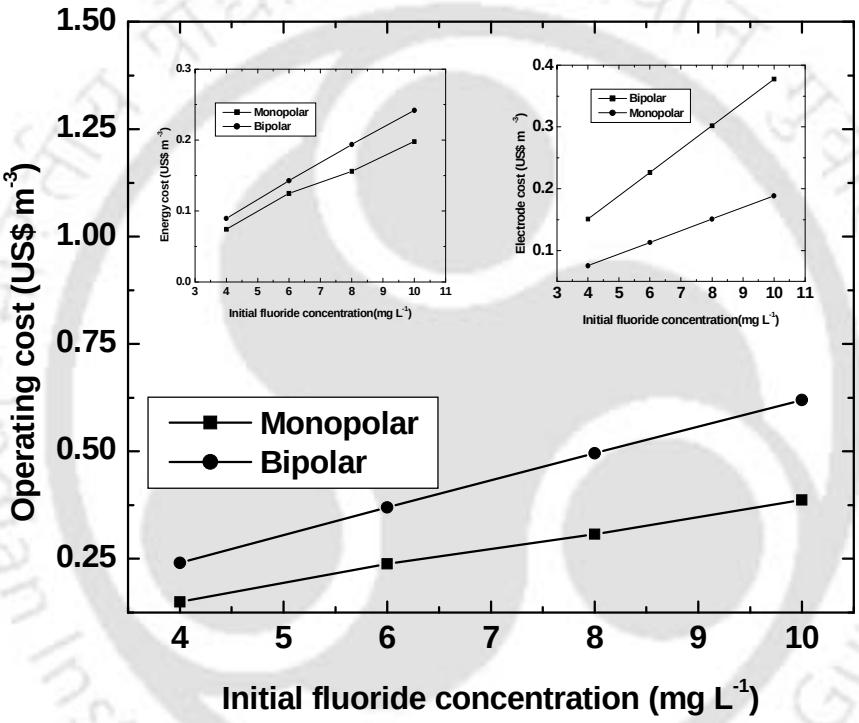

Fig. 3.10: Cost for the treatment of drinking water containing different concentration of fluoride. Current density: 625 A m^{-2}; interelectrode distance 0.005 m; duration of the experiment: 45 min; temperature: 25 °C. **Inset:** Cost for electrode and energy required for monopolar and bipolar connections.

Figure 3.10 also evidences that the operating cost for the treatment of drinking water containing initial fluoride concentration 10 mg L^{-1} in bipolar and monopolar connections under the same operating conditions (current density of 625 A m^{-2}, interelectrode distance of 0.005 m, 45 min of operation, 25 °C and pH ~ 8) were 0.62 and 0.38 US$ m^{-3}, respectively. The highest operation cost for the bipolar connection could be related to its greater surface area compared to the monopolar one.

3.1.10 Characterization of the by-products obtained from the EC bath

A whitish precipitate was formed at the bottom of the electrocoagulation bath at the end of EC process. The precipitate was taken out after the filtration using a filter paper (HM2, Indiachem, India) and dried inside a hot-air oven for 3-4 hours. It was then grinded to a fine powder and prepared for SEM, EDAX, FTIR and XRD analysis in order to characterize the by-product obtained from the EC bath.

Scanning electron microscopy and energy dispersive X-ray

The morphology of the by-products obtained from the EC bath using bipolar connection was shown in Fig. 3.11a. It might be seen from the figure that the by-products formed during the process were whitish and the amount of aluminium hydroxides and dissolved electrode were much higher than that of fluoride present in the EC bath. It was seen from Fig. 3.11b that the by-products formed during electrocoagulation were composed of elements like Al, O and F. This analysis confirmed that fluoride was entrapped within the aluminium hydroxide complex and formed sludge.

Fourier transform infrared spectroscopy (FTIR)

FTIR was performed using potassium bromide pellets and the result was shown in Fig. 7c. The wave numbers ranged from 4000-450 cm^{-1}. Peaks at 3466, 1020 and 605 cm^{-1} corresponding to H-O-H, Al-O and Al-F-Al bond stretching, respectively, can be observed in Fig. 3.11c. Al-F-Al bond stretching was matched with the analysis made by Gross et al. (2007) [133] for various amorphous trifluoride complexes. From this analysis, it was confirmed that fluoride was linked with aluminium hydroxide complexes and precipitated at the bottom of EC bath.

Powder X-ray diffraction

The X-ray diffraction of the by-product was recorded by a diffractometer operating with a Cu Kα radiation source and nano-bragg mode. The XRD analysis result is shown in Fig. 3.11d. The 2θ scans were recorded from 5 to 90°. The spectrum of the analyzed by-products showed broad and diffuse peaks. Therefore, the identification of peaks with such broad humps is a well known confirmed characteristic of phases which are amorphous or poorly crystalline in nature [134].

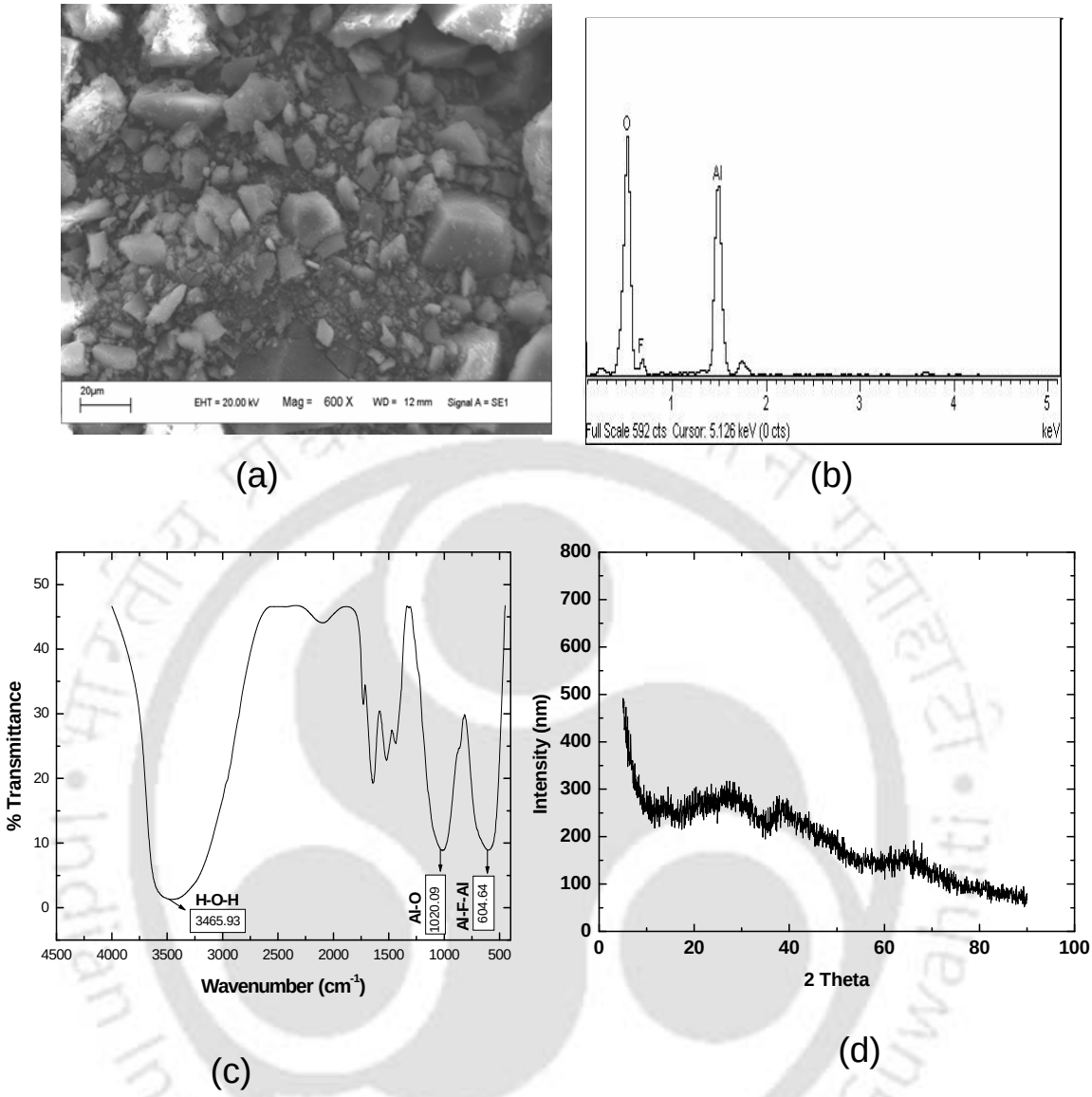

Fig. 3.11: Characterization of by-products obtained from EC bath. Current density: 625 A m^{-2}, initial fluoride concentration: 10 mg L^{-1}; duration of the experiment: 45 min; temperature: 25 °C; electrode connection: bipolar. (a) SEM image; (b) Elemental analysis; (c) FTIR analysis; (d) XRD analysis.

3.2 Iron removal

Electrocoagulation (EC) technique was adopted for the treatment of iron containing drinking water using a reactor of around 2.8 L capacity having 1 L liquid volume. Experimental investigation was carried out to observe the effect of different operating parameters such as pH, current density, inter electrode distance, conductivity on the removal of iron from the iron-rich aqueous solution prepared with deionized water. Aluminium sheet was used as the electrode material and inter electrode distance was varied from 0.005 m to 0.015 m. All the experiments are performed using monopolar electrode connection.

3.2.1 Effect of initial iron concentration

The Fe (II) solutions with different initial concentrations of 5 mg L^{-1}, 10 mg L^{-1}, 15 mg L^{-1}, 20 mg L^{-1} and 25 mg L^{-1} are treated by EC at a current density of 400 A m^{-2}. Variations of percentage removal of Fe (II) are shown in Fig. 3.12. It is seen from the figure that the percentage removal increases with time. Up to the concentration of 10 mg L^{-1}, complete removal is observed at the end of 5 minutes of operation. Again, the required time for 100% Fe (II) removal increases with initial Fe (II) concentration up to 25 mg L^{-1}. It is well known that among the salts of Fe (II), Fe (III) and Al^{+3}, only Fe (III) gives brown color in its hydroxide form. The formation of a gelatinous reddish-brown precipitate was observed at the bottom of the batch cell after the electrocoagulation. This (reddish-brown color of the precipitate) revelation confirms the presence of Fe (III) in the precipitate. It seems that oxidation of Fe (II) to Fe (III) occurs which are subsequently trapped by the aluminum hydroxide with time. The Fe (II) removal has been increased with time

initially, later it has been decreased gradually as the total Fe (II) concentration was decreased. This decrease in both Fe (II) and Fe (III) concentrations may be due to the adsorption on to the freshly generated aluminum hydroxides hence precipitation in the bath.

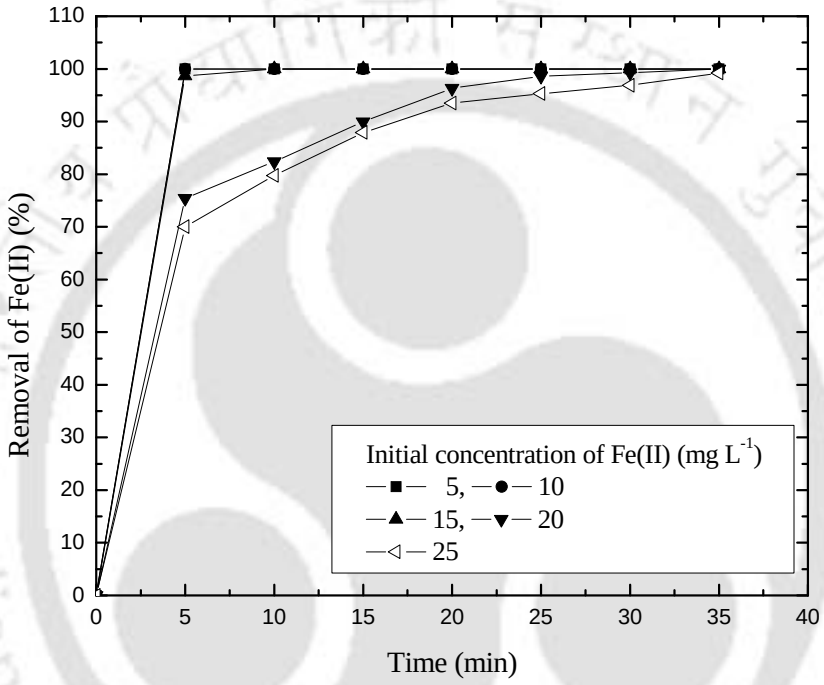

Fig. 3.12: Variation of extent of Fe (II) removal with time for different initial Fe (II) concentrations. Inter electrode distance: 0.005 m, current density: 400 A m^{-2}, pH: 7.5, conductivity: 12 S m^{-1}.

In EC process, Fe (II) is removed in two steps. Fe (II) is converted to Fe(III) in first step and then it is adsorbed in aluminum hydroxide complexes in second step. At lower concentration (up to 15 mg L^{-1}) available aluminum hydroxide complexes are sufficient to remove the Fe (II) molecules within 10 minutes with suitable oxidizing environment.

The rate of generation of Aluminum hydroxide complexes are not sufficient to remove high Fe (II) concentration (>15 mg L^{-1}) within 10 minutes of operation. For example, 35 minutes is required for complete removal of 25 mg L^{-1} of initial Fe (II) solution. Hence longer residence time is required for EC of high Fe (II) concentration. Therefore, it is quite clear that under the present experimental conditions up to 10 mg L^{-1} of initial Fe (II) concentration complete removal of Fe (II) is possible within 5 minutes.

3.2.2 Variation of Fe(II) removal with interelectrode distance

The set up of electrode assembly is very important for required effective surface area of electrode and inter electrode distance. Variation of percentage removal of Fe (II) with inter electrode distance is shown in Fig. 3.13. It may be observed from the figure that with the increase of inter electrode distance, percentage removal of Fe (II) decreases. It is well known that, during the electrucoagulation as the potential is applied to the electrodes initially, the anodic oxidation is started. Now as the time proceeds a very fine film of metal hydroxides would get formed on the anode generating an extra resistance that even increases with increasing inter-electrode distance. Therefore, as a result, after some time of the operation current falls down. To maintain a constant current, applied potential has to be increased. Now it is very much clear that current is remained constant but the resistance is increased. Therefore the ohmic loss (IR resistance) increases which in turn inhibits the rate of anodic oxidation. This may be the reason behind the lower iron removal efficiency at higher inter electrode distance as discussed early. At minimum inter electrode distance the resistance for current flow in the solution medium is lower than that facilitates the electrolytic process for enhanced Fe (II) removal.

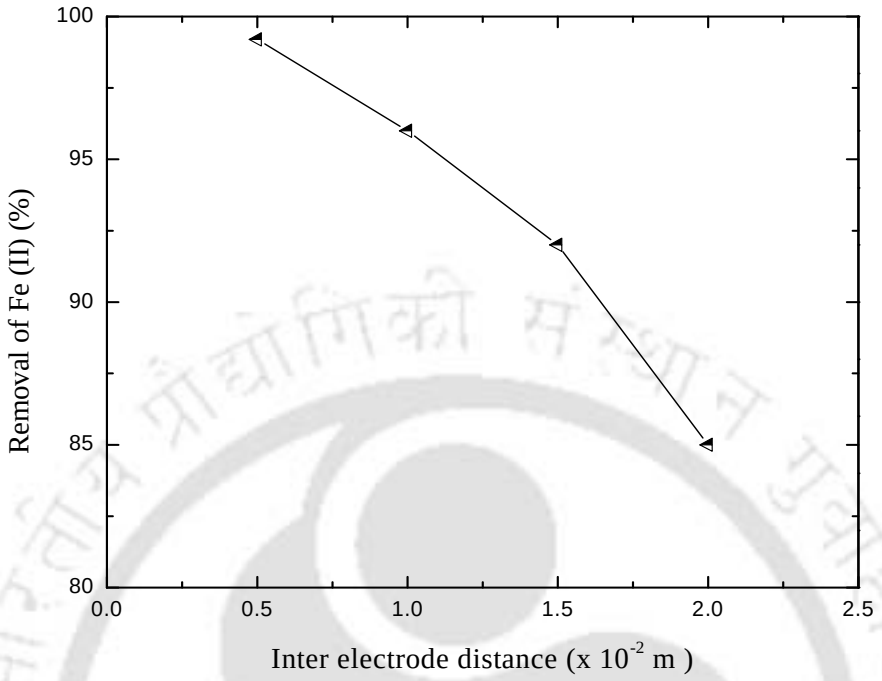

Fig. 3.13: Effects of inter electrode distance on the Fe (II) removal. Current density: 400 A m^{-2}, conductivity: 12 S m^{-1}, initial Fe (II) concentration: 25 mg L^{-1}, time: 35 min, pH: 7.5.

The variation in IR drop is governed by following equation

$$\eta_{IR} = I \cdot \frac{d}{A \cdot \kappa} \qquad (3.5)$$

Where,

I = current (A)

d = distance between the electrodes (m)

A = active anode surface (m^2)

κ= specific conductivity (10^{3} mS m^{-1}). [74].

Above equation infers that at constant anodic surface area and conductivity of solution, voltage drop (IR) increases with the increase of inter electrode distance. The increase in IR drop is not recommended for EC process in order to have acceptable energy consumptions as well as desired effective separation. In order to achieve 100 % removal for the initial Fe (II) concentration of 25 mg L^{-1}, the optimum inter electrode distance is 0.005 m.

3.2.3 Effect of current density

Figure 3.14 shows the removal of Fe (II) from tap water as a function of time for four different current densities. It may be seen from the figure that a steep increase in Fe (II) removal just at the beginning of the process for all the current occurred and becomes gradual there after. It may also be found that lower current density has lesser effect on the final total Fe (II) removal, but removal is rapid with high current density. From the figure it may be observed that the removal of iron is 55 % at the end of 5 minutes and 67% at the end of 35 minutes of operation at current density of 100 A $m^{-2}$for the initial iron concentration of 25 mg L^{-1}. Almost complete removal is observed at the end of 35 minutes of operation when current density increases to 400 A m^{-2}. In electrocoagulation, initially the aluminum cations contribute to charge neutralization of the pollutant particles as the isoelectric point is attained. Here a sorption coagulation mechanism occurs resulting in the formation of loose aggregates. As time progresses, further aluminum cation addition results in amorphous aluminum hydroxide precipitation that promotes pollutant aggregation via a sweep coagulation followed by precipitation mechanism. During the final stages, coagulated aggregates interact with bubbles and float to the

surface or settle to the bottom of the reactor. As shown in the figure there is sharp decrease in concentration due to fresh electrodes surfaces initially but the concentration reduction is achieved further as the time progresses with more generation of aluminum hydroxides for coagulation of the particles.

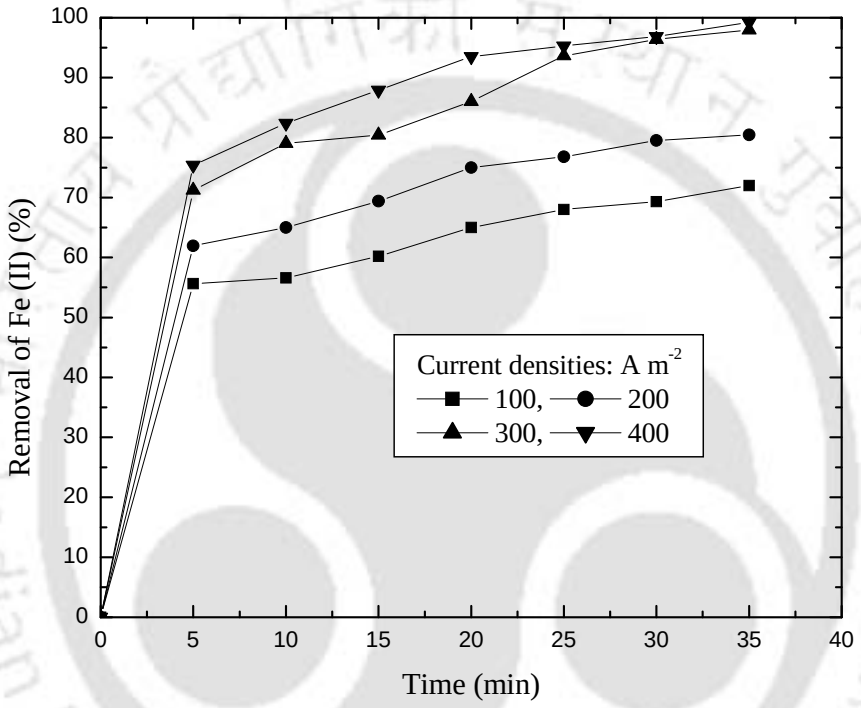

Fig. 3.14: Variation of percentage removal of Fe(II) with time at different current densities. Inter electrode distance: 0.005 m, initial Fe(II) concentration: 25 mg L^{-1}, pH: 7.5, conductivity: 12 S m^{-1}.

3.2.4 Change in pH

The solution pH plays an important role in the autocatalytic disappearance of aqueous Fe (II) with the motivation of iron removal in slightly basic (pH >7)range.

Electrocoagulation is believed to be a favorable technology due to the formation of more OH^- ions in the electrolysis of water [135]. Therefore, in the present investigation, initial pH of the solution has been kept at 7.5 in association with the application of different current densities (100 A m^{-2}, 200 A m^{-2}, 300 A m^{-2} and 400 A m^{-2}) for an initial iron concentration of 25 mg L^{-1}.

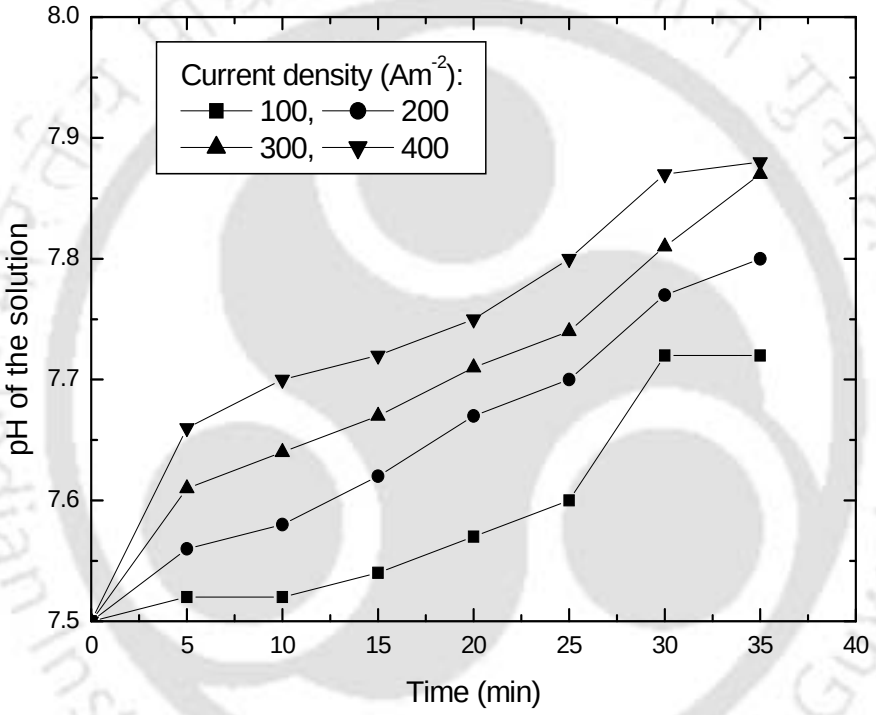

Fig. 3.15: Variation of pH of Fe(II) with time at different current densities. Inter electrode distance: 0.005 m, initial Fe(II) concentration: 25 mg L^{-1}, initial pH: 7.5, conductivity: 12 S m^{-1}.

Duration of the process was 40 minutes and after every 5 minutes pH of the solution has been checked using a digital pH meter (CONSORT, C863, Make: Belgium). At the end

of the process pH has been reached to a value of 7.70, 7.77, 7.82 and 7.88, respectively for different current densities. A reddish-brown sludge due to the formation of iron hydroxide (as discussed in chapter 2) was observed at the bottom of the cell shortly after the completion of the experiment. It might be the generation of more aluminum hydroxides which in turn adsorbed iron hydroxide from the solution and got precipitated at the bottom. Hence, it confirms the above mentioned phenomenon (sweep-flock mechanism). From Fig.3.15 it was seen that with the variation of current density, pH increases slowly and reaches to it's maximum value 7.88 at the end of 35 minutes with an applied current density of 400 A m^{-2}. It seems that the pH of the solution changes a little or in other words it remains merely constant throughout the process.

3.2.5 Variation of conductivity

Conductivity plays a major role in the EC process by improving the ionic strength of the solution. When the conductivity of solution increases, ohmic loss (IR resistance) decreases, which, in turn, reduces the electrical energy consumption. Figure 3.16 shows the dependency of the iron removal performance on the conductivity of the treated iron-contaminated drinking water having an initial iron concentration of 15 mg L^{-1}. It may be seen from the figure that at no-electrolyte dosing condition iron removal was nearly 89% and correspondingly conductivity was 0.4 Sm^{-1}. It is also seen from the figure that the iron-removal increases with solution conductivity which is increased by the addition of electrolyte. In the present investigation, NaCl was added into the EC bath with an amount of 2 gL^{-1}, 4 gL^{-1} and 6 gL^{-1} separately in order to investigate the effect of initial conductivity on removal performance. With an addition of 2 gL^{-1} NaCl, it was observed

that the conductivity value was enhanced from 0.4 Sm^{-1} to 1.2 Sm^{-1} and the iron-removal was achieved more than 99%. Furthermore, it was seen that with an addition of 4 gL^{-1} and 6 gL^{-1} of NaCl, the conductivity value was increased to 3.4 Sm^{-1} and 5.6 Sm^{-1}, respectively.

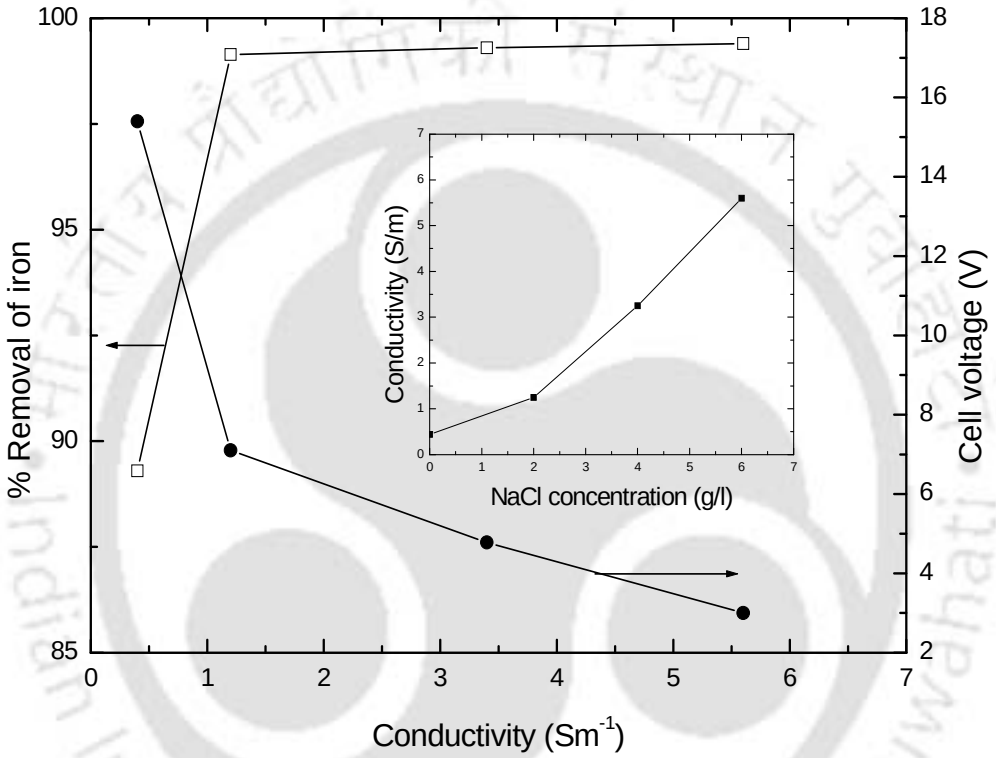

Fig. 3.16: Effect of solution conductivity on the removal efficiency of iron and cell voltage. Initial iron concentration 15 mg L^{-1}, inter electrode distance: 0.005 m, pH of the solution: 8, time: 40 minutes.

At the initial stage of investigation of the present work when no electrolyte was added the cell voltage was 15.4 V. It decreased up to 54%, 69% and 80.5% with an addition of 2 gL^{-1},4 gL^{-1} and 6 gL^{-1}, respectively. In connection with the conductivity enhancement it is

seen that the cell voltage dropped down from 15.4 V to 3 V making the process energy-efficient.

3.2.6 Variation of energy consumption

Current efficiency (φ) is very important economical parameters in EC process. Different parameters such as current density and dissolved amount of contaminants affect the current efficiency. Lower current density would not be sufficient to achieve the desired separation, however, it lowers the possibility of the film-formation on the anode surface. Higher current density shows a better removal of dissolved contaminants. If the amount of dissolved contaminant is large then the removal process gets slowed down due to the accumulation of gelatinous aluminium hydroxide film on the anode even on the application of higher current density. As a result current efficiency falls down.

After each experiment the electrodes were cleaned, dried and weighed to estimate the amount of dissolved of the electrodes. Noticeable amount of weight loss was observed due to anodic dissolution only. The extent of anodic dissolution varied with different operating condition considered herein. For example, 7.4 mg and 8.12 mg of anode dissolution were estimated for the treated tap water containing initial iron concentration of 5 mg L^{-1} and 10 mg L^{-1}, respectively, at current density of 400 A m^{-2}.

Current efficiency (φ) for different operating conditions are calculated as:

$$\varphi = \frac{\Delta M_{exp}}{\Delta M_{theo}} \times 100 \qquad (3.6)$$

This calculation is based on the comparison of experimental weight loss of Aluminum electrodes ($\Delta M_{\exp}$) during EC process with theoretical amount of Aluminum dissolution (ΔM_{theo}) according to the Faraday's law:

$$\Delta M_{theo} = \frac{MIt_{EC}}{nF} \qquad (3.7)$$

Where, M is the molecular weight of the Aluminum (g mol^{-1}), n the number of electron moles, F is the Faraday constant (F = 96487 C mol^{-1}) and t_{EC} is the time (sec) of EC operation. As $Al(OH)_3(s)$ is supposed to be the formed species, the number of electron moles in dissolution reaction is equal to 3. Current efficiency (φ) depends on anodic dissolution which is also varied with time of EC and other operating condition as well.

The specific electrical energy consumption (S_{eec}) is calculated as a function of Aluminum electrodes weight consumption during EC in kWh/ (kg Al) [136, 137].

$$S_{eec} = \frac{n \times F \times U}{3.6 \times 10^3 \times M \times \varphi} \qquad (3.8)$$

Effect of current density on the percentage removal of Fe (II) and specific electrical energy consumption is shown in Fig. 3.17. The result shows that an increase in the current density causes an increase in Fe (II) removal as well as specific electrical energy consumption. So, to achieve an optimized current density, both percentage removal of Fe (II) and specific electrical energy consumption should be evaluated. More current density favors formation of more number of Aluminum complexes, which also enhances the removal of Fe (II) as expected. This causes the higher weight loss of Aluminum electrode and therefore increases the specific electrical energy consumption. Sludge formed during the electrocoagulation experiment was filtered out of the chamber, dried and weighed. It was observed that with the increase in the initial iron concentration and current density,

sludge production increased. On the other hand sludge production was decreased with the increase in inter electrode distance. At current density of 400 A m^{-2} and inter electrode distance of 0.005 m, the weight of sludge estimated as 30.95 mg, 42.56 mg and 96.3 mg for treating the tap water having initial iron concentration of 5 mg L^{-1}, 10 mg L^{-1} and 25 mg L^{-1}, respectively.

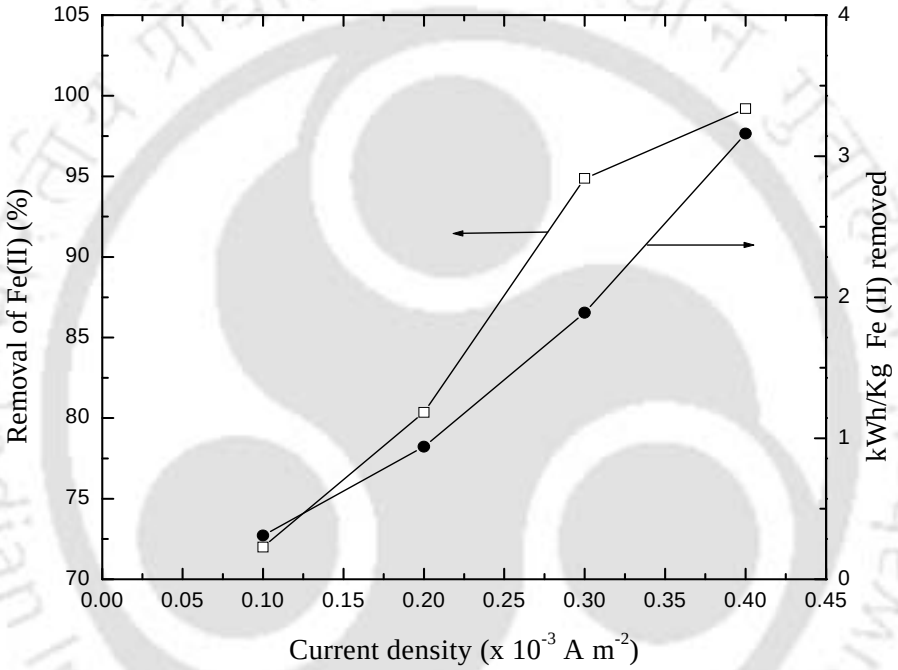

Fig. 3.17: Effect of current density on the removal of Fe(II) and specific electrical energy consumption. Inter electrode distance: 0.005 m, initial Fe (II) concentration: 25 mg L^{-1}, pH: 7.5, conductivity: 12 S m^{-1}.

3.2.7 Operating cost for EC of iron

In any electrical process cost is incurred due to electrical energy demand, which affect the operating cost. For EC process the operating cost includes material, mainly electrodes

and electrical energy costs, as well as labor, maintenance, sludge dewatering and disposal, and fixed costs. The latter costs items are largely independent of the type of the electrode material [138, 139]. In this preliminary economic investigation, energy and electrode material costs have been taken into account as major cost items in the calculation of the operating cost (US$ m^{-3} of Fe (II) solution).

Operating cost = a C_{energy} + b $C_{electrode}$ (3.9)

Where, C_{energy} (KWh m^{-3} of Fe (II) solution) and $C_{electrode}$ (kg Al m^{-3} of Fe (II) solution) are consumption quantities for the Fe (II) removal, which are obtained experimentally. "a" and "b" given for Indian market in June 2007, are as follows: "a" electrical energy price 0.0065 US$/ kWh; "b" electrode material price 0.3 US$ kg^{-1} Al. Cost due to electrical energy (KWh m^{-3} Fe (II) solution) is calculated as

$$C_{energy} = \frac{U \times I \times t_{EC}}{v} \quad (3.10)$$

Where, U is cell voltage (V), I is current (A), t_{EC} is the time of electrolysis (s) and v is the volume (m^3) of Fe (II) solution. Cost for electrode (Kg Al m^{-3} Fe (II) solution) is calculated by the following equation by Faraday's Law

$$C_{electrode} = \frac{I \times t \times M_w}{z \times F \times v} \quad (3.11)$$

Where, I is current (A), t is time of electrolysis (s), M_W is molecular mass of aluminum (26.98 g mol^{-1}), z is no of electron transferred (z =3), F is Faraday's constant (96487 C mol^{-1}) and v is volume(m^3) of Fe (II) solution [75].

Cost due to electrical energy consumption as well as electrode assembly is calculated for different initial Fe (II) concentration (up to 25 mg L^{-1}) and shown in Fig. 3.18 for 100% Fe (II) removal at optimum operating conditions. Details of procedure are discussed in

section 3.2.7 and a model calculation is shown in the preceding section. It may be seen from the figure that both the consumption quantities (electrical and electrode) remains almost unchanged up to the initial concentration of 15 mg L^{-1}, beyond that it increases with the initial Fe (II) concentration. Operating cost also increases with the initial Fe (II) concentration as shown in the inset of Fig. 3.18.

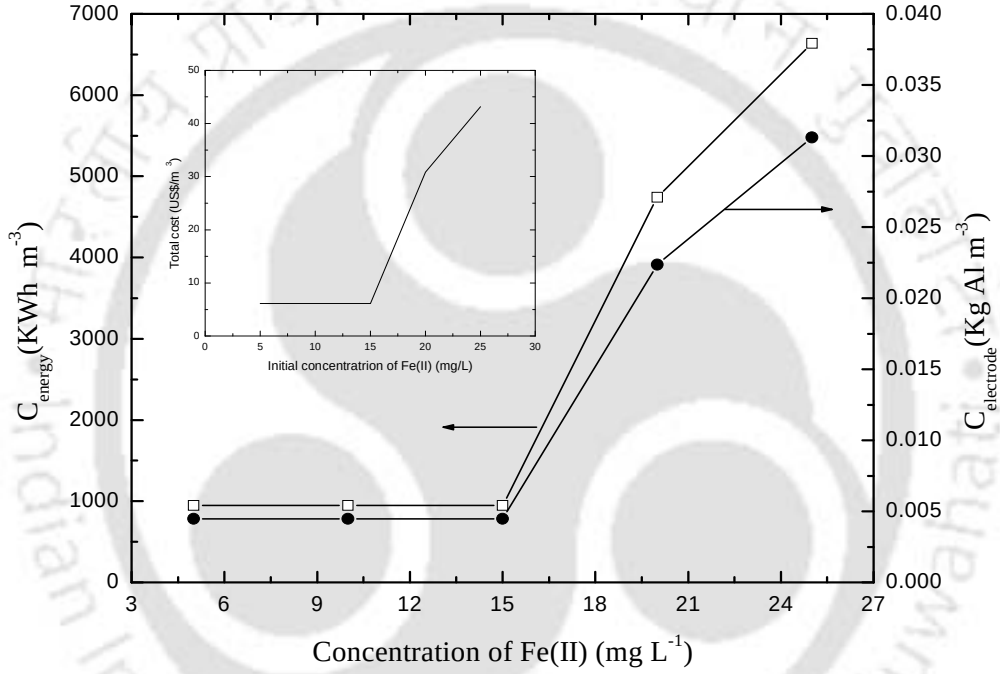

Fig. 3.18: Cost for the treatment tap water containing different concentration of Fe(II). Current density: 400 A m^{-2}, conductivity: 12 S m^{-1}, pH: 7.5, inter electrode distance 0.005 m.

It is found that about 6.05 US$ m^{-3} is required for the treatment of water containing initial iron concentration up to 15 mg L^{-1} at the end of experiment at 400 A m^{-2}. Kobya et al. [75] have also determined the operating cost for the treatment of potato chips

manufacturing waste water using EC process. They found that operating costs were varied 0.48– 5.42 \$ m^{-3} wastewater at 50–300 A m^{-2}, and 0.62 and 6.32 \$ m^{-3} wastewater at 5 and 40 minutes, respectively. The Fig. 3.19 represents the variation of operating cost with applied current densities. It seems that the operating cost is increased almost linearly due to increase in consumption of electrical energy as well as electrode material.

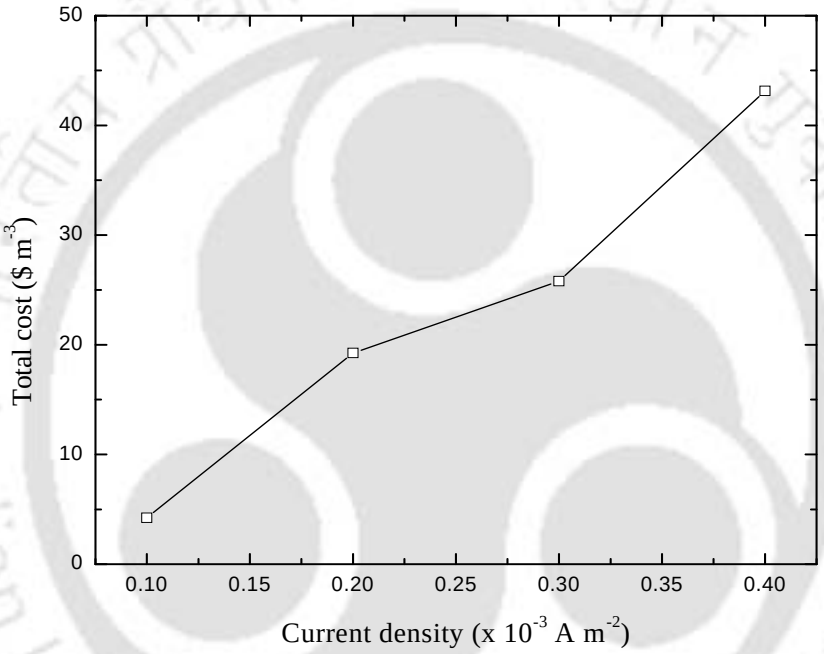

Fig. 3.19: Effect of current densities on total cost for the treatment of tap water. Conductivity: 12 S m^{-1}, pH: 7.5, inter electrode distance: 0.005 m, initial concentration of Fe (II): 25 mg L^{-1}.

Model calculation:

Calculation of operating cost for the initial concentration of 10 mg L^{-1}.

Operating cost is determined using the following relation as mentioned in section 4.4.

Operating cost = a C_{energy} + b $_{electrode}$

Where,

a = 0.0065 US$/ kWh;

b = 0.3 US$ /kg

$$C_{energy} = \frac{U \times I \times t_{EC}}{v}$$

U = 19.75 V

I =0.16 A

t_{EC} = 300 sec

V= 1×10^{-3} m^3

Cost due to electrical energy is calculated using above values.

C_{energy} = 948 kWh m^{-3}

$$C_{electrode} = \frac{I \times t \times M_w}{z \times F \times v}$$

M_w=26.98 g mol^{-1}

z = 3

F= 96487

Cost for Aluminum electrode is calculated using above values.

$C_{electrode}$= 0.0149 Kg m^{-3}

Operating cost: 6.16 US$ m^{-3}

3.2.8 Analysis of sludge obtained after EC

Scanning electron microscopy (SEM) and electron dispersive X-ray analysis are used to characterize any sample by revealing information about the morphology and elemental constitution, respectively. In EC process, by products formed are aggregated species followed by adsorption. Hence characterization of byproducts formed during EC are determined using SEM and EDAX. SEM image and EDAX spectra of solid precipitate (by product of EC) are presented in Figs. 3.20 and 3.21, respectively. SEM image shows the morphology of various aluminium hydroxide precipitates that have been impregnated with iron hydroxide. From Fig. 3.20a it may be observed that few whitish chunks of material along with large amount of coloured ones (appeared as black in the image) formed the backbone of the sludge during the EC process. The whitish portion was mainly of the gelatinous aluminium hydroxides formed due to the anodic oxidation and the black ones are of adsorbed iron hydroxide on the surface of aluminium hydroxide. Fig. 3.20b is a magnified morphological outlook of a small size flock as shown in Fig. 3.20a. This image confirmed with its low brightness that almost all the whitish surface provided by the aluminium hydroxide had been filled up by brown coloured iron hydroxide by means of adsorption. Furthermore, it can also be stated that affinity towards the interaction between iron hydroxide and aluminium hydroxide is high that favored the adsorption process during the experiment. EDAX analysis has been done for the byproducts obtained from the EC bath. The observation of peaks and trends in the EDAX graph (Fig. 3.21) convey that the by product of EC consisted of aluminium (Al), Oxygen (O), Iron (Fe), Sodium (Na), Chloride (Cl). Presence of Silica (Si) is due to glass slit used for EDAX analysis of the sample.

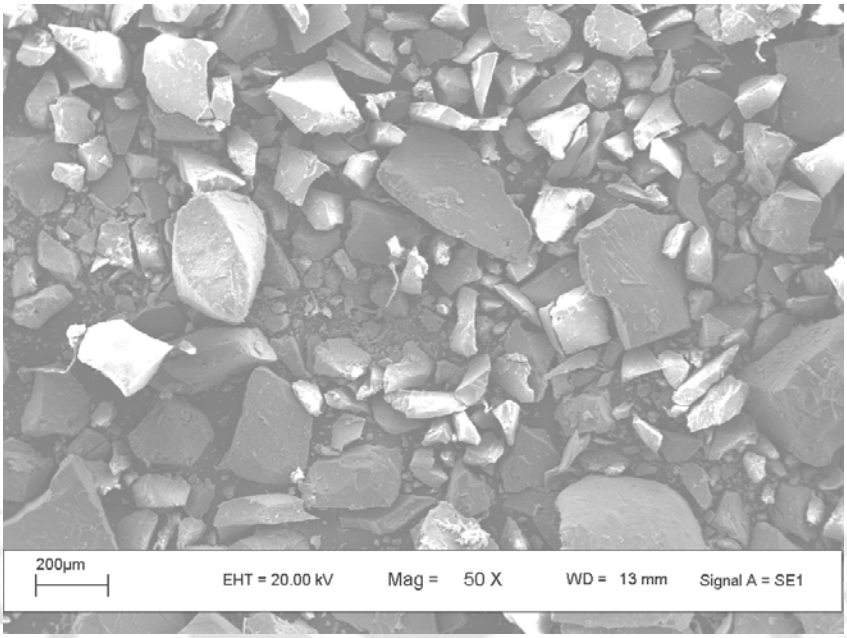

(a)

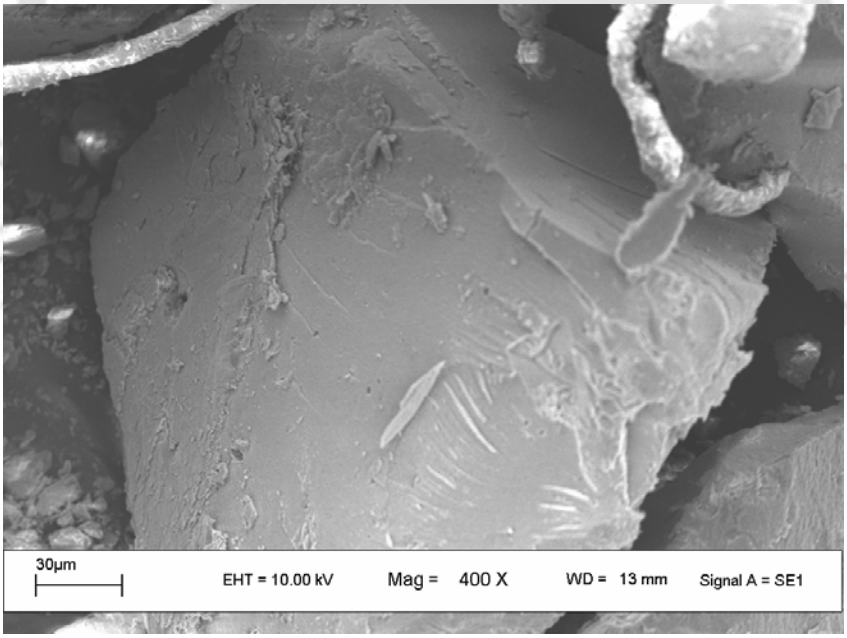

(b)

Fig. 3.20 a) SEM image of by products obtained from EC bath. b) Enlarged SEM image of by products obtained from EC bath.

By-products formed were mainly composed of iron-hydroxide and aluminium hydroxide. These by-products can be further used as hybrid adsorbents for the removal of arsenic from drinking water [140].

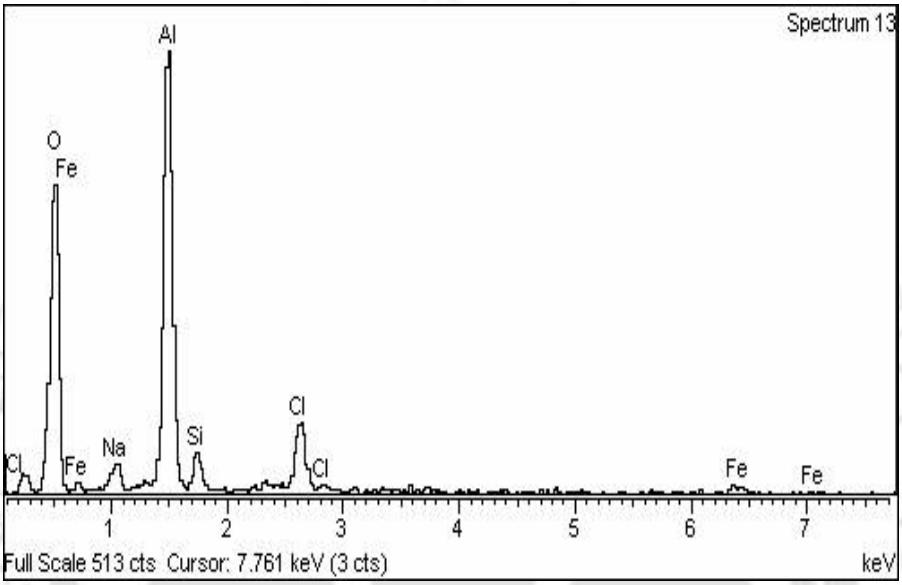

Fig. 3.21: Elemental analysis of by products obtained from EC bath.

3.3 Arsenic removal

Electrocoagulation (EC) was employed to investigate its feasibility in monitoring arsenic contamination in drinking water. Different parameters like initial arsenic concentration, current density, pH, interelectrode distance were found to be dominating in order to remove arsenic from the contaminated water. Both monopolar and bipolar electrode connection were used and explained well.

3.3.1 Effect of initial arsenic concentration

Arsenic concentration in untreated drinking water claims its toxicity due to its carcinogenic potential. Figure 3.22 shows the changes in arsenic concentration observed with time of EC for different initial arsenic concentrations. It was seen that with an increase in initial arsenic concentration, the removal of arsenic was decreased under the maintained operating conditions.

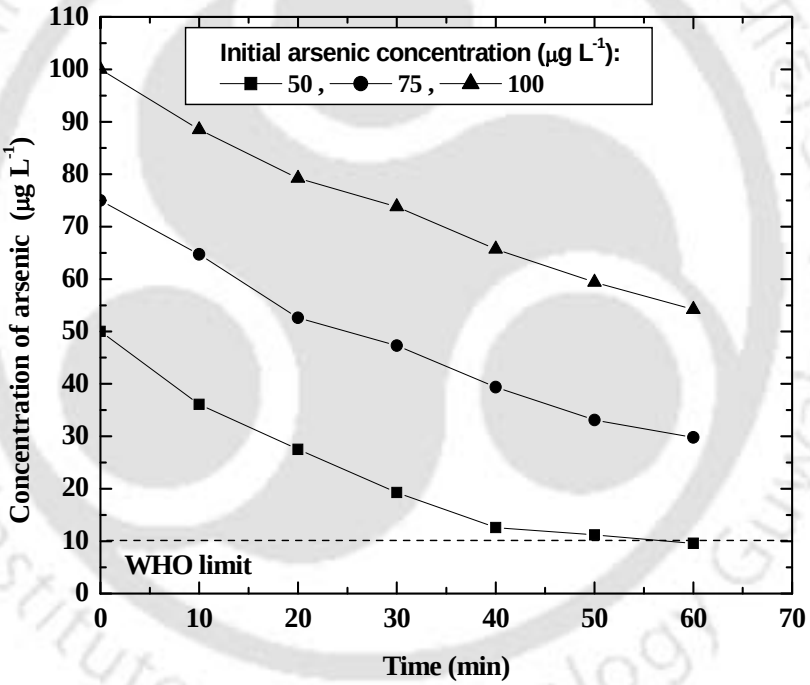

Fig. 3.22: Effect of initial arsenic concentration on the arsenic removal with time. Current density: 125 A m^{-2}, interelectrode distance: 0.005 m. (Monopolar)

It can also be observed from Fig 3.22 that after 60 minutes of electrocoagulation of drinking water with initial arsenic concentration of 50 and 75 μg l^{-1}. The final arsenic

concentrations were 9.6 and 29.8 μg l^{-1}, at an applied current density of 125 Am^{-2} and interelectrode distance 0.005 m. Higher arsenic concentration in drinking water needs sufficient time as well as sufficient aluminium hydroxide species formed during the anodic oxidation in order to get removed from the drinking water. Under the present operating conditions, insufficient aluminium hydroxide was formed and therefore the process could not remove arsenic sufficiently from contaminated drinking water with higher initial arsenic concentration**.**

3.3.2 Effect of electrode connection

Arsenic removal was investigated employing different electrode connection to understand the essence of the mode. It was observed that the concentration declination trend for arsenic using bipolar electrode connection was improved than monopolar connection at an applied current density of 250 A m^{-2} after an hour operation. It can be seen from Fig. 3.23 that final arsenic concentration was 40.8 and 12.5 μg L^{-1} after 60 minutes of operation of electrocoagulation of drinking water with initial arsenic concentration of 100 μg L^{-1} using monopolar and bipolar electrode connection, respectively. It is a well-known fact that in bipolar connection, sufficient aluminium hydroxide is formed than in monopolar connection which subsequently helps in removing the arsenic adequately from the contaminated drinking water. Bipolar connection showed prominent improvement in the final arsenic concentration which was at a proximity of the safety limit recommended by WHO.

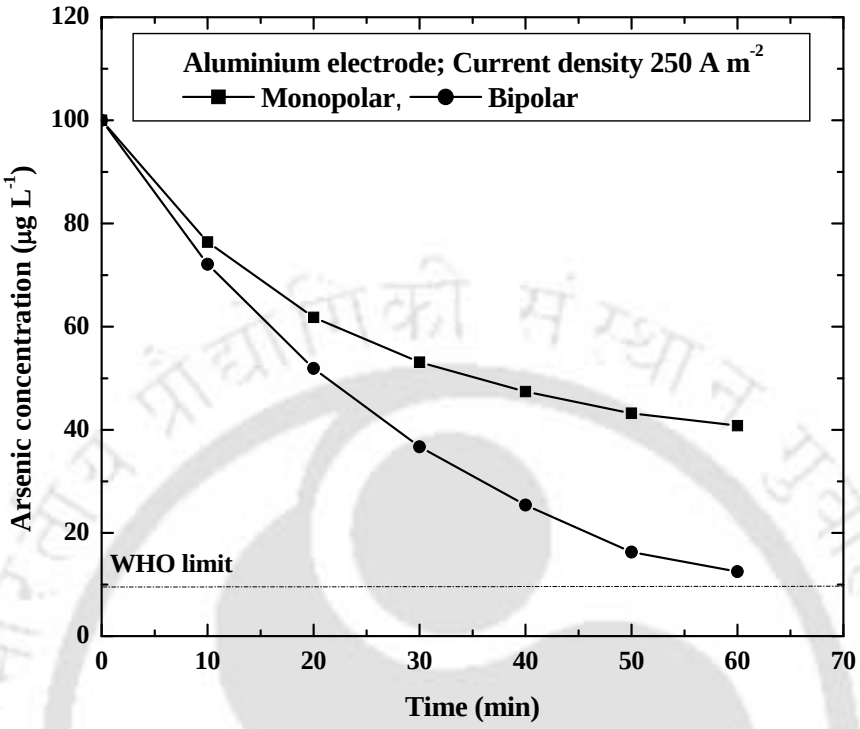

Fig. 3.23: Variation of arsenic concentration (µg L^{-1}) in the EC bath with time (min) for different electrode connection (bipolar and monopolar). Interelectrode distance: 0.005 m, initial arsenic concentration; 100 µg L^{-1}, current density: 250 A m^{-2}, temperature: 25 °C, duration of the experiment: 60 minutes.

However, under the specified conditions (i.e. 250A m^{-2} current density, inter electrode distance of 0.005 m and 60 minutes of treatment time), it was observed that none of the cases could retain the success of attaining the final arsenic concentration in the water at its recommendable limit. At this situation, the investigation was further extended by increasing the current density to 375 A m^{-2} considering bipolar electrode connection.

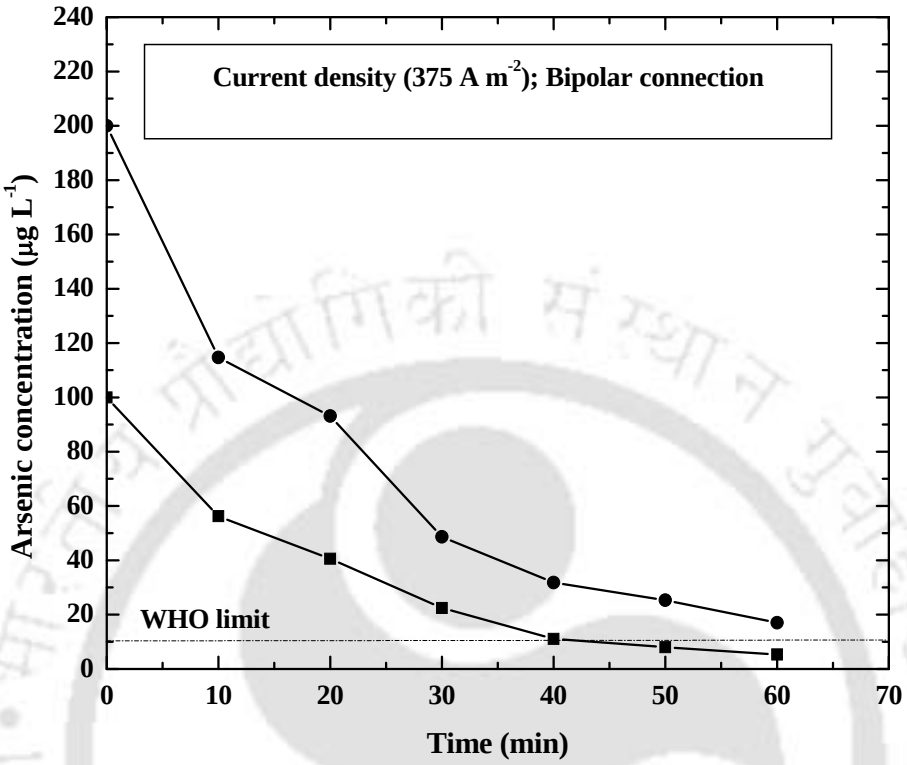

Fig. 3.24: Variation of the arsenic concentration in the EC bath with time. Current density 375 A m^{-2}, Interelectrode distance: 0.005 m, electrode connection:bipolar, temperature: 25 °C, duration of the experiment: 60 minutes.

Figure 3.24 shows the concentration declination with time using bipolar connection. It was observed that, with an increase in current density using bipolar connection, final concentration was found to come down to the recommendable limit. For an example, final arsenic concentration was observed to be 8 µg L^{-1} after 50 minutes of the electrocoagulation treatment of drinking water with initial arsenic concentration of 100

μg L^{-1}. However, at the end of 60 minutes of operation for the drinking water with initial arsenic concentration of 200 μg L^{-1}, the final arsenic concentration was observed 17 μg L^{-1} which was approached nearly the safety limit. Bipolar connection is believed to improve the anodic oxidation process which in turn generates adequate aluminium hydroxide species during the experiment. Therefore, it remained clear that with an increase in current density using bipolar connection, final arsenic concentration can be better monitored for the treatment of drinking water with higher arsenic concentration.

3.3.3 Arsenic removal with varying interelectrode distance

In any electrochemical process, interelectrode distance is one of the important parameters which governs the mobility of charges (electrons) carrying current from one electrode to the other and hence affects the performance of the process. Figure 3.25 describes the effect of interelectrode distance on the performance of the arsenic removal from drinking water by electrocoagulation with time. It was observed that with the passage of time, final arsenic concentration in drinking water was decreased with decreasing the interelectrode distance using monopolar connection. It can be seen from Fig 3.25 that after 60 minutes of electrocoagulation, the final arsenic concentrations were 15.2, 12.4 and 9.6 μg L^{-1} when interelectrode distances were maintained at 0.15, 0.1 and 0.005m, respectively, at a current density of 125 A m^{-2} and initial arsenic concentration of 50 μg L^{-1} in the drinking water. This is because of the fact that the anodic oxidation can not be well promoted during electrocoagulation for the larger interelectrode distance due to the extra resistance which restricted the ionic mobility between the electrodes with an increase in their spacing [2]

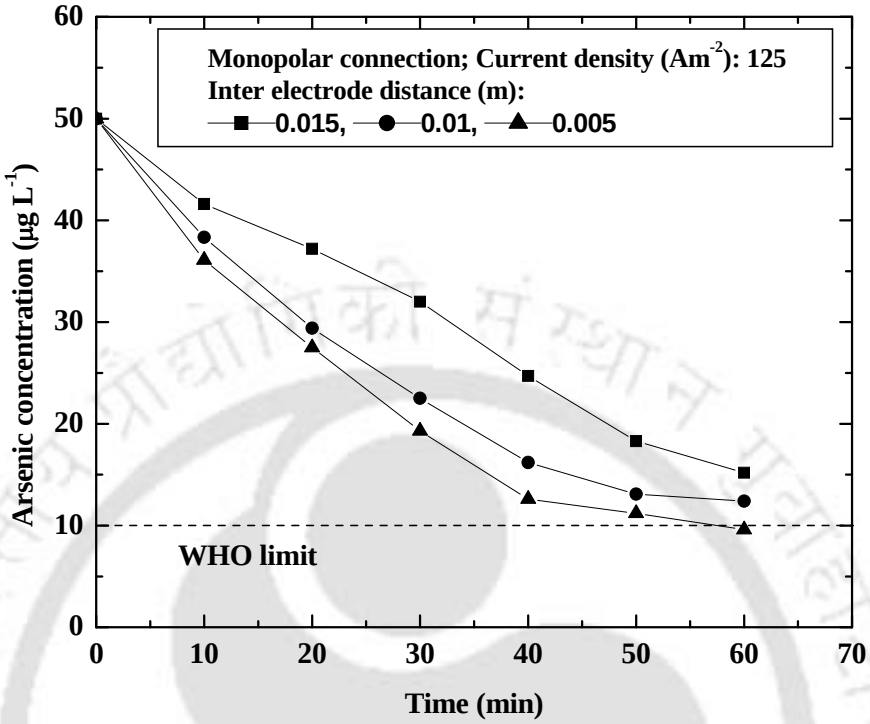

Fig. 3.25.: Effect of interelectrode distance on the arsenic removal with time. Initial arsenic concentration: 50 µg l^{-1}. Current density: 125 A m^{-2}.

3.3.4 Variation of arsenic removal with current density

Current density was increased to intensify the process performance using monopolar connection so as to find out the viability in monitoring contamination in drinking water containing higher initial arsenic concentration. Figure 3.26 depicts the effect of current density varied from 187.5 to 625 A m^{-2} in arsenic removal from drinking water with initial arsenic concentration of 100 µg L^{-1}. It was seen that with an increase in current density final arsenic concentration was also decreased. It was observed that, after 60 minutes of such operation for the drinking water with initial arsenic concentration of 100

μg L^{-1}, the final arsenic concentration was found to be 6.2 μg L^{-1} at a current density of 625 A m^{-2} and interelectrode distance 0.005 m. The decreasing trend of arsenic concentration in the EC bath with increase in current density was well explained in section 3.1.4 for the removal of fluoride.

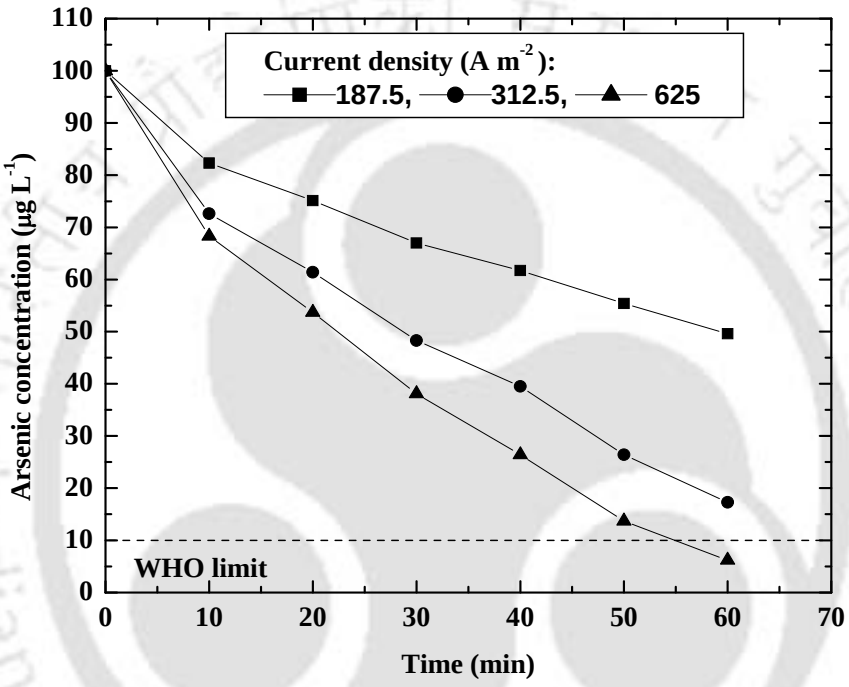

Fig. 3.26: Effect of current density on the arsenic removal with time by electrocoagulation. (Monopolar), initial arsenic concentration: 100 μg L^{-1}.

Similar observation was noticed for the case of bipolar connection with current densities varied from 375 to 625 A m^{-2} for the treatment of drinking water with initial arsenic concentration of 200 μg L^{-1} which is shown in Fig 3.27. It is also necessary to mention that the final arsenic concentration after the electrocoagulation treatment was found to be

3.7 and 6.8 μg L^{-1} at 500 and 625 A m^{-2} current densities for 60 and 50 minutes of operations, respectively.

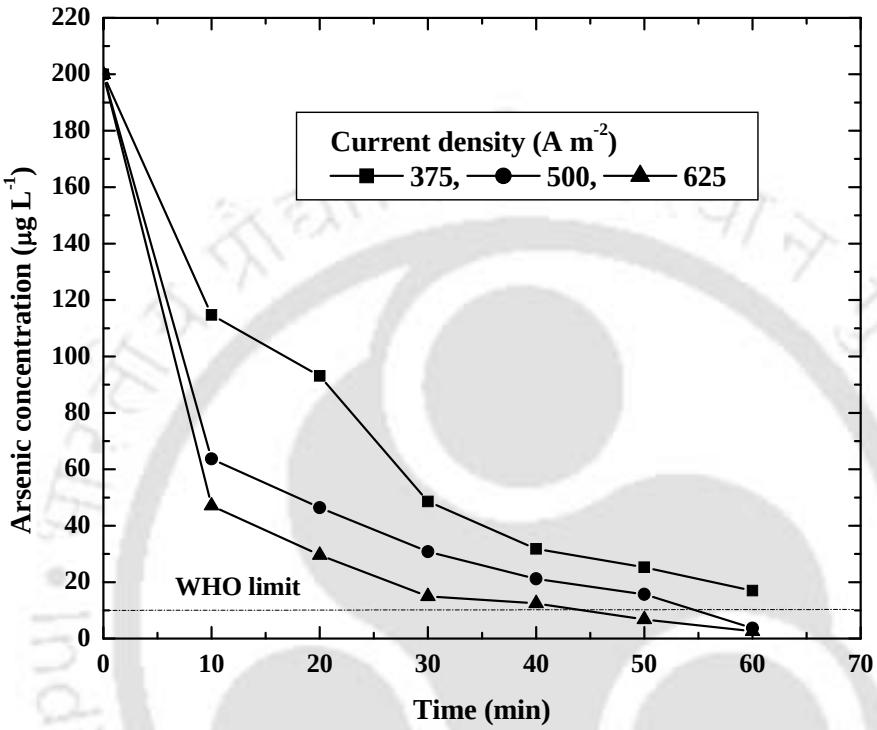

Fig. 3.27: Effect of current density on the arsenic removal from drinking water by electrocoagulation. Initial arsenic concentration: 200 μg L^{-1}, interelectrode distance: 0.005 m, electrode connection: bipolar, temperature: 25° C, duration of the experiment: 60 minutes.

3.3.5 Variation of pH

The solution pH was investigated in order to check the water quality. Figure 3.28 shows the variation of pH with time during the electrocoagulation treatment of drinking water containing initial arsenic concentration of 100 μg L^{-1}. It was seen that pH increased from

6.1 to a final value of 8.1 which is safe for drinking**.** During electrocoagulation, OH^- ion was produced due to the electrolysis of water which took part in charge neutralization with the positive metal ions formed from the anodic oxidation. The overall contribution of the interactions occurred between such hydroxides were believed to increase the solution pH with time. Consequently, it is to be stated that with an increase in current density, anodic oxidation was favoured as well as the formation of insoluble gelatinous aluminium hydroxide species in the EC bath. These species are believed to take part in the entrapment of arsenic molecules followed by agglomeration via charge neutralization.

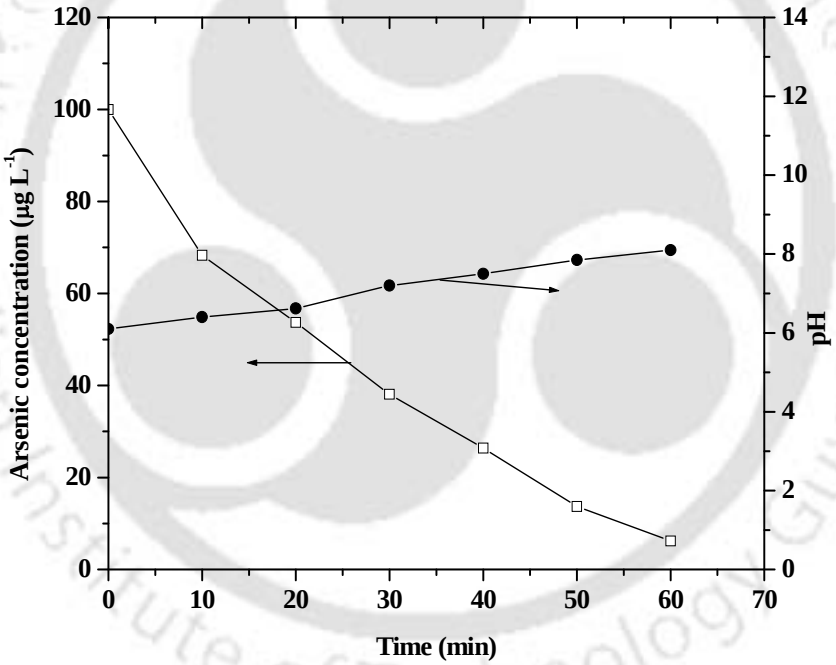

Fig. 3.28: Variation of pH with time during the experiment. Initial arsenic concentration: 100 µg L^{-1}, interelectrode distance: 0.005 m. (Monopolar)

3.3.6 Variation of sludge formation

In electrocoagulation process, dissolution of electrodes depends mainly on the applied current density and so does the sludge formation during the treatment. Therefore, it is important to quantify both the amount depending upon the initial concentration of the contaminant species and the applied current density. Figure 3.29 shows the corrosion of the electrodes estimated whereas Fig. 3.30 represents the sludge formation observed during the treatment of arsenic contaminated drinking water with different initial concentration. It was observed from the Fig. 3.29 that with an increase in current density and initial arsenic concentration, the electrode dissolution was also increased.

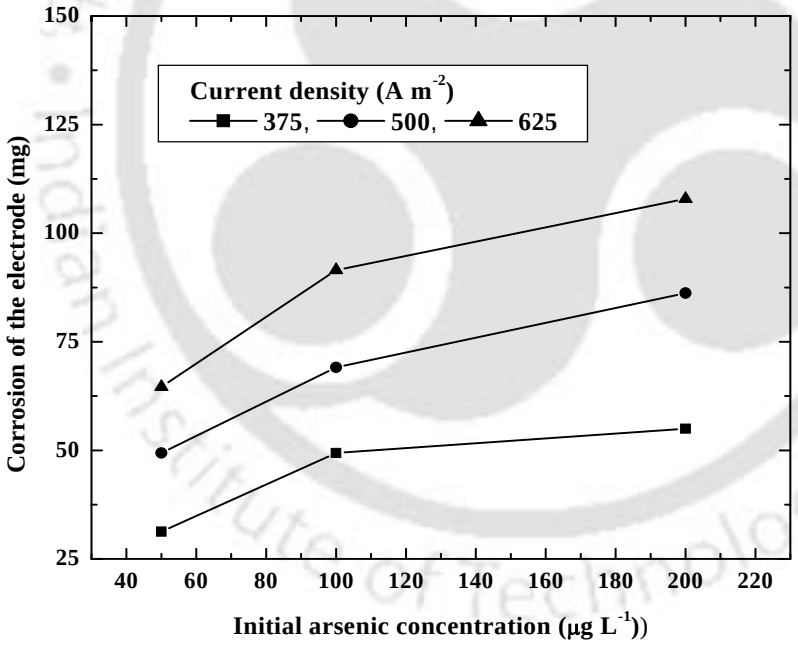

Fig. 3.29 Variation of electrode corrosion with bipolar connection at different current densities. Interelectrode distance: 0.005 m, duration of the experiment: 60 min, temperature: 25 °C.

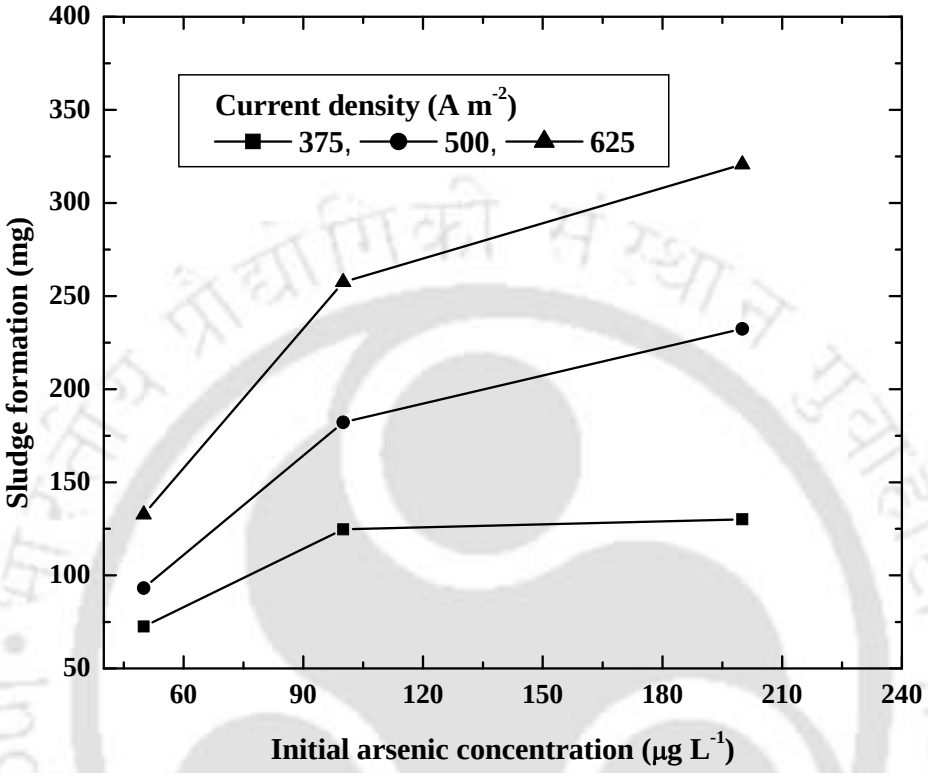

Fig. 3.30: Variation of sludge formation with bipolar connection at different current densities. Interelectrode distance: 0.005 m, duration of the experiment: 60 min, temperature: 25 °C.

For example, it was noticed that at 375 Am^{-2} current density, the electrode dissolution was increased from 31.3 mg to 55 mg during the treatment of drinking water when initial arsenic concentration was increased from 50 to 200 μg L^{-1}. The dissolution was found to be drastically increased from 64.6 to 107.9 mg at an applied current density of 625 Am^{-2}. In addition to this, it can be seen from the Fig. 3.30 that the similar trend was

followed for the sludge formation during the process. For an example, it is mention worthy that sludge formation was found to increase from 72.5 to 132.7 mg when current density was increased from 375 to 625 Am^{-2} during EC of contaminated water with initial arsenic concentration of 50 μg l^{-1}. The above mentioned observation was due to the intensified anodic oxidation which favoured the sufficient generation of gelatinous aluminium hydroxides. Therefore, it was possible to retain arsenic adequately by such insoluble metal hydroxides. As a result, the dissolution of electrodes as well as the sludge formation were found to increase with an increase in current density.

3.3.7 Change in film thickness

Film of sticky aluminium hydroxide is formed during the electrocoagulation treatment which in turn affect the voltage to drop down. Therefore to maintain a constant current density, it is necessary to estimate the film property in terms of its thickness over the electrode surface after the experiment. Figure 3.31 shows the change in film thickness at different current density during the bipolar electrocoagulation treatment of drinking water with initial arsenic concentration varied from 50 to 200 μg l^{-1}. It can be noticed from the Fig 3.31 that with an increase in current density and initial arsenic concentration, the film thickness over the electrode surface was also increased. With an increase in current density, aluminium hydroxide was started forming at the vicinity of the electrode and due to its gelatinous nature a film of such hydroxide was deposited over the electrode surface to some extent. This deposition also contained the contaminant particles retained by the metallic hydroxides. Therefore it can be believed that the film thickness is likely to be

dependent on the extent of the anodic oxidation and the initial concentration of the contaminant (Arsenic as in the present case). However, anodic oxidation is likely to be dependent on the current density as discussed earlier. Therefore, it can be clearly stated without doubt that the film thickness was increased with the increase in current density. As a needful requirement of justification, it would be mention worthy that film thickness was increased from 89.2 to 135.4 nm for the treatment of drinking water with initial arsenic concentration of 50 μg l^{-1} when the applied current density was increased from 375 to 625 Am^{-2}, respectively.

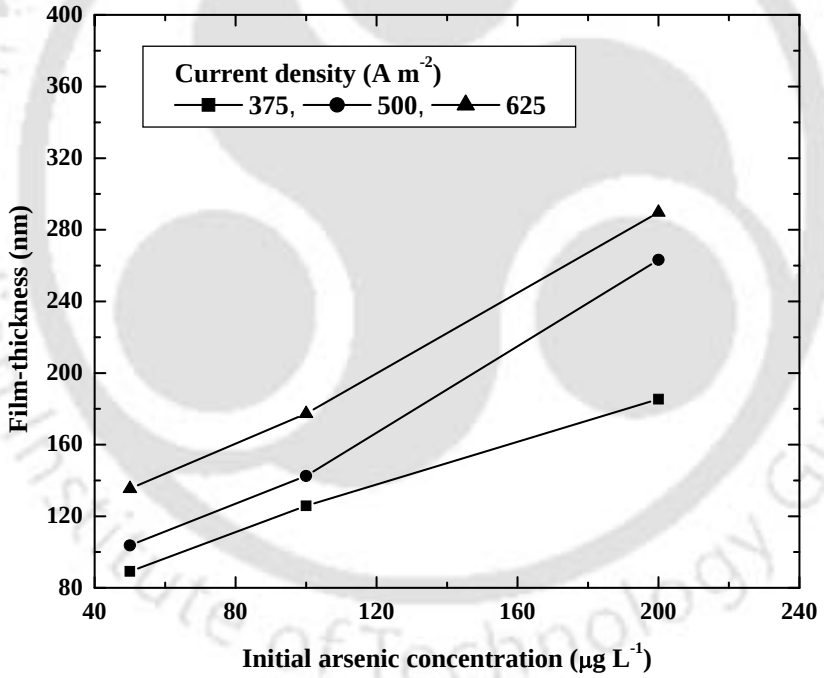

Fig. 3.31: Variations of film thickness over electrode surface with different current densities and initial arsenic concentrations. Interelectrode distance: 0.005 m, duration of the experiment: 60 min, electrode connection: bipolar, temperature: 25 °C.

In addition to this, film thickness was also increased from 89.2 to 185.4 nm when the initial arsenic concentration in drinking water was increased from 50 to 200 μg l^{-1}, respectively at an applied current density of 375 Am^{-2}.

3.3.8 Determination of cost for the removal of arsenic using EC

The total operating cost along with the other costs such as energy cost and electrode cost would predict a better understanding about the economic aspect of such technique employed for the treatment of arsenic contaminated drinking water. For EC process the operating cost was estimated by taking into account only the energy and electrode material cost as major cost item which has been reported in section 3.1.9.

Figure 3.32 shows the variation of electrical energy (US$ m^{-3})cost and total operating cost (US$ m^{-3}))estimated for the treatment of drinking water with different initial arsenic concentrations. Energy cost was mainly dependent on the extent of the experiment, the applied voltage and the current density. It is very much obvious that the experiment time mainly depends upon the initial concentration of the contaminant in the solution under treatment. On the other hand, electrode cost was mainly due to the amount of dissolved electrodes during the treatment. In other words, it can be stated that electrode cost is also dependent on the applied voltage, current density and the initial concentration of the contaminant in the solution under consideration. It is also dependent on the electrode material itself. Hence, it remained an essential part of the present work to investigate such parameters.

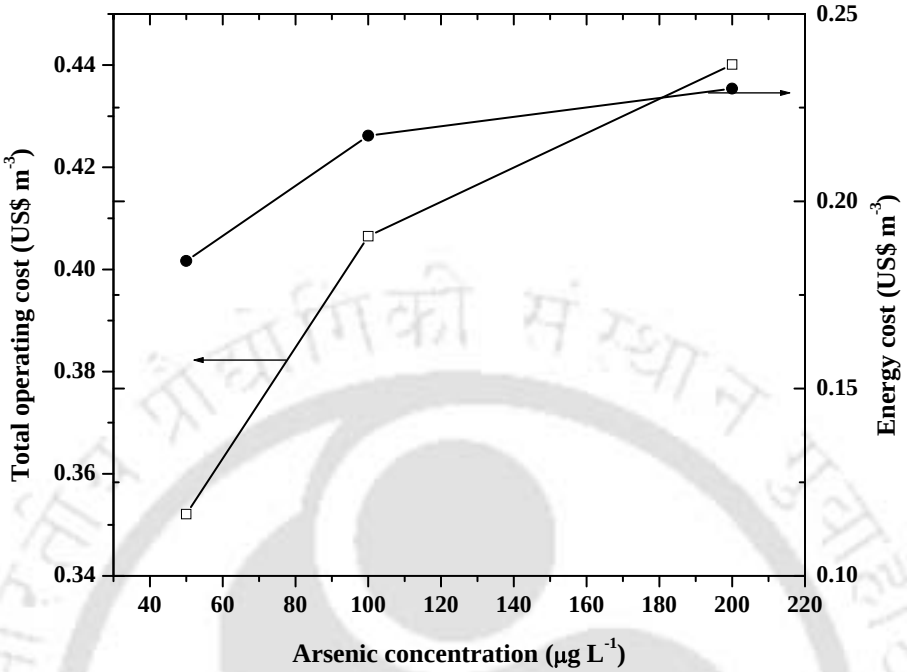

Fig.3.32: Total operating cost and energy cost estimation during the electrocoagulation treatment of drinking water with different initial arsenic concentration. Current density: 625 A m^{-2}, Bipolar connection.

It can be viewed from the Fig. 3.32 that with an increase in initial arsenic concentration in drinking water, both the cost (i.e. total operating cost and energy cost) were increased. It was also noticed that both the total operating cost and the energy cost were increased sharply. With an increase in initial concentration of arsenic in the drinking water under interest, the treatment time was also increased for the acceptable removal limit of the contaminant as detailed above. Therefore, undoubtedly the electrode cost as well as the energy cost was increased. Consequently the total operating cost which was comprised of these two costs was also increased. For an example, the total operating cost was

appeared to be increased from 0.3521 to 0.4401 US$ m^{-3} along with the energy cost increased from 0.1841 to 0.2301 US$ m^{-3}, respectively during the treatment of drinking water with initial arsenic concentration varying from 50 to 200 μg l^{-1}, respectively.

3.3.9 Characterization of electrocoagulated byproducts

In addition to this, characterization of by-products was done using XRD, SEM, EDAX and FTIR spectroscopy. Figure 3.32a reveals the phase nature of the electrocoagulated by-product formed during the experiment. It can be visualized from the Fig. 3.32a that irregular reflections from the samples that appeared in the form of noises confirmed the amorphous nature of the byproducts. Furthermore, Fig. 3.32b shows the morphology of the by-product at a magnification of 2KX using SEM. It was seen that the whitish lump with irregular shape and size was formed during the experiment which also confirmed the absence of crystalline phase in the by-product characterized by XRD and is shown in Fig. 3.32a.

Figure 3.32c shows the elemental detection using energy dispersive X-ray analysis popularly known as EDAX. It can be clearly seen from the Fig. 3.32c that elements like Al (aluminium), O (oxygen), C (carbon), Si (silica) and As (arsenic) were present in the byproduct. Aluminium and oxygen were due to the aluminium hydroxide, carbon was detected due to the carbon tape used for holding the sample in position during the analysis and silica may have an assay source during sample preparation. Nonetheless, in order to confirm the arsenic presence in the byproduct formed during the electrocoagulation treatment, FTIR (Fourier Transform Infrared Raman spectroscopy) was performed and is represented in the Fig 3.32d.

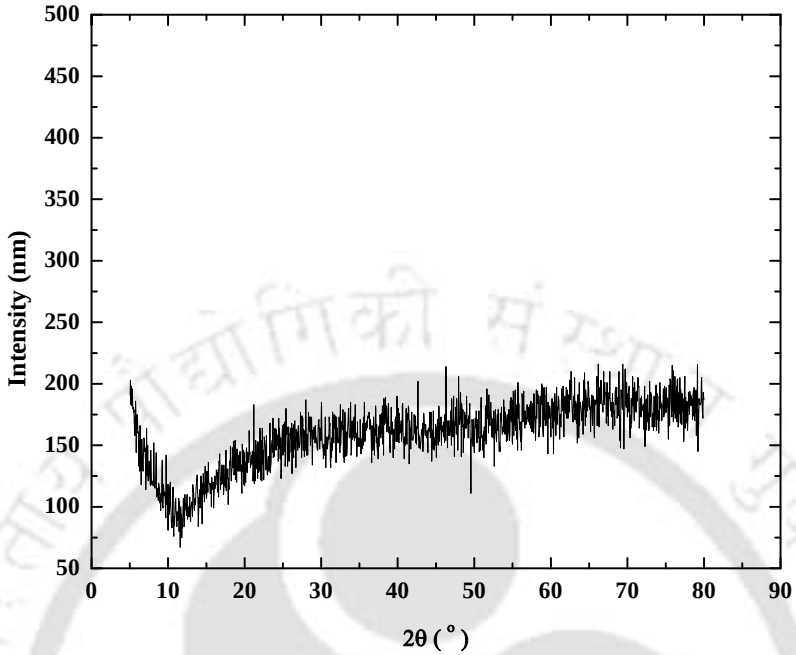
Intensity (nm)
500
450
400
350
300
250
200
150
100
50
0
10
20
30
40
50
60
70
80
90
2θ (°)

(a)

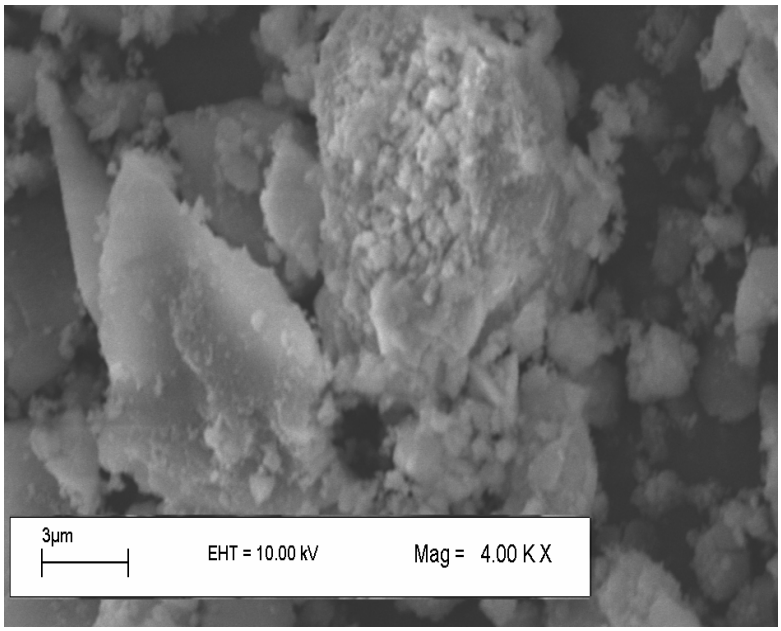
3µm
EHT = 10.00 kV
Mag = 4.00 K X

(b)

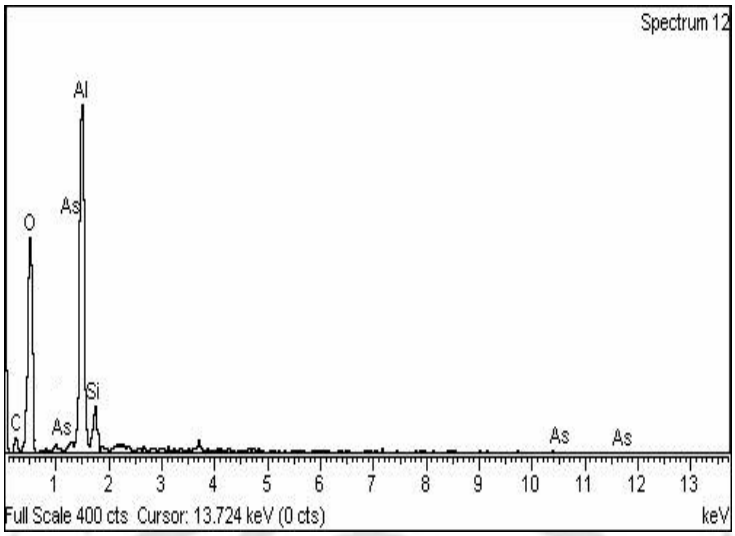

(c)

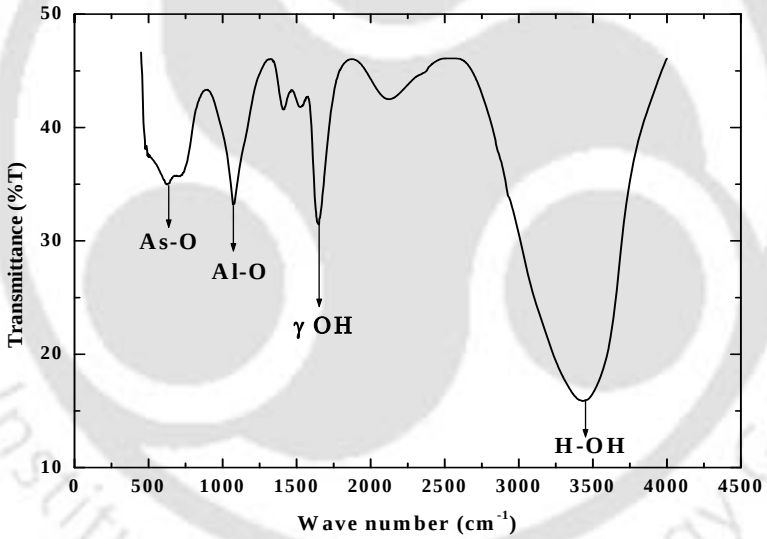

(d)

Fig. 3.32: Characterization of byproducts obtained from EC bath. Current density: 625 A m^{-2}, initial fluoride concentration: 200 µg L^{-1}, duration of the experiment: 45 min, temperature: 25 °C, electrode connection: bipolar. (a) XRD analysis, (b) SEM image, (c) EDX analysis (d) FTIR analysis.

FTIR was introduced to a transmitting pellet formed by a mixture of the grinded byproducts and potassium bromide as discussed in the chapter 2 in detail. It can be observed from the Fig. 3.32d that the presence of As-O, Al-O, overtunes of hydroxyl (γOH) and H-OH bond stretching by the peaks identified at wave numbers 619, 1066, 1634 and 3446 cm^{-1}, respectively. These findings confirmed the arsenic entrapment on the surface of whitish amorphous aluminium hydroxide.

3.4 Summary

Initial concentration of the pollutants indicates the contamination level of the water source and depending upon that the treatment time also comes into the picture as one of the dependent variables. Electrocoagulation (EC) is solely dependent on the extent of the anodic oxidation occurred with an application of certain voltage to the electrodes connected through a electrical source such as DC. source. In other words, the extent of anodic oxidation can be viewed dependable on electrode material, current density and electrode connection and the interelectrode distance. During the EC treatment, the pH is an another important indicator which depicts the overall effect of different ion-ion interactions. Hence, several parameters like initial fluoride, iron and arsenic concentration, duration of the experiment, interelectrode distance, electrode connection, current density and pH were investigated during EC treatment of contaminated drinking water containing fluoride, iron and arsenic.

The following are the excerpts of the experimental findings:

1) Different concentrations of fluoride, iron and arsenic in drinking water were treated in an electrocoagulation bath of 1 liter capacity. The highest initial concentration of fluoride, iron and arsenic were considered as 10 mg L^{-1}, 25 mg L^{-1} and 200 μg L^{-1}, respectively. It was observed that fluoride, iron and arsenic concentrations came down from 10 to 1 mg L^{-1} (WHO limit) in 40 minutes, 25 to 0.3 mg L^{-1} (WHO limit) in 35 minutes and 100 to 10 μg L^{-1} (WHO limit) in 55 minutes, respectively, using monopolar electrode connection.

2) The results showed that the removal efficiency increases with the increase in current density. Current density of 625 A m^{-2} was found to be effective for the efficient removal of fluoride and arsenic whereas for iron it was found to be around 400 A m^{-2}. It was observed that the final fluoride, iron and arsenic concentration of 0.76 mg L^{-1}, 0.2 mg L^{-1} and 6.2 μg L^{-1} in drinking water was attained by electrocoagulation at an applied current density of 625 A m^{-2} , 400 A m^{-2} and 625 A m^{-2} in 45 minutes, 35 minutes and 60 minutes using monopolar electrode connection.

3) It was observed that with an increase in interelectrode distance the removal efficiency decreased. The mobility of ions carrying currents in terms of their charges from one electrode to the another is mostly dependent on the interelectrode distance. Therefore, electrocoagulation is also favored with decreasing interelectrode distance. It was observed that the final fluoride concentration decreased from around 3 mg L^{-1} to 0.8 mg L^{-1} when interelectrode distance decreased from 0.015 to 0.005 m, respectively.

4) The results also confirmed that the bipolar connection can serve better than the monopolar connection. However, electrode corrosion as well as sludge formation was more in the bipolar connection. In bipolar electrode connection, fluoride and arsenic concentrations were found to be dropped down from 10 to 1.7 mg L^{-1} and 100 to 12.5 μg L^{-1} in 45 and 60 minutes, respectively. On the other hand, in monopolar electrode connection, the fluoride and arsenic concentrations were found to be declined from 10 to 2.2 mg L^{-1} and from 100 to 40.8 μg L^{-1}, respectively. The final fluoride and arsenic concentration of 0.8 mg L^{-1} and 6.8 μg L^{-1} were noticed at the end of 40 and 50 minutes, respectively using bipolar connection and at an applied current density of 625 A m^{-2}.

5) Solution pH was found to be increased insignificantly with time for all the cases. During the electrocoagulation treatment, with the passage of time, sufficient amount of metallic hydroxide species generated inside the bath which compelled the pH to be increased with time in all the cases (varied from 6.4 to 8.1). It was also observed that for bipolar connection, the pH of the solution was marginally higher than the monopolar connection. For example, at a current density of 625 A m^{-2} and an initial fluoride concentration of 10 mg L^{-1}, the solution pH was always around 8 at the end of all trials. However, in iron removal process by electrocoagulation, at the end of 35 minutes, the pH has been reached to a value of 7.70, 7.77, 7.82 and 7.88, respectively for different current densities.

6) The operating costs for monopolar and bipolar connections were 0.38 and 0.62 US$ m^{-3}, respectively, for the initial fluoride concentration of 10 mg L^{-1}. The operating cost was estimated equal to 0.44 US$ m^{-3} of the contaminated drinking

water containing initial arsenic concentration of 200 μg l^{-1} using biopolar electrode connection.

7) Finally, the by- products formed inside the electrocoagulation bath were characterized using SEM, EDX, XRD and FTIR which confirmed the removal of above mentioned contaminants from drinking water during the treatment. It was observed that, by-products formed during the EC treatment were irregular in shape and size for all the cases and were supported by the XRD data. Elemental analysis along with the FTIR clearly supported the credential of the electrocoagulation using aluminium electrodes in entrapping the fluoride, iron and arsenic successfully from the contaminated drinking water.

These findings indicated that the health risk due to the adequacy of fluoride, iron and arsenic in drinking water can be well monitored by electrocoagulation and this investigation may be effective for developing an economical electrocoagulator in future.

Chapter 4

Preparation of Microfiltration Membrane: Experimental

This chapter describes the essential raw materials and/or ingredients, procedures of preparing ceramic microporous membranes and their characterization techniques. Details of permeation experiments are also discussed subsequently.

4.1 Raw materials

This work utilized six common inorganic raw materials such as kaolin (CDH, India), quartz (Research Lab Fine Chem Industry, India), Calcium carbonate (Merck, India), sodium carbonate (Merck India), boric acid (Merck India) and sodium metasilicate (GSC Fine Chem Ltd, India). All these raw materials used for inorganic fabrication were graded at least 99.5 % pure and were used without any further purification. Different raw materials used in this work for the fabrication of inorganic membrane served for different functional attributes. Kaolin and feldspar provided low plasticity and high refractory properties to the membrane. Quartz contributed to the mechanical and thermal stability of the membrane. Regulation of porous texture in the ceramic was realized by sodium carbonate which under sintering conditions dissociated into Na_2O and released CO_2 gas. The path taken by the released CO_2 gas thereby created the porous texture of the inorganic membrane and contributed to the membrane porosity during the sintering process. Boric acid increased membrane mechanical strength by the formation of metallic metaborates at sintering temperatures. Boric acid and sodium

carbonate also act as colloidal agents and improved dispersion properties of the inorganic precursors thereby addressing homogeneity in the membrane structure. In a similar way, sodium metasilicate acts as a binder by creating silicate bonds among the elements to induce higher mechanical strength in the ceramic membrane.

Three major clay materials kaolin used for the membrane fabrication process were characterized using X-Ray diffraction analysis (Make: Bruker Axs; Model: D8 ADVANCE) and particle size distribution analysis (Make: Malvern; Model: Mastersizer 2000). The XRD spectrum of the clay materials were matched with the JCPDS database file PDF-01-089-6538, PDF-01-075-0443 and PDF-01-072-2284 for kaolin, quartz and feldspar, respectively.

4.2 Membrane preparation

This section elaborates the procedures of ceramic porous self-supported membranes by paste method and uni-axial methods, respectively. Details of composition taken for both the methods are shown in Table 4.1.

Table 4.1: Composition of ceramic porous self-supported membrane

Material	**Composition (wt %)**	**Sources**
Kaolin	45	CDH, India
Calcium carbonate (calcite)	25	MERCK, India
Quartz	10	Research-Lab Fine Chem Industries, India
Sodium carbonate	10	MERCK, India
Boric acid	5	RANBAXY, India
Sodium meta silicate	5	GSC Lab Testing & Allied Industries, India

4.2.1 Paste method

Clay mixture was taken in a sieving mesh of size 40 and sieved it for 30 minutes to get all particles in the same size. All the chemicals were mixed properly for another 30 minutes to get the homogeneity after the sieving and mixed it with the de-ionized water (Millipore, Elix-3) to form a paste. The paste was used to fabricate the structure of membrane in the form of a disc with a circular cross-section and thickness of 55 mm and 5 mm, respectively. The structure thus developed was kept over a perfectly flat and smooth gypsum surface for over night under a pressure of around 21.045 kPa in order to reduce the water content by soaking. Furthermore, the circular disks so obtained were placed in an air oven to remove all of the remaining unbounded moisture at a temperature of 150 °C for 24 hours. Sintering process was then carried out using very low heating rate of 2 °C min^{-1} inside a muffle furnace. During sintering process care was taken to raise the temperature to minimize the formation of pinhole cracks due to the uneven thermal stress that is likely to be generated due to an uncontrolled heating. Finally, the sintering was ended at a temperature by setting the furnace controller a certain value (as in the present case these values were 750 °C, 800 °C, 850 °C, 900 °C and 950 °C, separately) and was kept constant for 5 hours. Then cooling down operation was initiated which took almost 48 hours to come to its initial point. All the ceramic membranes were thereafter taken out of the furnace and rubbed with an abrasive paper (C-220) to get a smooth polished flat surface. Then all the rubbed-membranes were kept under water in a beaker using an ultrasonic bath (Elma, T460) for 30 minutes to remove all of its loose particles formed during the rubbing and then again dried in an air oven for 3 hours. The preparation process is presented in the Fig. 4.1.

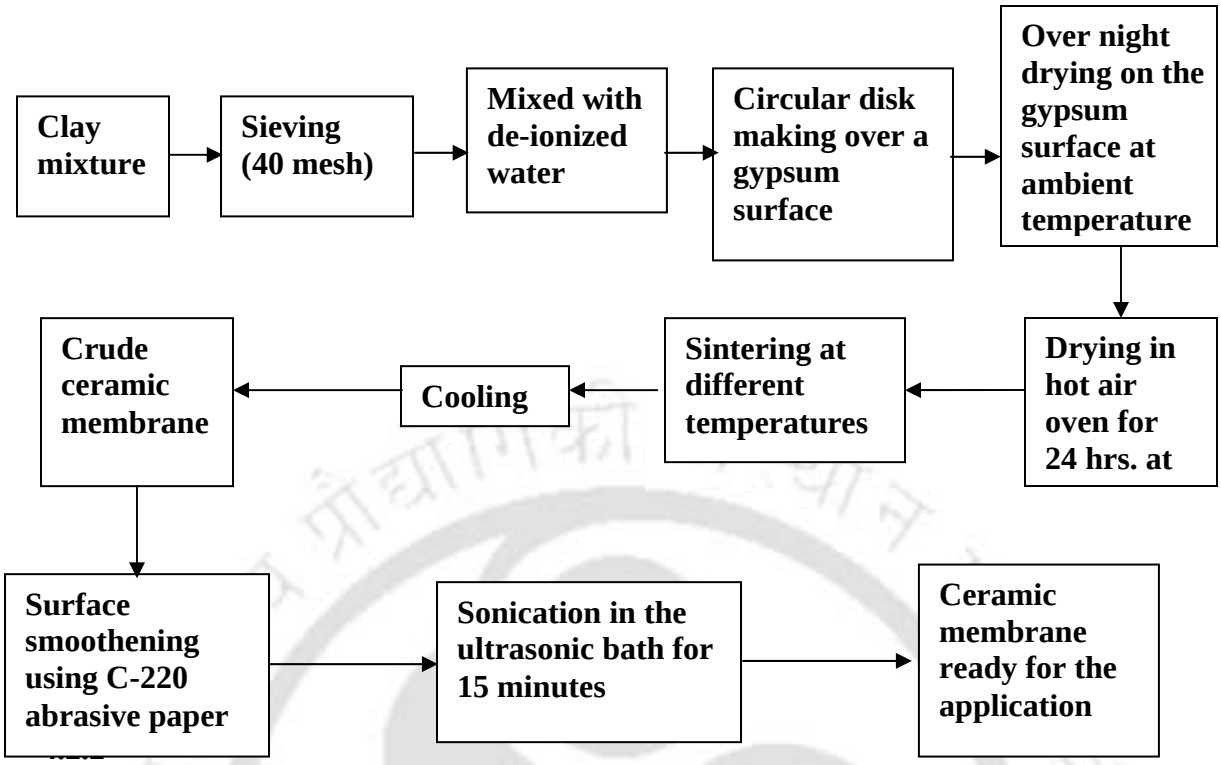

Fig. 4.1: Schematic representation of the procedure for the preparation of ceramic membrane using paste method

4.2.2 Uni-axial method

In this method, first the clay materials were taken in a 40 size mesh for sieving to get an uniform particle size of all materials in the mixture. After then sieved materials were received in a pot and mixed manually, a binder (2 wt% Poly vinyl alcohol) was added (10 wt% of the total mixture weight) to it and was finally mixed for 30 minutes in a ball mill so that the mixture would be a homogeneous one. It is necessary to mention that from 120 gm of this mixture some amount was lost inside the ball mill for the inability of scrubbing them out manually. So after the scrubbing out of the ball mill, the mixture was further sieved using the same mesh size and weighed using a high precision spring

balance which confirmed that around 2 gms. of the material was wasted. The mixture was then divided into several equally-weighed (30 g) segments. Each segment was experienced an uni-axial pressure of 52 MPa for 1 minute under the action of a hydraulic press that had been operated manually. The diameter and the thickness of the prepared membrane were 50 mm and 5 mm, respectively.

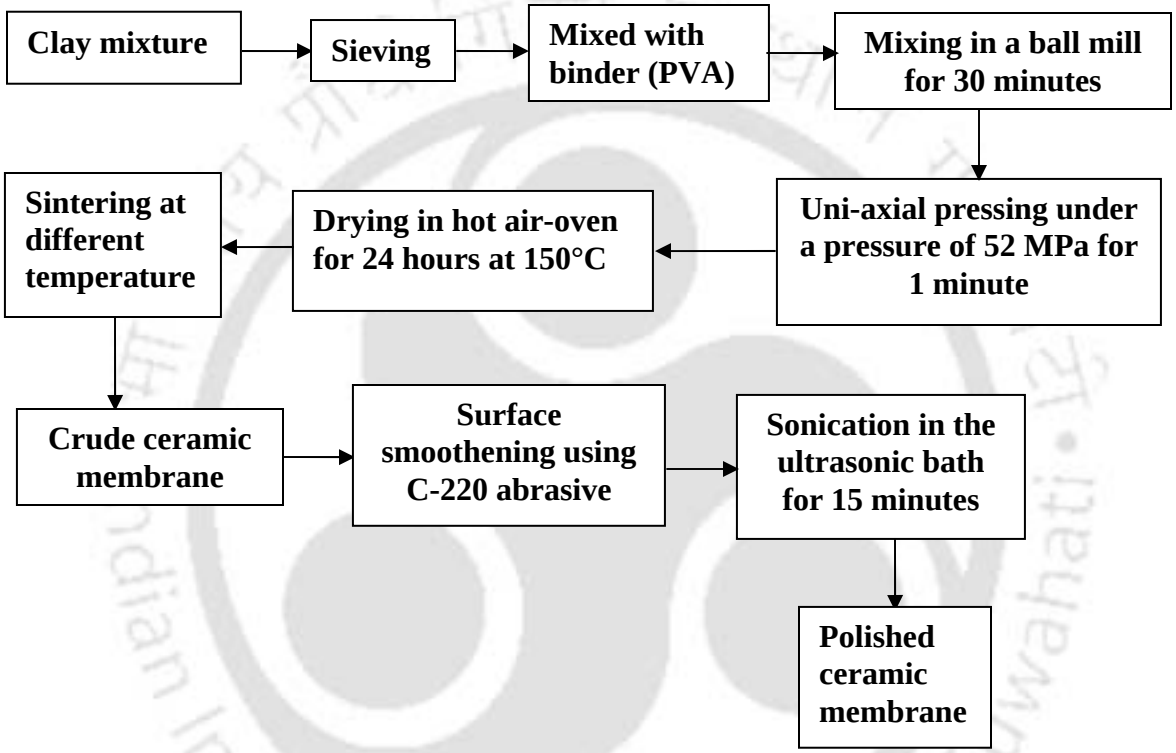

Fig. 4.2 Schematic representation of the procedure for the preparation of ceramic membrane using uni-axial method

Furthermore, disks were kept inside a hot air oven at 150°C for the overnight and then they were sintered inside a muffle furnace. Sintering process was then carried out using very low heating rate of 2 °C min^{-1} inside a muffle furnace and then cooled also in the same manner. It is very important that during heating and cooling of the supports, process should be as slower as much possible, otherwise during thermal treatment, a non-uniform

thermal stress is generated inside the ceramic body that can cause cracks inside which in turn would make them impossible to use. The preparation process is presented in the Fig. 4.2.

4.3 Characterization techniques

4.3.1 Structural Characterization

This section explains different structural characterization techniques employed for the ceramic microfiltration membranes prepared by paste and uni-axial cold pressing methods. Different characterizations of the membrane involve the structural characterization by particle size analyzer, thermogravimetric analysis (TGA), X-Ray diffraction analysis (XRD), scanning electron microscope (SEM), total porosity and average pore radius determination by water as permeation test.

Particular size analyzer (Make: Malvern, MASTERIZER 2000, UK) is used to determine the size distribution of different ingredients. Thermogravimetric analysis of the sample mixture was conducted (Make: Mettler Toledo, TGA SDTA 851^e, USA) to identify the weight transformations of the material at different thermal conditions. X-ray diffraction (Make: Brucker D8 ADVANCE, Germany) analysis of the porous ceramic membrane was conducted to investigate the extent of phase transformations. Scanning electron microscopy (Make: LEO 1430VP, UK) was carried out to analyze the presence of possible defects and estimate the membrane pore size. The estimation of average membrane pore size from SEM micrographs was carried out using well-known Image J software [22]. The bulk porosity of the membrane was evaluated using Archimedes method with water as the wetting liquid.

4.3.2 Permeation experiment

The membrane performance and presence of defects in the interior portion of the membranes was evaluated using liquid (water) flux characterization. For liquid permeation experiment a laboratory made permeation setup of capacity 125 ml is used. The setup (as shown in Fig. 4.3) used for this experiment consists of a Teflon tubular cell with a flat circular Teflon base plate which contains the membrane housing.

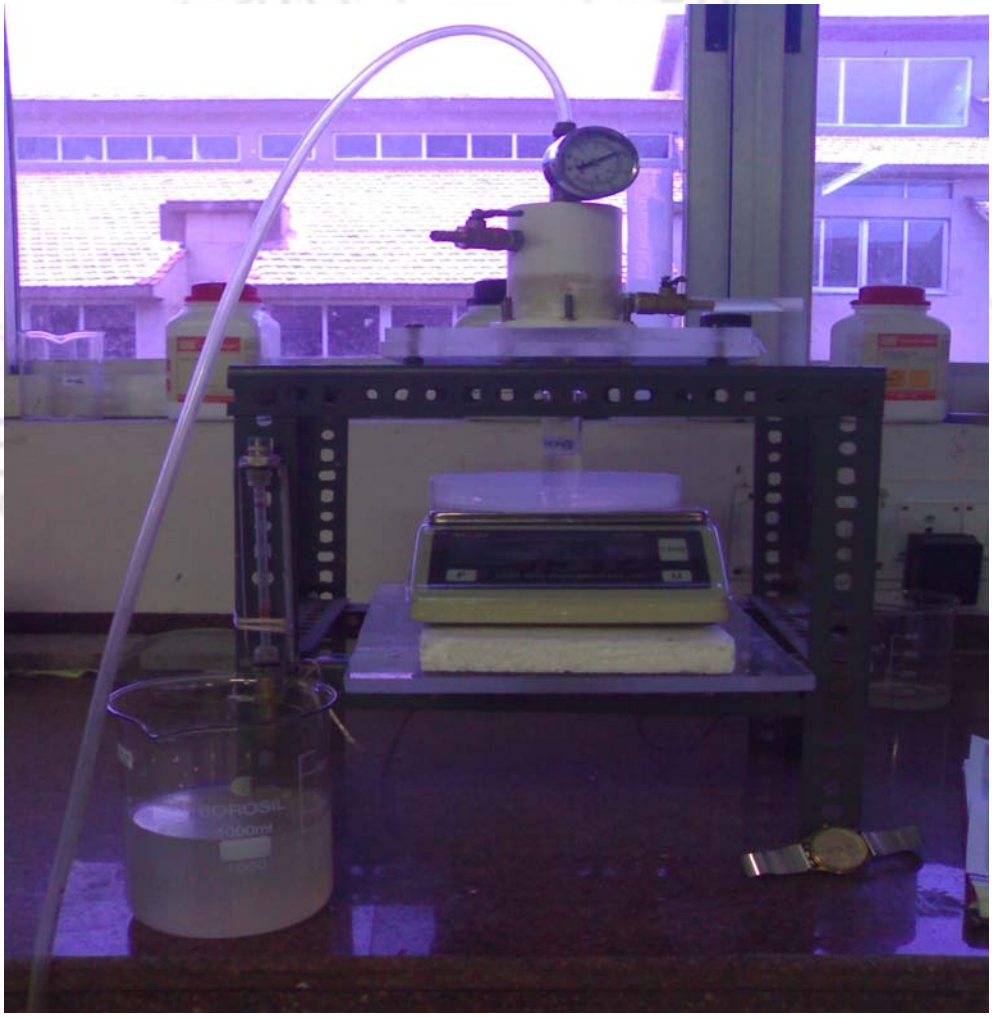

Fig. 4.3: Experimental setup for water permeation.

The deionized water was filled in the tubular section from the top. The membrane was placed in a Teflon casing and sealed with epoxy resin and then place in the membrane housing provided on the base plate. The cell was pressurized with compressed air. Liquid permeate flow rate was measured using a digital weight machine. The hydraulic permeability and the corresponding pore diameter of the membranes were also determined. All permeation experiments were conducted at a temperature of 25 ^{o}C.

4.4 Chemical stability

Chemical stability of the ceramic membranes were tested by immersing them inside a strong acid medium (pH 3) as well as in a strong base medium (pH 12) for 24 hours duration. Concentrated HCl and concentrated NaOH solution were used to maintain the pH of the medium. Wet membranes were collected and weighted after drying at 150 ^{o}C for 3 hours. Weight losses of the membranes were estimated for all the membranes sintered at different temperatures. In order to minimize the error in estimating the weight loss of the supports, an average was taken for every three ceramic porous supports sintered at a particular temperature.

Chapter 5

Preparation of Microfiltration Membrane: Results and Discussion

This chapter discusses about the different structural and physical characteristics studied for the ceramic microfiltration membranes prepared by paste and uni-axial cold pressing methods.

5.1 Structural characterization of prepared MF membrane

Structural characterization consists of different types of methods employed for the clay mixture and for the supports after sintering. Morphological characterization of the sintered ceramic porous supports was made by XRD, SEM and water permeation test. Furthermore, pore size distributions, surface pore density were calculated from the SEM images and the average pore size estimated based on the pore size distribution. Chemical stability of the inorganic ceramic microporous membranes prepared by paste and uni-axial cold pressing method were discussed in detail. Furthermore cost of the membranes was also taken into account in order to validate their market acceptance for certain applications as discussed in the section later in this chapter.

5.1.1 Particle size distribution

Particle size analysis is useful to study the particle size distribution of the clay mixture before sintering. In association with the preparation of ceramic membranes, most of the particles of every ingredients in the clay mixture would be necessarily equal in size i.e. each ingredient should have narrow particle size distribution. Apart from this, it is also

required that clay mixture must have a wide particle size distribution so that during sintering, it is likely to be expected that the smaller particles would fill-up the void spaces between bigger particles and thus making the structure more compact in the sense of homogeneous porosity with the increase in temperature [141]. It is therefore necessary to select certain clay mixtures with wide range particle size distribution for the preparation of ceramic membranes. In the present work, the clay mixture was selected in such a way that the particle size distribution of its ingredients is believed to have been widely distributed which was analyzed by the particle size analyzer before initiating the sintering process. Figure 5.1 shows the particle size distribution of the clay mixture. From the figure it was revealed that most of the ingredients in the clay mixture had a sharp particle size distribution. This observation also supported the fact that particle size of the clay mixture was widely distributed. Particle size of the different ingredients in the clay mixture was studied using the particle size analyzer. From the figure it was observed that the particle size of the kaolinite had the smallest value of 2.0465 μm with a vol % 6.41 compared to the other materials used to prepare the clay mixture for the preparation of ceramic porous membranes by both the methods as was explained elsewhere in this chapter. It was also noticed that the largest particle was observed for the case of sodium-carbonate with a value of 447.7 μm with the vol % 9.91 (nearly 10% roughly). While calcite and quartz had most of their particle size falling in the range of 4.36 μm with 7.81 vol% and 42.76 μm with 5.53 vol%, respectively.

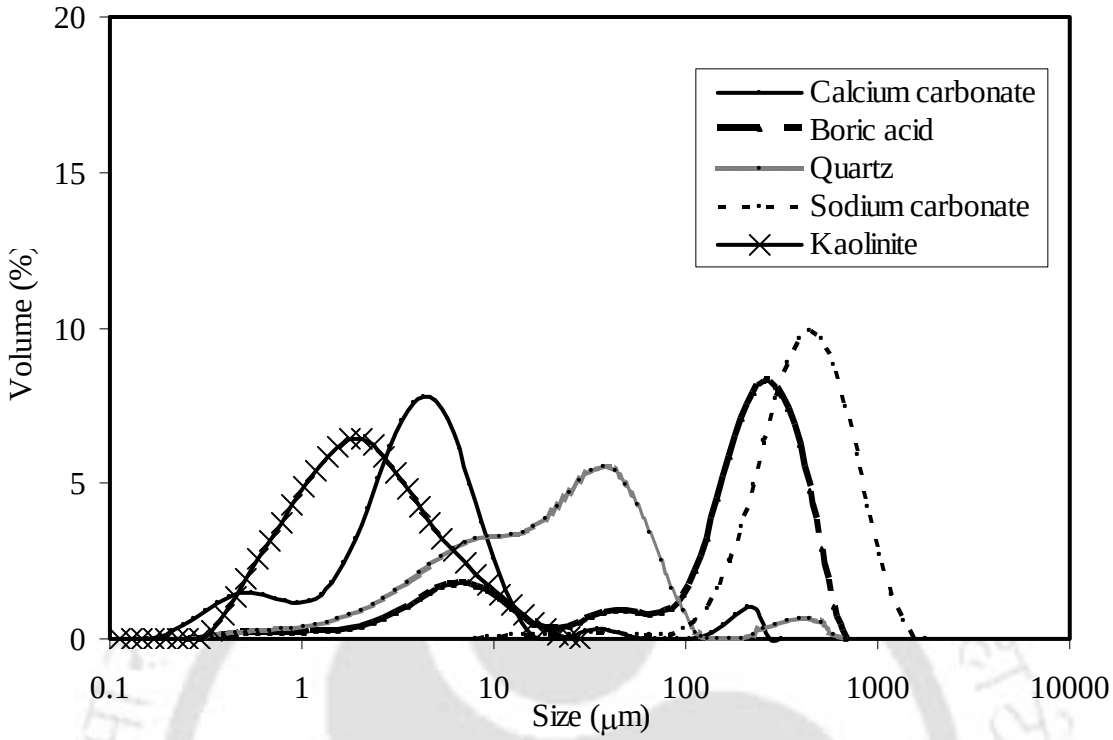

Fig. 5.1 Particle size distribution of the clay mixture

5.1.2 Thermogravimetric analysis

Thermogravimetric analysis (TGA) is an essential investigation to understand the thermal behavior of the sample. Figure 5.2 reveals the temperature sensitivity of the clay mixture during sintering. It was seen from the TGA analysis of the clay mixture that with increase in temperature at a certain heating rate the weight loss was increased at three distinct location of temperature which is accounted for the three decay points in the graph and a 27 % overall weight loss was observed. It was also observed that the weight loss of the clay mixture was found to be insignificant above 850 °C temperature. From the graph (Fig 5.2) it was seen that the three declined regions which were accounted for the loss of

hydrated water molecules from the kaolinite structure, decomposition of sodium carbonate (Na_2CO_3) and of calcite ($CaCO_3$), respectively as was indicated by the arrows in the figure displayed below. A sharp declination was observed at the temperature 500 °C corresponds to a weight loss of 2.72 %. This may be due to the decomposition of sodium carbonate as this little amount of decrease in weight can be accounted if the amount of carbon-di-oxide released is very small in amount.

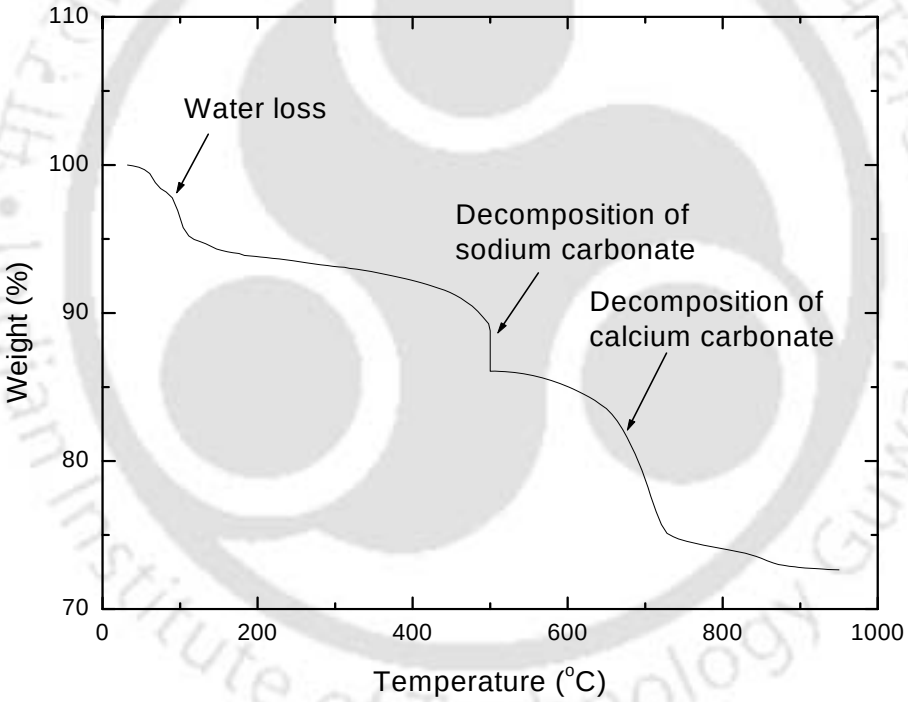

Fig. 5.2 TGA of the materials used for membrane preparation.

5.1.3 X – ray diffraction analysis

X-ray diffraction study was used to confirm the phase transformation as well as the nature of phases (crystalline, semi-crystalline or amorphous) present in the sample during sintering at different temperatures. Figure 5.3 reveals the nature of the phases present in the porous ceramic membranes sintered at different temperatures followed by X-ray diffraction (XRD) analysis. The analysis was done with a step size of 0.05° and scanning rate of 1° min^{-1}. The range of 2θ for all the samples were scanned from 5° to 90° using a diffractometer with Cu K_α (λ= 1.54178 Å) radiation source. From the figure it was seen that with the increase in sintering temperatures crystalline phases were more prominent. Some kaolin peaks disappeared after 750 °C and some of them were shifted may be due to the transformation of phases beyond this temperature range. At 750 °C, more number of peaks came with a low intensity range, thus makes the task almost impossible to find out the exact material after matching their relative intensity with the JCPDS (Joint Committee on Powder Diffraction Standards) files. It might be the presence of more number of semi-crystalline phases at this particular temperature. It was also felt that the transformation of phases was mostly occurred at 750 °C. At the higher temperatures like 800 °C, 850 °C, 900 °C and 950 °C this trend was absent. Besides, for all the cases beyond the 750 °C, distinct peaks of calcite, wollastonite and kaolinite were observed and matched with the values reported in JCPDS files as reported in the Table 5.1. Figure 5.4 shows the grain size of the crystallites estimated by well-known Scheer's formula [142]. It was observed that with an increase in sintering temperature grain size was increased. For an example, grain size of the calcite was found increasing from 30.34 nm to 40.02

nm at 750 °C and 950 °C, respectively. This observation confirmed the transformation of amorphous phase towards the crystalline phase.

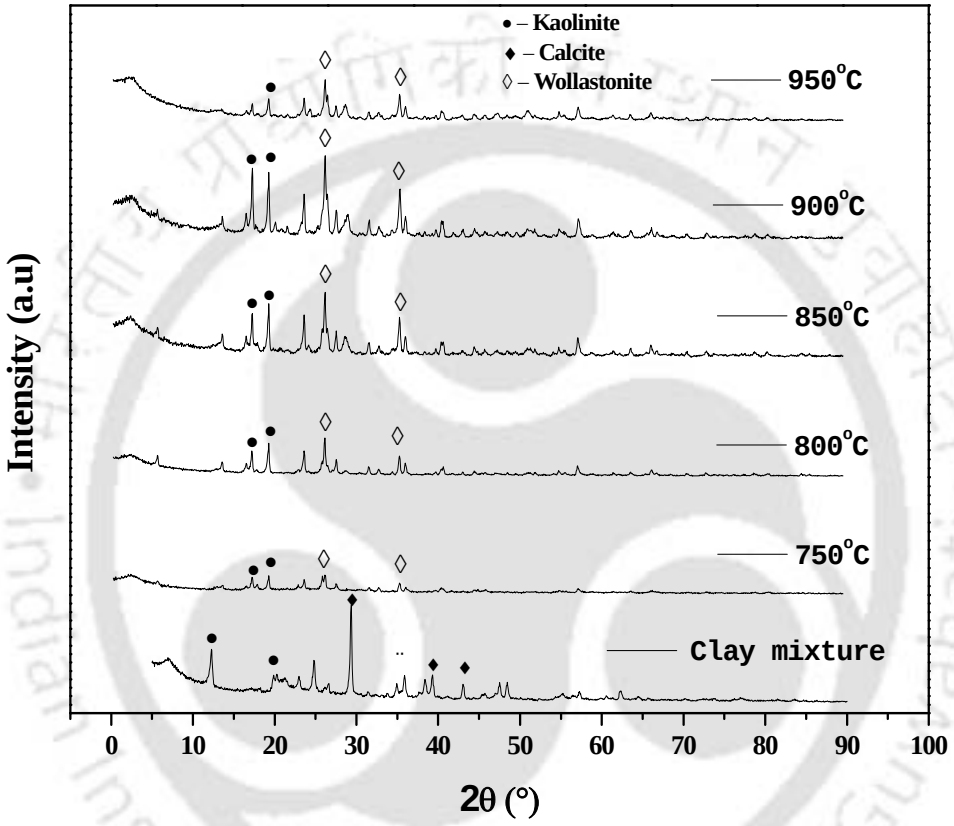

Fig. 5.3: XRD of ceramic membranes sintered at different temperatures.

Table 5.1: JCPDS files of elements detected from XRD graph.

Element	Highest intensified peak (2θ)	Miller indices (h k l)	# JCPDS file
Calcite	29.408	(1 0 4)	00-005-0586
Quartz (α-SiO_2)	26.642	(1 0 1)	01-075-0443
Wollastonite	26.55	(-1 0 2)	01-072-2284
	29.66	(1-1 0)	01-072-2284
	29.66	(1 2 0)	01-072-2284
Kaolinite	14.24		01-089-6538

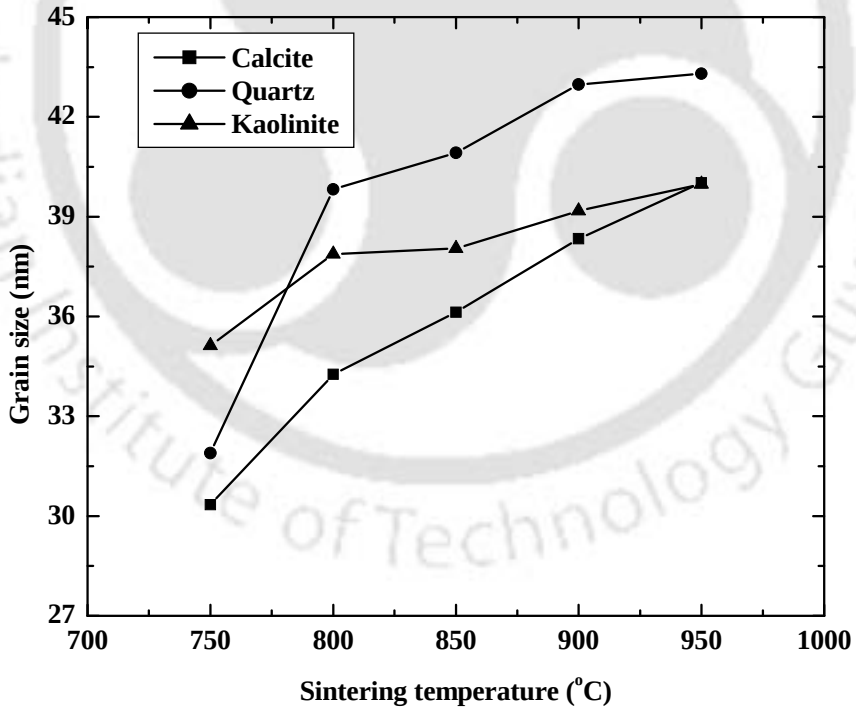

Fig. 5.4: Effect of sintering temperature on the grain size.

5.1.4 Scanning electron microscopy

Scanning electron microscopy provides the morphological information of the sample. Porous sample is consisted with different shape and size of the pores. In the present study, the surface morphology was investigated to visualize the shape, size as well as the distribution of pores. The micrographs related to the evolution of the microstructure of ceramic membranes with the increasing sintering temperature are shown in Fig. 5.5 and 5.6 revealed the morphological outlook of the ceramic porous surfaces sintered at 750 °C, 800 °C, 850 °C, 900 °C and 950 °C by paste and uni-axial method, respectively. It was seen that the surface of microporous membranes were well compacted with an increase in sintering temperature from 750 to 950 °C. All the samples were analyzed by a scanning electron microscope with a 2KX magnification which showed that the membranes sintered at higher temperatures had more densified structure. It can be visualized from the Figs. 5.5e and 5.6e that the narrower shape and size of the pores were found for the membranes sintered at 950 ^{o}C for both the methods.

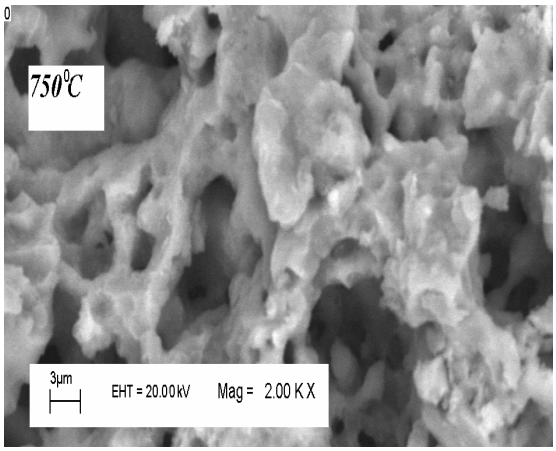

(a)

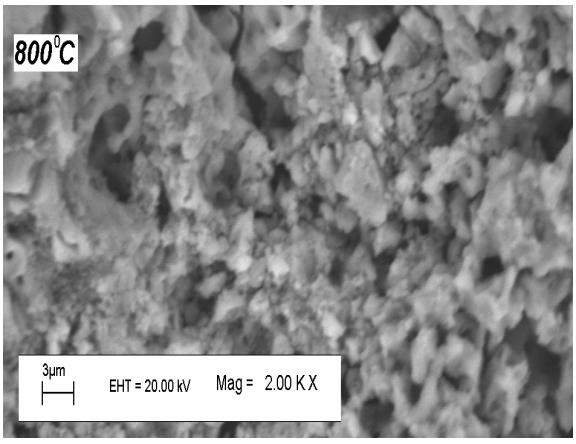

(b)

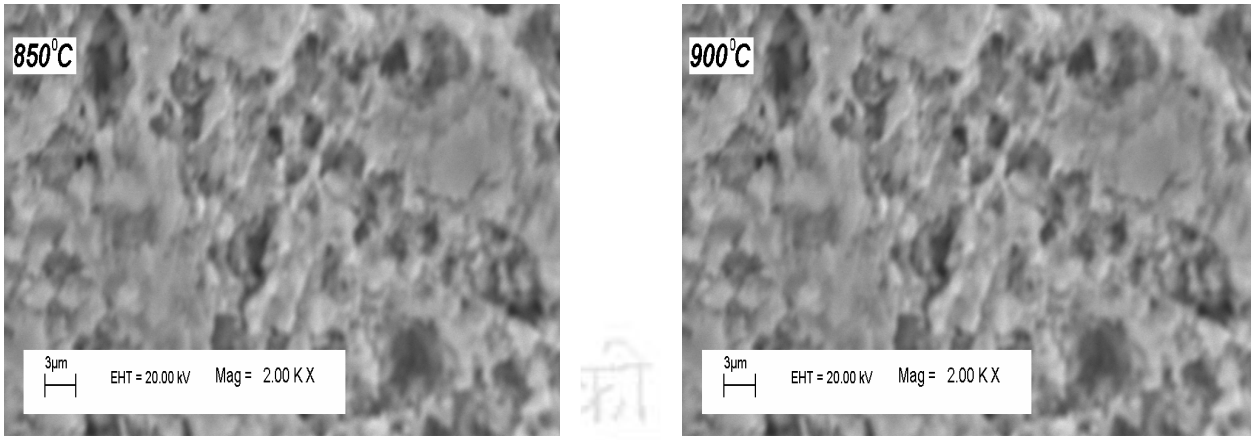

(c) **(d)**

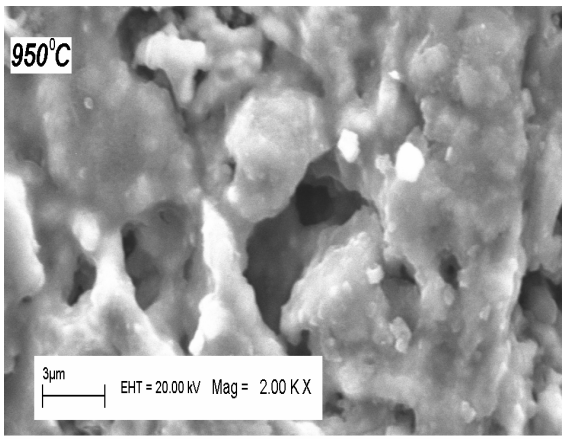

(e)

Fig. 5.5 SEM (2X magnification) images of ceramic membranes at different temperatures. (paste method)

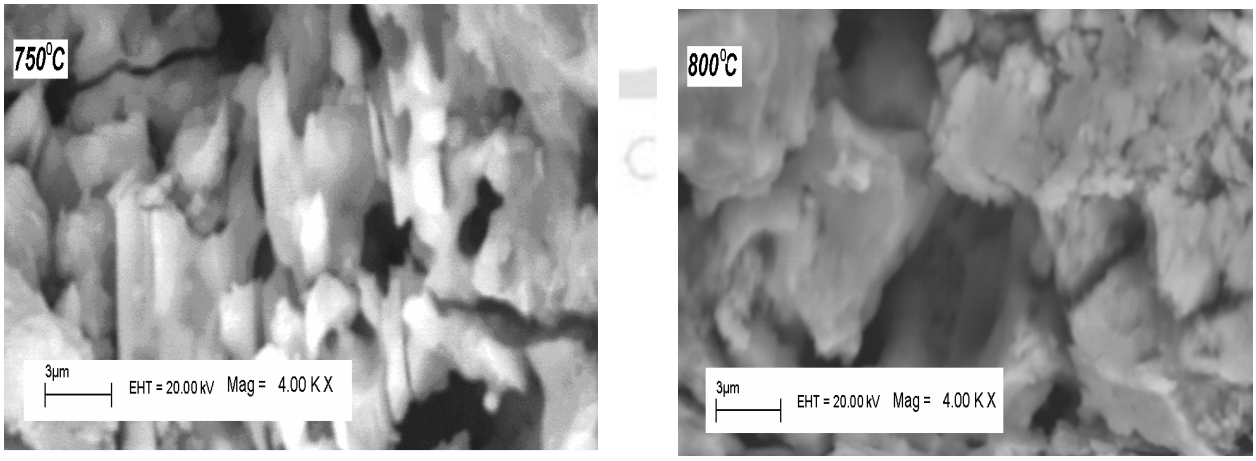

(a) **(b)**

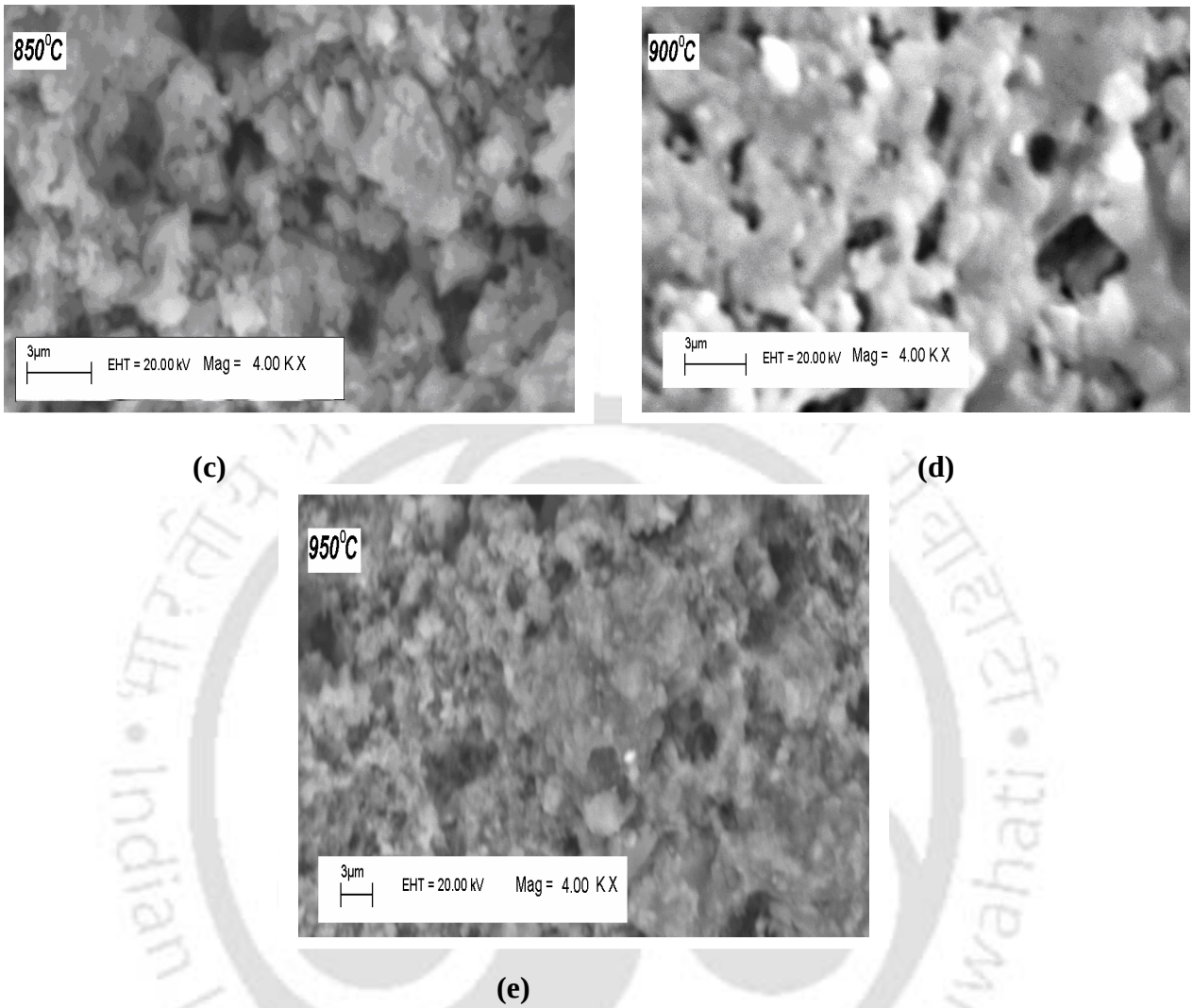

Fig 5.6 SEM (4X magnification) images of ceramic membranes at different temperatures. (**uni-axial method**)

5.1.5 Pore size distribution

Pore size distribution of the ceramic microporous membranes sintered at different temperatures was estimated from the SEM images using well-known ImageJ software. The result is shown in the Fig. 5.7 and Fig 5.8 which describes the distribution of pores of various sizes on the surface of the ceramic membranes are prepared by paste and uni-

axial methods, respectively, sintered at different temperatures. It can be seen from figures 5.7 and 5.8 that with an increase in sintering temperature, the area average pore diameter was decreased in both the methods. This observation was also supported by the porosity result which was described in the section later on. Estimation of average pore size was done by following the mathematical expression considering all the pores were of cylindrical in nature,

$$d_s = \left[\frac{\sum_{i=1}^{n} n_i d_i^{\,2}}{\sum_{i=1}^{n} n_i} \right]^{0.5} \qquad (5.1)$$

where d_i is the diameter of the ith pore estimated from the image, d_s is the area averaged pore diameter, n_i is the number of pores with diameter d_i and n is the total number of pores calculated from the SEM images. The area averaged diameters of membranes prepared by paste method thus estimated were of 5.2, 3.33, 2.36, 2.03 and 1.58 μm at 750 °C, 800 °C, 850 °C, 900 °C and 950 °C temperatures, respectively. Ceramic membranes prepared by uni-axial cold pressing method possessed the area averaged diameter of 2.47, 2.44, 1.87, 1.46 and 1.14 μm at 750 °C, 800 °C, 850 °C, 900 °C and 950 °C temperatures, respectively. Hence it clearly confirmed of the structure densification at the higher temperatures for ceramic microporous membranes prepared by both methods. It is therefore obvious to achieve a narrow pore size distribution of the ceramic membranes sintered at higher temperatures.

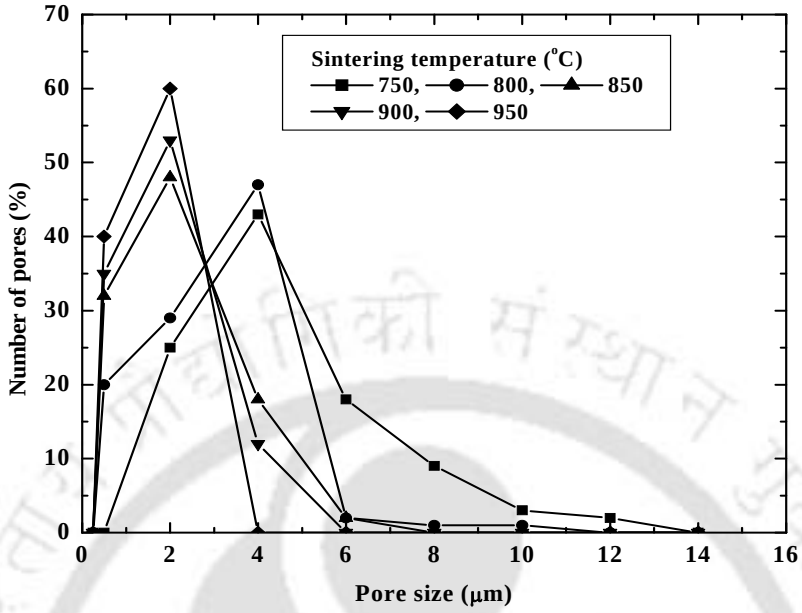

Fig. 5.7: Pore size distribution at different sintering temperatures. **(Paste method)**

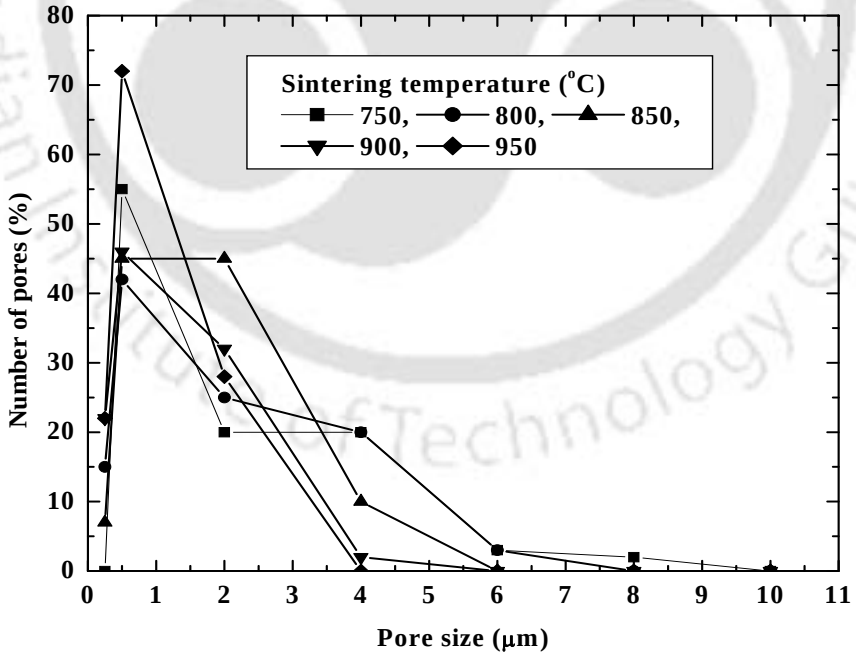

Fig 5.8: Pore size distribution at different sintering temperatures. **(Uni-axial method)**

Surface pore density

Surface pore density was calculated using the following expression:

$$N_S = \frac{N}{A_{\text{Image}}} \times 10^{12} \qquad (5.2)$$

Where, N_S is the surface pore density (m^{-2}), N is the number of pores in the image under consideration, A_{Image} is the image area (μm^2), this area was calculated by following the expression:

$$A_{\text{Im}age} = \frac{L_1}{N_L} \times \frac{L_2}{N_L} \qquad (5.3)$$

Where, L_1 represents the number of pixels accounted for the length of the image along x-direction (μm) whereas L_2 is the number of pixels accounted for the length of the image along y-direction (μm), N_L is the number of pixels measured for the standard length size given in the image (μm).

The surface pore density variation in ceramic membranes sintered at different temperatures was shown in the Fig. 5.9. It was observed that, with an increase in sintering temperature, surface pore density was decreased for the ceramic membranes irrespective of their preparation procedures. However, the surface pore density was found to be much lower for the ceramic membranes prepared by uni-axial cold pressing method. Correspondingly, it can be reported that the surface pore density was decreased from 140×10^8 m^{-2} to 93.93×10^8 m^{-2} for the membranes prepared by paste method followed by sintering at 750 °C and 950 °C, respectively. The similar observation was noticed for the ceramic membranes by uni-axial cold pressing method with surface pore density decreasing from 100.12×10^8 m^{-2} to 70.27×10^8 m^{-2} after sintering at 750°C and 950

°C, respectively. In paste method, void spaces in ceramic membranes were generated more compared to those prepared by uni-axial cold pressing due to the insufficient compressive force applied during preparation. Besides, water was added more to make the membranes by paste method. Therefore, during sintering, ceramic membranes prepared by paste method could give a significant rise in surface pore density than the membranes prepared by the uni-axial cold pressing method. Furthermore, with the increase in sintering temperature, the ceramic structures were also more densified irrespective of their preparation procedure. Therefore, the surface pore density was decreased with temperature.

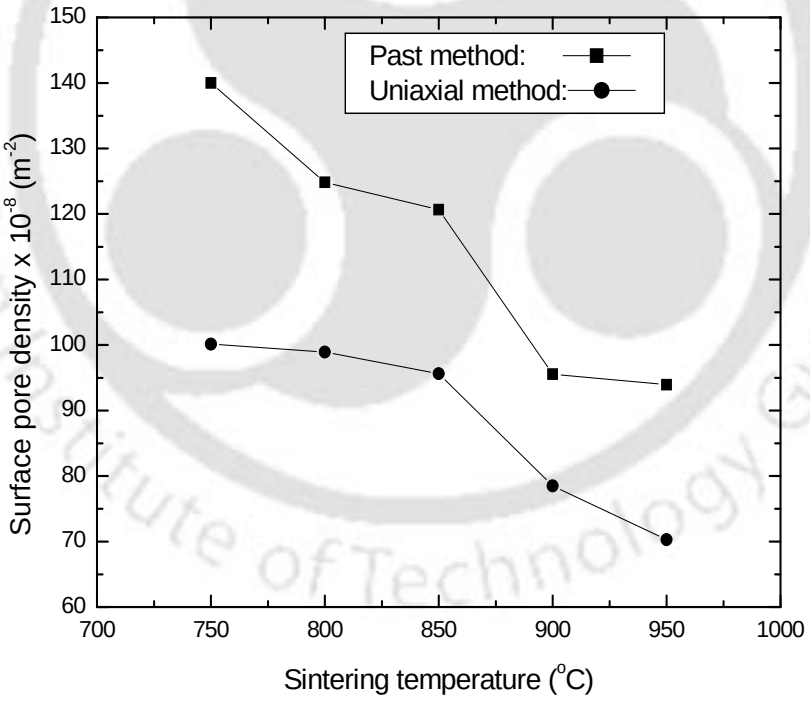

Fig. 5.9: Variation of surface pore density with sintering temperatures

5.1.6 Porosity measurement

Porosity (p) of the ceramic microporous membranes was estimated following Archimedes's principle. According to the principle, the porosity (p) can be estimated using the following equation:

$$p = \frac{(M_w - M_d)}{(M_w - M_a)} \times 100 \qquad (5.4)$$

Where, M_w is the mass of the ceramic microporous membranes saturated with water, M_d is the dry mass of the ceramic microporous membranes and M_a is the mass of the support taken at its dipping condition inside the water. Fig. 5.10 shows the variation of the bulk porosity with sintering temperature for the ceramic microporous membranes prepared by paste and uni-axial cold-pressing, respectively. It was seen from the figure that with an increase in temperature during sintering the porosity of the ceramic porous structure was decreased.

It was also observed that the bulk porosity was found to be a little higher in ceramic membranes prepared by paste method followed by sintering at different temperatures. Consequently, in uni-axial cold pressing, the bulk porosity of 0.8 and 0.43 were observed for ceramic membranes sintered at 750 °C and 950 °C, respectively. The similar trend was noticed for ceramic membranes prepared by paste method with a bulk porosity of 0.85 and 0.55 when the sintering temperature during preparation was maintained at 750 °C and 950 °C, respectively. During sintering , the gaseous products due to the thermal decomposition makes the surface porous and further the void spaces thus generated is filled up with the other materials through structural densification. The densification is favored with the increase in sintering temperature followed by the phase transformation

(i.e. amorphous to crystalline) of the raw materials (mainly clay) used for the preparation of ceramic membranes. Hence, it was clear for the bulk porosity to be low for the ceramic membranes prepared by both the methods. In paste method, amount of added water was more and could not be taken out sufficiently just after the preparation due to the lack of pressure applied during the operation. Furthermore, during paste method excess pressure was avoided due to the absence of organic binder used in the clay mixture. This could possibly generate excess void spaces than that could be formed in the ceramic membranes prepared by uni-axial method. Therefore, during sintering, bulk porosity was higher in ceramic membranes prepared by paste method.

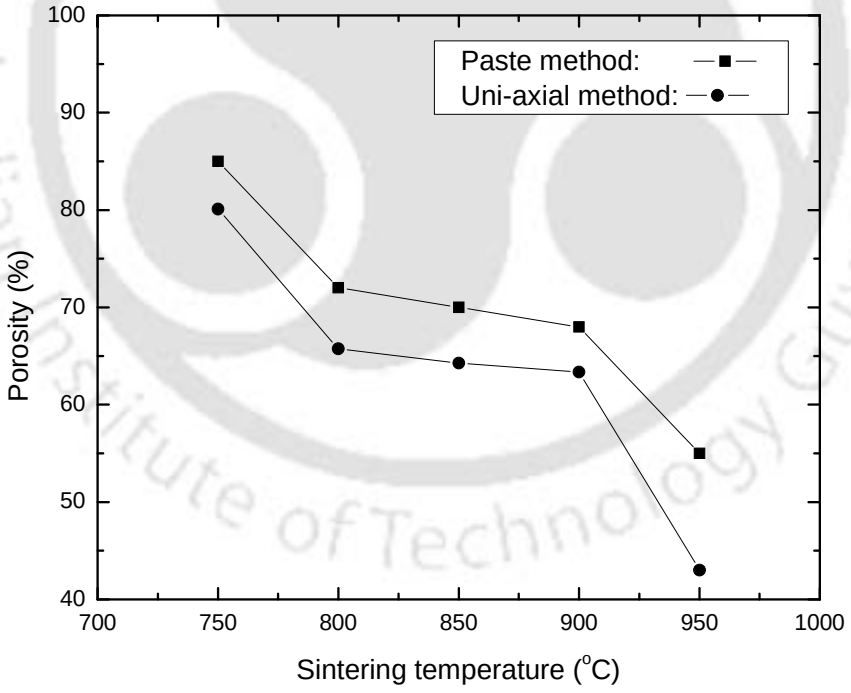

Fig. 5.10: Variation of porosity of ceramic membranes at different sintering temperatures

5.2 Permeation experiments

The inorganic membranes are subjected to liquid permeation test using deionized water in batch mode operation. Trans-membrane pressure drop for water permeation tests are maintained at 0 – 202 kPa (micro-filtration range). Before using each fresh membrane, membrane compaction has been conducted using deionized water at a transmembrane pressure of 250 kPa (which is higher than the maximum operating pressure for the set of experiments conducted). During compaction, the membrane flux was observed to be high initially and reduced to the steady value after two hrs of operation for all the membranes. At the beginning of compaction flux is 40.2×10^{-5} m^3 m^{-2} sec^{-1} which reaches to a steady state value of 38.7×10^{-5} m^3 m^{-2} sec^{-1} at the end of compaction for the membrane sintered at 950 ^oC. The permeation tests involve the measurement of permeates liquid volume as a function of time at specific values of trans-membrane pressure drop. The flux of liquid is measure at an interval of 10 seconds to verify the variation of flux with time. These experiments are performed until the total liquid permeate collected is 80 ml at a specific pressure differential.

Permeate flux (J) is determined by using the following equation:

$$J = \frac{Q_w}{A\Delta t} \qquad (5.5)$$

where Q_w is volume of water permeated (m^3), A is effective membrane area (m^2) and Δt is sampling time (hr). The term, ($J / \Delta p$), also known as permeability (L_h), is determined from the slope of the linear relationship between the pure water flux (J) and transmembrane pressure.

Figure 5.11 (a) shows the variations of steady state water permeate flux with transmembrane pressure drop for membranes prepared by paste method at different sintering temperatures. It may be seen from the figure that with the increase in pressure, the permeate flux was increased. Again, permeate flux was decreased with the increase in sintering temperature. . It was observed that the permeate flux increased from 5.4×10^{-5} m^3 m^{-2} sec^{-1} to 33.4×10^{-5} m^3 m^{-2} sec^{-1} when pressures increased from 33.77 to 202.65 kPa, respectively, for the ceramic membranes prepared by paste method. Furthermore, it can be seen that the permeate flux was decreased from 20.4×10^{-5} m^3 m^{-2} sec^{-1} to 15×10^{-5} m^3 m^{-2} sec^{-1} at 101.32 kPa when sintering temperature increased from 750 °C to 950 °C. The similar observation was also noticed for the ceramic membranes prepared by uni-axial cold pressing method which is shown in Fig 5.11(b). Comparing both the figures it may be seen that at same condition the obtained flux value is less in case of membranes sintered by uni-axial method. For example, membrane prepared by paste method showed a permeate flux of 10.7×10^{-5} m^3 m^{-2} sec^{-1} at 67.55 kPa and 950 °C whereas 4.2×10^{-5} m^3 m^{-2} sec^{-1} for uni-axial method at same temperature and pressure. With increase in pressure caused the gradual increase in driving force. Therefore, the permeate flux was found to be increased with the increase in sintering temperature. With increase in temperature, the ceramic structure became more compacted and thus active volume to flow was restricted. As a result, the permeate flux was observed to follow a decreasing trend in the ceramic membranes sintered at higher temperatures. Furthermore, it is also mention-worthy that, the higher flux in ceramic membranes prepared by paste method can be accounted for their higher non-homogeneity compared to those prepared by uni-axial cold pressing method.

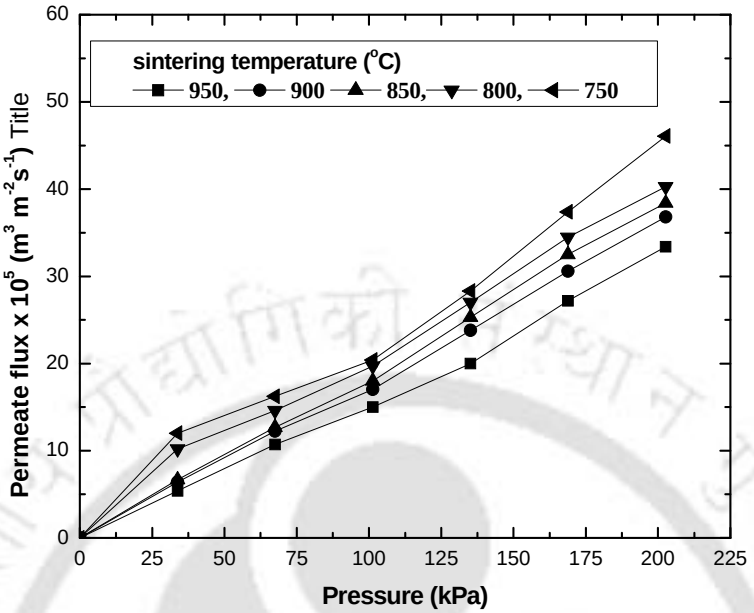

Fig. 5.11a: Variation of permeate flux with pressure for microfiltration membranes sintered at different temperatures using paste method.

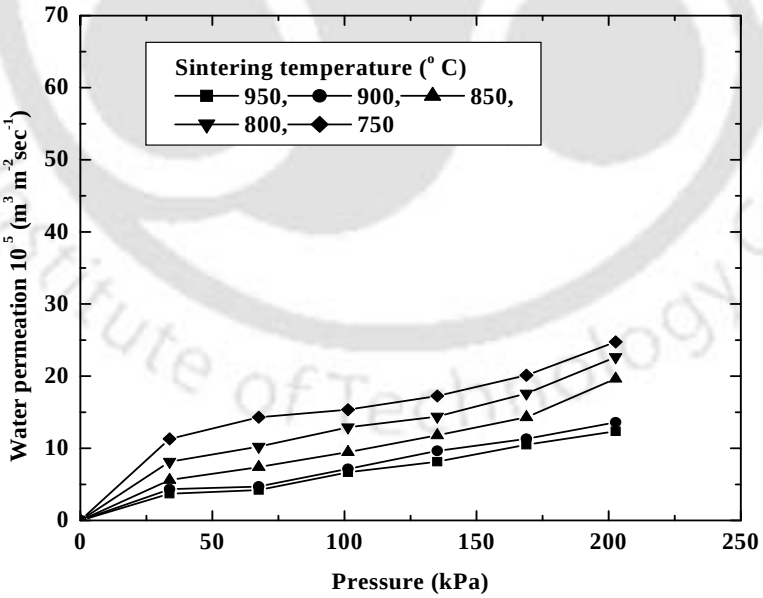

Fig 5.11b: Variation of permeate flux with pressure for microfiltration membranes sintered at different temperatures using uni-axial method.

The hydraulic permeability (L_h)of the membrane can be estimated according to the following expression [107]

$$J = \frac{n\pi r^4 \Delta P}{8\mu l} = L_h \Delta P \qquad (5.6)$$

Where J ($m^3m^{-2}s^{-1}$) is the liquid flux through the membrane, ΔP (kPa) is the trans-membrane pressure drop across the membrane, μ is the viscosity of water, l is pore length and $\varepsilon(=n\pi r^2)$ is the porosity of the membrane. Permeability of each membrane was determined from the slop of the plot permeate flux vs. transmembrane pressure. The calculated values of permeability (L_h) at different sintering temperatures using paste and uni-axial methods are shown in Table 5.2 and 5.3, respectively. Both the tables also summarize different correlation coefficients (R^2) for different sintering temperatures. From tables it can be observed that R^2 values varied from 0.988 to 0.999 for the range of sintering temperatures considered in this work. The high values of R^2 (~1.0) dictate the more accurate values of membrane permeability

Table 5.2: Variation of permeability of membranes with sintering temperature prepared by paste method

Temperature (°C)	**ε (porosity)**	**$L_p \times 10^9$ ($m\ Pa^{-1}\ s^{-1}$)**	**R^2**
750	0.85	2.22	0.994
800	0.72	2.02	0.998
850	0.7	1.89	0.998
900	0.68	1.79	0.989
950	0.55	1.58	0.989

Table 5.3: Variation of permeability of membranes with sintering temperature prepared by uni-axial cold pressing method

Temperature (°C)	**ε (porosity)**	**$L_p \times 10^9$ (m Pa^{-1} s^{-1})**	**R^2**
750	0.8008	1.31	0.989
800	0.6575	1.13	0.999
850	0.6428	0.93	0.998
900	0.6336	0.69	0.988
950	0.43	0.62	0.995

Figure 5. 12(a) shows the changes in hydraulic permeability (*Lp*) with sintering temperatures for membranes prepared by both paste and uni-axial cold pressing methods. It was found that with the increase in sintering temperature, the hydraulic permeability of the ceramic membranes was decreased irrespective of their permeation procedure. From the figure it may be seen that for the membranes prepared by paste method the permeability was 2.221×10^{-9} and 1.588×10^{-9} m/Pa.s when sintering temperature were 750 °C and 950 °C, respectively. The hydraulic permeability increased from 0.622×10^{-9} to 1.315×10^{-9} m/Pa.s when temperature increased from 750 °C and 950 °C in case of uni-axial method.

The decrease in permeability with sintering temperature is due to the decreasing trend in permeate flux (Fig. 5.11a and 5.11b) with temperature. Again, the decreasing trend in permeate flux with temperature is because of structural densification as discussed in section 5.1.5. It was also noticed that the hydraulic permeability was profound in ceramic

membranes prepared by paste method. In paste method, void spaces were generated more which was discussed earlier in detail. Therefore, the hydraulic permeability was found to be higher in ceramic membranes prepared by the paste method.

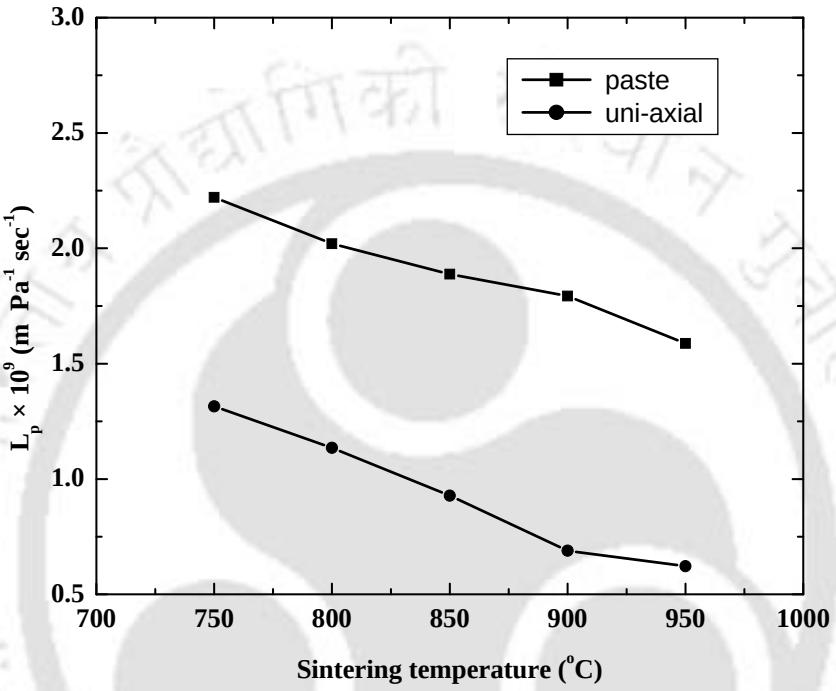

Fig. 5.12(a): Variation of hydraulic permeability (L_p) of prepared membranes with varying sintering temperatures

The average pore radius (r_l) of the membrane is evaluated by assuming presence of cylindrical pores in the membrane matrix using the following equation deduced from equation [143] as

$$r_l = \left[\frac{8\mu l L_h}{\varepsilon}\right]^{0.5} \qquad (5.7)$$

The porosity ($\varepsilon(=n\pi r^2)$) of the membrane is determined by the pycnometric method using water as wetting liquid. The calculated values of porosity of different membranes are shown in Tables 5.2 and 5.3.

Figure 5.12 (b) shows the variation of average pore size (estimated from SEM images and water permeation test) with sintering temperature for ceramic membranes prepared by two methods It was observed that with an increase in sintering temperature, the average pore size was decreased for membranes prepared by both the methods. It was found that in the paste method average pore size estimated from SEM decreased from 5.22 to 1.58 μm at 750 ^{o}C and 950 ^{o}C, respectively. The similar observations was noticed in the uni-axial method with average pore size decreased from 2.47 to 1.14 μm at 750 ^{o}C and 950 ^{o}C, respectively. The average pore size obtained by the water permeation method is found to be less compared to that of SEM analysis. For an example. In uni-axial method the average pore size estimated from the water permeation test was found to be reduced from 1.1 μm to 0.56 μm while sintering temperature increased from 750 ^{o}C to 950 ^{o}C

The decreasing trend of pore size with increase in sintering temperature, irrespective of preparation method adopted, is due to the densification of ceramic structures which is confirmed by the pore size measurement (Fig. 5.12 b).

From the figure it is seen that the average pore size calculated by the ImageJ software from SEM photographs are higher than those obtained from the water permeation test. It is because of the fact that in SEM analysis, there is a possibility of overestimating the mean pore size by considering the wider pores on the surface which may not even continue till the end of the membrane disk. Mean pore size obtained by water permeation

test correspond to the pores through which water permeates. It is also seen that though there are differences between the values, the decreasing trend of mean pore size and porosity with increasing sintering temperature are agreed by both the techniques.

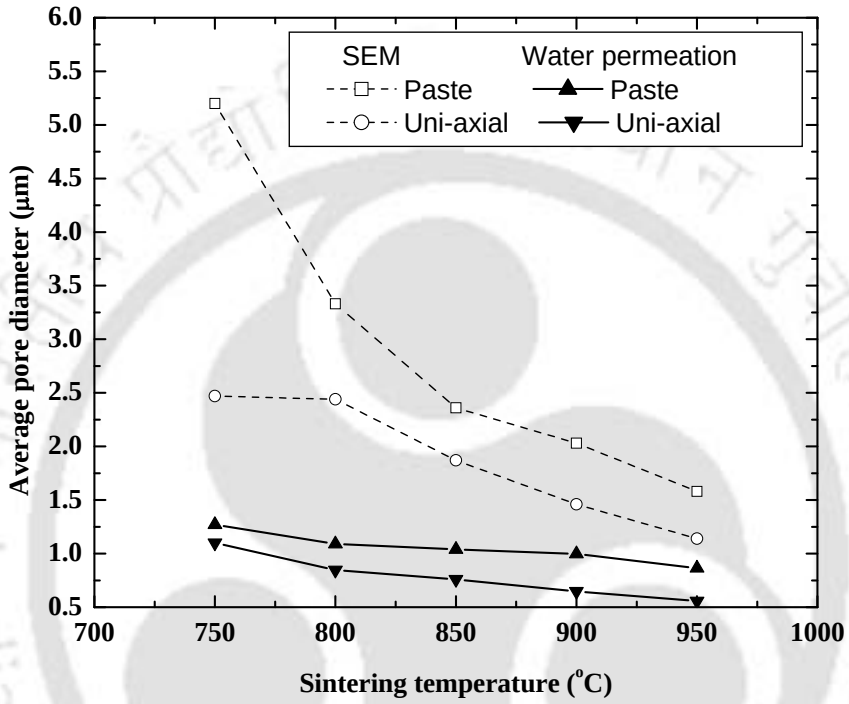

Fig. 5. 12 (b): Variation of average pore size estimated from SEM images and water permeation test for different membranes.

Thus from the above study, it may be inferred that though SEM analysis predicts a reasonable trend of membrane morphology in terms of pore size distribution; but for actual separation application, water permeation test may be considered to have more significance in assessing the mean pore size and porosity of the prepared membranes quantitatively. So, it can be concluded that SEM analysis is mostly suitable to estimate

membrane morphology qualitatively i.e. to have the idea regarding the structure of the membrane. However, since the present study is associated with liquid stream, the subsequent chapter (chapter 6) analyzes the membrane performance considering the morphological properties (e.g. mean pore size, porosity and pore size distribution) obtained from the water permeation test.

5.3 Chemical stability analysis

Figure 5.13 describes the weight loss of the ceramic membranes sintered at different temperatures in both acidic and basic medium. Details of experimental procedures are discussed in chapter 4.

It was observed that the averaged percentage weight loss of the ceramic membranes under acid and base treatment was decreased with the increase in sintering temperature irrespective of their preparation procedures. It was also noticed that percentage weight loss was more during acid treatment for the ceramic membranes prepared by both the methods. In addition to this, the percentage weight loss was more in ceramic membranes prepared by paste method. It can be elaborated that the averaged percentage weight loss were found to be 10.7% and 0.07 % after the acid treatment for the ceramic membranes prepared by paste method followed by sintering at 750 °C and 950 °C, respectively. The similar trend was also noticed after the base treatment with averaged percentage weight loss of 2.53% and 0.01% for the ceramic membranes prepared by paste method followed by sintering at 750 °C and 950 °C, respectively. At higher sintering temperature, the structure is believed to be converted to the properties similar to that of the ceramics. It is well known that ceramic material is likely to be insensitive to corrosive chemicals such as

strong acid and base. Therefore, with increasing the sintering temperature, the averaged percentage weight loss was found to be lower and finally almost be significant. It confirmed the attainment of ceramic properties for the membranes prepared by paste and uni-axial cold pressing method, respectively. In uni-axial cold pressing, organic binder was used instead of only water which intended to make all the ingredients in the clay mixture bonded together through cross-linking during the sintering better compared to those prepared by paste method. Therefore, the residual basic elements in the ceramics prepared by the unit-axial cold pressing were less compared to those prepared by paste method. Hence an averaged percent weight loss under acid treatment was less in the membranes prepared by the uni-axial cold pressing.

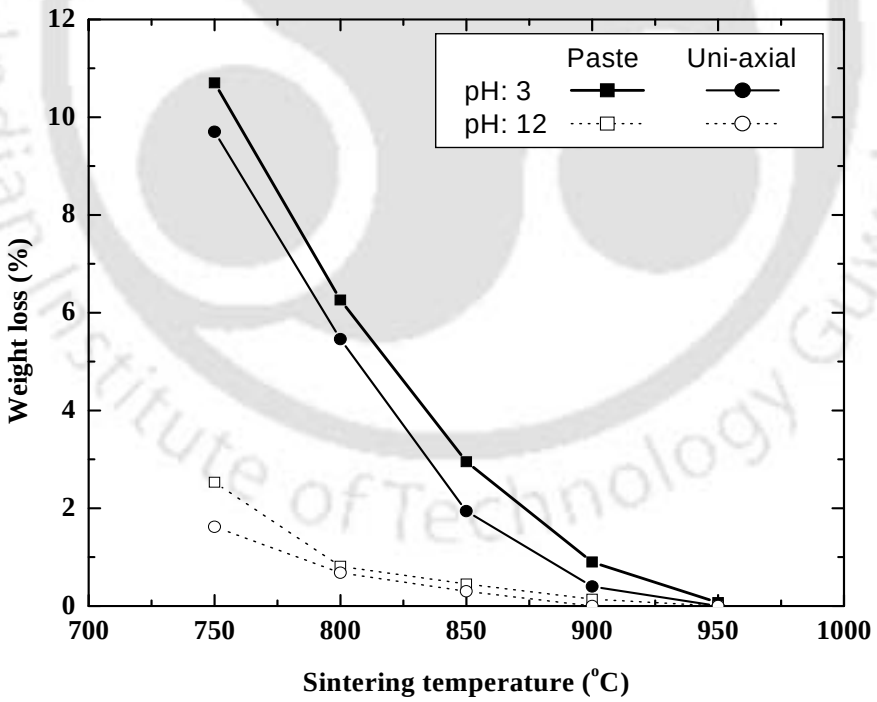

Fig. 5.13: Average weight loss of the prepared ceramic microfiltration membranes in strong acidic and basic medium

.

5.4 Membrane cost

In connection with the membrane preparation and its characterization, cost evaluation is an important perspective to validate the viability of such membranes compared to those which are available in the market. Conventionally, industrially applicable polymeric membranes cost around 50-200$ m^{-2} [144] whereas, inorganic membranes are claimed to be more expensive such as 500-1000$ m^{-2} [145]. The present work aimed at evaluating the membrane cost based on the raw material cost and electrical energy consumption during sintering as well as mechanical machining. Hence, the estimated cost for the ceramic micro porous membrane preparation is a combinational contribution of raw material cost and energy cost for electrical consumption during the whole process of ceramic micro porous membrane preparation. Electrical energy consumption was estimated by the following formula $E = P \times t_{total}$, where E is the total electrical energy consumption (kWhr) during the processing of materials and t is the total time of operation in hours and P is the power rating of the electrically driven machines such as muffle furnace. The total operation time of a muffle furnace was determined using the simplified approach described below mathematically:

$$t_{total} = \frac{\Delta T}{(dT/dt) \times 60} + t_{dw} \qquad (5.8)$$

where, t_{total} is the total operation time in hours of the muffle furnace, ΔT is the temperature difference (°C) between the final and starting temperature of the muffle furnace, (dT/dt) is the heating rate (°C min^{-1}) applied during the process and t_{dw} is the dwelling time at 950°C(as in the present investigation t_{dw} was equal to 5 hours).

Electrical energy price given for Indian market in June, 2007 is 0.0065 US$/ kWhr Therefore, the energy cost is equal to $0.0065 \times E$ US$. This cost was attributed for a membrane of surface area A_M m^2. Hence the energy cost for the membrane preparation would be equal to $\frac{0.0065E}{A_M}$ US$ m^{-2}. The cost of the raw materials needed for preparing the membrane was 110.62 US$ m^{-2} and 135.75 US$ m^{-2} and was shown in the Table 4 and Table 5, respectively. Finally, the total estimated membrane cost including raw materials cost and energy consumption cost was found to be around 172.7 US$ m^{-2} and 197.82 US$ m^{-2} for ceramic microporous membranes prepared by paste and uni-axial cold pressing method, respectively. A sample calculation is shown in appendix A. Therefore, it can be strongly recommendable from the cost analysis presented in this work (Tables 5.4, 5.5 and appendix A) that the inorganic membrane based on kaolin would be competitive to the cost of market available polymeric membranes.

Table 5.4 Economical analysis of the prepared membrane (Paste method)

Raw materials	Wt (Kg) x 10^3	Unit price ($ Kg^{-1})
Kaolin	9	5.0
Quartz	2	64.0
Calcite	5	4.2
Sodium carbonate	2	4.6
Boric acid	1	5.6
Sodium meta-silicate	1	8.4
Total dry basis formulation	20	110.62 $ m^{-2}

0.02 Kg clay mixture (dry-basis) was needed to develop one membrane (50 mm diameter and 5 mm thickness)

Table 5.5 Economical analysis of the prepared membrane (uni-axial method)

Raw materials	Wt (Kg) x 10^3	Unit price ($ Kg^{-1})
Kaolin	13.5	5.0
Quartz	3	64.0
Calcite	7.5	4.2
Sodium carbonate	3	4.6
Boric acid	1.5	5.6
Sodium meta-silicate	1.5	8.4
Total dry basis formulation	30	135.75 $ m^{-2}

0.03 Kg clay mixture (dry-basis) was needed to develop one membrane (50 mm diameter and 5 mm thickness)

Appendix A: Sample calculation for membrane cost

$$t_{total} = \frac{\Delta T}{(dT/dt)\times 60} + t_{dw}$$

$\Delta T = (950 - 50)$ °C
$= 900$ °C
$(dT/dt) = 2$°C min^{-1}, $t_{dw} = 5$ hours

$t_{total} = (7.5 + 5)$ hours
= 12.5 hours

P = 1.5 kW

$E = P \times t_{total}$
= $1.5 \times$ 12.5 kWhr
= 18.75 kWhr

A_M = membrane area = $\pi / 4(50 \times 10^{-3})^2$ m^2
= 19.635×10^{-4} m^2

Energy cost = $(18.75 \times 0.0065)/(19.635 \times 10^{-4})$ US\$ m^{-2}
= 62.07 US\$ m^{-2}

Raw material cost = 110.62 US\$ m^{-2} (Table 4)

Total cost for the membrane preparation (paste method) = (Raw material cost + Energy cost) US\$ m^{-2}
= (110.62 + 62.07) US\$ m^{-2}
= 172.7 US\$ m^{-2} (approximately)

Total cost for the membrane preparation (uni-axial cold pressing) = (Raw material cost + Energy cost) US\$ m^{-2}
= (135.75 + 62.07) US\$ m^{-2}
= 197.82 US\$ m^{-2}

5.5 Comparison of paste and uni-axial methods

It is important that several parameters such as porosity, pore size distribution, surface pore density mainly determine the membrane characteristic and therefore the procedure of preparation remains very vital in predicting the qualitative aspects of particular membrane. This section therefore pays attention to distinguish the preparatory methods applied for the present work to describe their dependence over several parameters as mentioned above in order to prepare cost-effective ceramic microporous membrane of

expected quality. It was observed that with the increase in temperature, crystallinity as well as densification of the ceramic membranes prepared by paste and uni-axial cold pressing was confirmed by the XRD and SEM images, respectively. This observation was also supported by the fact of sharp pore size distribution estimated from the SEM images by well-known ImageJ software. It was observed that pore size distribution was much narrower in the ceramic microporous membranes prepared by uni-axial cold pressing method. Therefore, it is very much clear that retention of particles with sizes bigger than the estimated pore size would be better separated by such membranes compared to those prepared by the paste method. This was also observed that the surface pore density was lower in the ceramic membranes prepared by uni-axial cold pressing. It ensured the better mechanical strength of such membranes compared to those prepared by the paste method. Porosity of the ceramic microporous membranes prepared by the paste method had a higher value compared to those prepared by the uni-axial cold pressing method. However the flux was low in the case where membranes were prepared by uni-axial cold pressing. In association with the formation of less number of pores over the membrane surface as well as the less porosity, the water flux through the membranes prepared by the uni-axial cold pressing was found to be less. In addition to this, the average pore size estimated was also lower than it was estimated in membranes prepared by the paste method from the water permeation test. For an example, membranes by paste method sintered at 950 ^{o}C, had an average pore size of 0.86 μm whereas membranes by uni-axial cold pressing sintered at same temperature had an average pore size estimated was equal to 0.56 μm. Furthermore, surface pore density in the ceramic membranes by uni-axial cold pressing was 25.17% less than that was estimated in the ceramic microporous membranes sintered

at 950 ^{o}C by paste method. In view of microfiltration application, it would be always better to follow uni-axial cold pressing method to prepare ceramic microfiltration membranes for achieving a particular separation by retaining the particles of bigger sizes than the pore size of the membranes. Although the cost of the membrane preparation by uni-axial cold pressing was found to be slightly higher than the paste method as explained earlier in the previous section.

5.6 Summary

Ceramic microporous membranes were prepared by paste and uni-axial cold pressing method. The prepared membranes were characterized by XRD, SEM and other well-known techniques such as water permeation. Several parameters such as surface pore density, pore size distribution, average pore size were estimated followed by different techniques. The present investigation had the following findings:

1) Membranes prepared by the uni-axial cold pressing are less porous than the ceramic membranes prepared by the paste method which was supported by the porosity and surface pore density value estimated by Archiemedes principle and ImageJ software from SEM images. Therefore it can be concluded that ceramic membranes prepared by the uni-axial cold pressing are less prone to the mechanical failure during the permeation experiment under certain applied pressure.

2) The average pore diameter was 1.58 and 1.14 μm calculated from the pore size distribution of the ceramic microporous membranes prepared by paste and uni-axial cold pressing method at 950 °C, respectively. In addition to this, it is

necessary to mention that pore size distribution was found to be narrower with the increase in temperature for the ceramic membranes prepared by the methods mentioned above. Hence it can be concluded that at higher temperature ceramic microporous membranes prepared by uni-axial cold pressing can be able enough to retain particles of sizes bigger than 2 µm compared to the membranes prepared by paste method.

3) Bulk porosity was found to be around 0.55 and 0.43 in ceramic membranes by paste and uni-axial methods, respectively, sintered at 950 ^{o}C. This was supported by the bulk porosity value as 0.55 and 0.43 for the membranes prepared by paste and uni-axial cold pressing, respectively. This can be also concluded that the ceramic membranes prepared by the uni-axial cold pressing were better consolidated than those prepared by the paste method.

4) Finally, the cost of the ceramic microporous membranes prepared were found to be around 172.7 and 197.82 US$ m^{-2} for the ceramic microporous membranes prepared by paste and uni-axial cold pressing, respectively. This estimation is likely to validate the preparation procedures used in the work cost effective compared to the market available costly processes.

Chapter 6

Electrocoagulation Followed by Microfiltration

This chapter deals with the hybrid process adopted for the effective separation of fluoride, iron and arsenic contamination from drinking water using electrocoagulation (EC) followed by microfiltration (MF).

6.1 Introduction

Ground water contamination due to the presence of fluoride, iron and arsenic in significant amount has several disadvantages as discussed in Chapter 1. Mixture of fluoride, iron and arsenic is treated using the combination method, i.e., electrocoagulation followed by microfiltration. In chapter 3, the applicability of the EC technology for the removal of fluoride, iron and arsenic from drinking water was studied separately. In this chapter, the applied aspect of the proposed combination method is verified with a mixture of fluoride, iron and arsenic dissolved in drinking water. The mixture was first treated in a batch EC process. The treated water along with the electrocoagulated byproducts was then passed through a MF unit for further treatment. The schematic representation of the hybrid process is shown in Fig. 6.1.

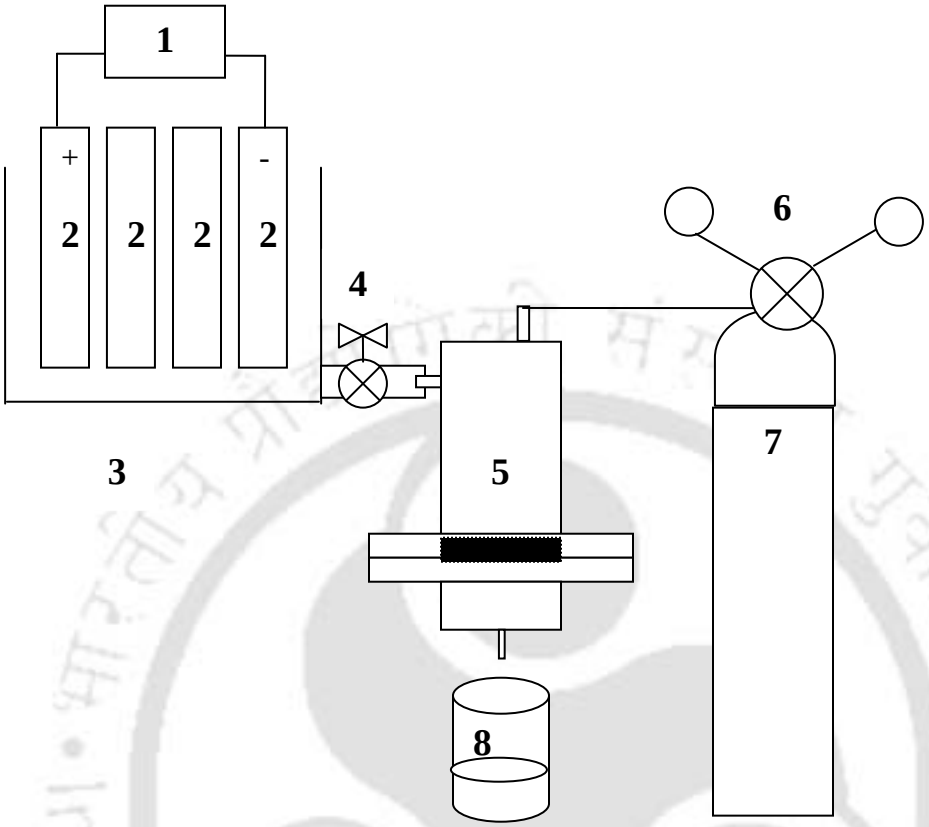

Fig. 6.1 Schematic diagram of the hybrid process

1: DC source, 2: Electrodes, 3: Electrocoagulation bath,
4: Exit, 5: Membrane cell, 6: Regulator, 7: Nitrogen cylinder
8: Permeate collector.

6.2 Experimental

An electrocoagulation bath (as discussed in chapter 2) with four electrodes made of aluminium sheet having dimension 0.15 m × 0.05 m × 0.002 m in bipolar mode of connection was used for the EC treatment. The working volume of 1 L was considered for the treatment of contaminated water containing mixture of fluoride (10 mg L^{-1}), iron (25 mg L^{-1}) and arsenic (200 μg L^{-1}). Electrocoagulation was continued for 45 minutes.

Current density and interelectrode distance were maintained at 625 A m^{-2} and 0.005 m, respectively. A membrane cell (elaborated in Chapter 4) of 125 ml capacity was used for microfiltration experiments. The outlet of the electrocoagulator was introduced to the membrane cell. The ceramic membrane prepared by uni-axial methods sintered at 950 ^{o}C was used in the MF cell. The membrane cell was pressurized by N_2 gas upto 202 kPa. During the experiments the pressure was kept constant and after every 5 min interval, the permeate was collected and the flux (J) was measured using following equation.

$$J = \frac{Q}{A \times t}$$

Where Q is the volume of permeate, A is the effective membrane area and t is the time of permeation. Permeate conductivity, pH and concentrations of fluoride, iron and arsenic were measured to ensure water quality for drinking purpose. At the end of the filtration treatment by the ceramic microfiltration membrane, the retained electrocoagulated sludge was collected from the membrane surface by scrubbing them out and dried in an air oven at 125°C for 4 hours. Thereafter the dried sludge was grinded into the powder and made ready for the SEM, EDX and XRD analyses in order to investigate the morphology, qualitative elemental visualization and phase transformations, respectively. In addition to this, the ceramic microfiltration membrane used for the EC experiments was also dried at the same condition as mentioned above and was subjected for the SEM analysis to visualize the morphological changes occurred to the membrane surface before and after the treatment due to the blocking of active pores by the electrocoagulated sludge.

6.3 Results and discussion

6.3.1 Particle size distribution of electrocoagulated by-product

The by-products formed during the electrocoagulation treatment were analyzed with the help of particle size analyzer to get confirmed about the size of the suspended flocks that were to be separated out of the solution in order to use it for drinking purpose. Figure 6.2 demonstrates the particle size distribution of the electrocoagulated by-products. From the figure it can be viewed that most of the particles generated during the treatment were in the range of 10 µm with volume % of more than five. Some of the bigger size particles were also formed due to the agglomeration amongst flocks so that particle size distribution had two other nodes, one at 100 µm and the other at 1000 µm with the volume percentage of 1.4 and 2, respectively. This observation undoubtedly supported the agglomeration of particles between the generated electrocoagulants. Comparing the particle size distribution of membranes prepared by uni-axial method (as discussed in chapter 5) and the particle size distribution of electrocoagulated by-product, it might be concluded that the MF membrane would be suitable for the separation of electrocoagulated by-product.

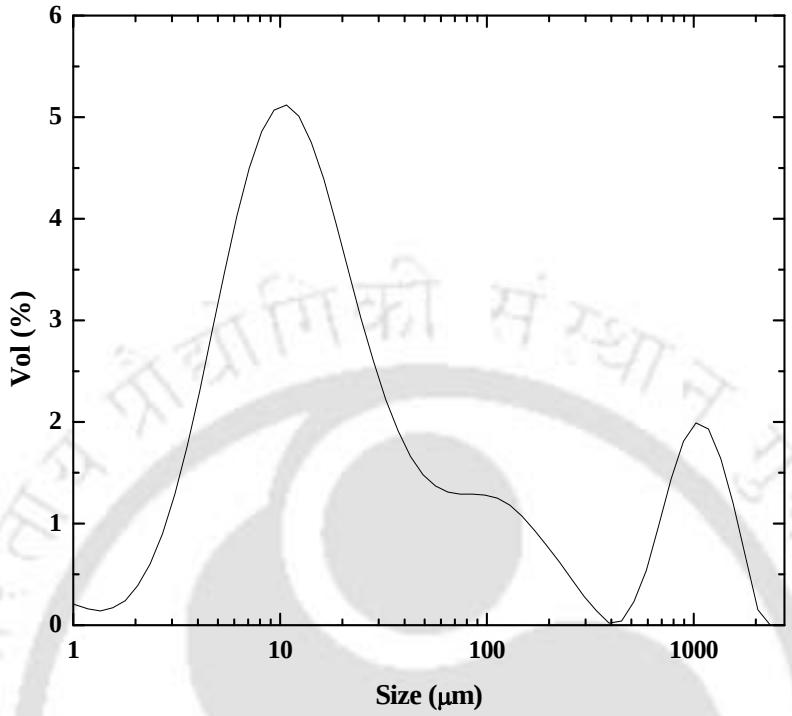

Fig. 6.2 Particle size distribution of the electrocoagulated by-product before the membrane filtration

6.3.2 Removal performance of fluoride, iron and arsenic

This subsection elaborately discusses the performance of the hybrid process for the treatment of drinking water containing mixture of fluoride, iron and arsenic. The EC followed by MF experiment was conducted with conditions mentioned in section 6.2. The performance of EC and MF was analyzed separately in terms of removal efficiency of fluoride, iron and arsenic, conductivity and pH of the treated water. Figure 6.3 clearly shows the experimental observation of percentage removal of the contaminants during EC. It was seen that with the passage of time, the percentage removal of all the contaminants were increased sharply initially and became gradual thereafter. It may be

found from the figure that after 45 minutes of electrocoagulation, percentage removal of fluoride, iron and arsenic were 93.2, 98.74 and 95.65, respectively. This is due the formation of aluminum hydroxide complex and availability of contaminants during EC process as discussed in section 3.1.1, 3.2.1 and 3.3.1.

Figure 6.3 shows the removal performance of fluoride, iron and arsenic, respectively, during EC process in terms of concentrations. Figure 6.4a shows the change in fluoride concentration with time during the EC treatment. It was seen that concentration was decreased with time and final concentration was observed to be below the recommendable limit (i.e., 1 mg L^{-1}) at the end of 35 minutes of the experiments. For an example, the fluoride concentration was decrease from 10 mg L^{-1} to 0.92 mg L^{-1} at the end of 35 minutes. Figure 6.4b shows variation of iron concentration with time during the EC process. It was also observed that concentration was decreased with time. The final concentration of iron was at the recommendable limit after 45 minutes of the experiments. For an example the iron concentration was declined from 25 mg L^{-1} to 0.3 mg L^{-1} at the end of 45 minutes. Similar trend of concentration declination was also observed for arsenic as shown in Fig. 6.4c. The arsenic concentration was found to be declined from 200 μg L^{-1} to 10 μg L^{-1} at the end of 42 minutes of EC operation. In summary, from figures 6.4a to 6.4c it may be concluded that the concentrations of fluoride, iron and arsenic in treated water was below the WHO limit after 40 minutes of EC process.

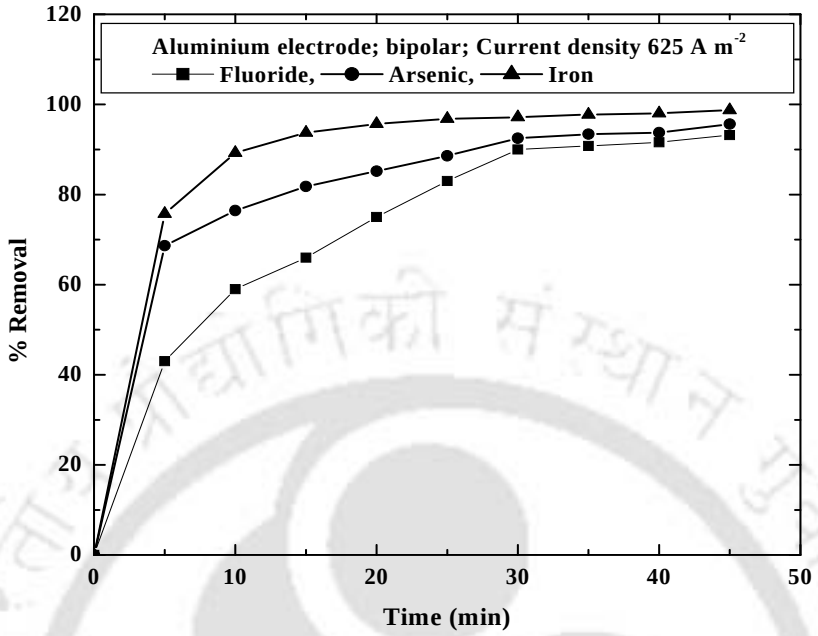

Fig.6.3 Percentage removal of fluoride, iron and arsenic from their mixture during EC process.

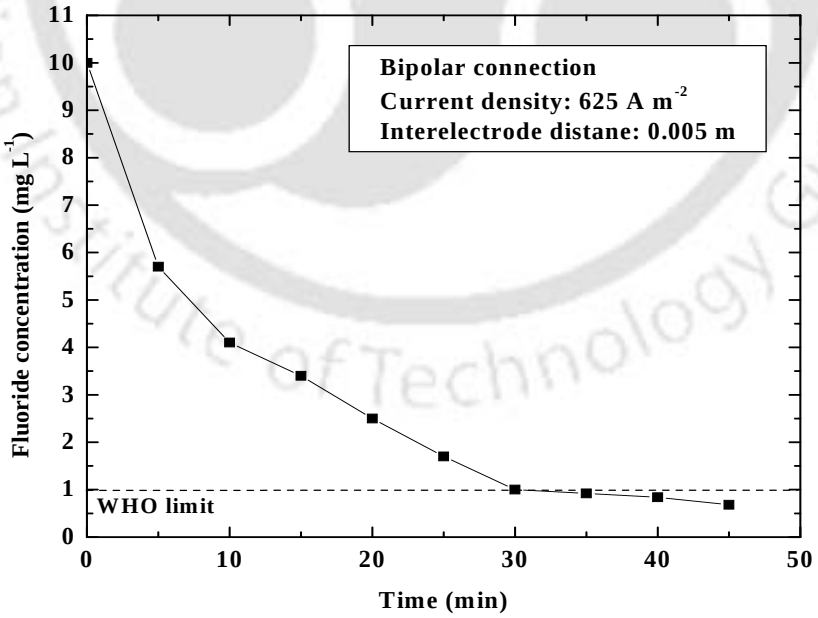

Fig.6.4a Concentration of fluoride from the mixture of fluoride, iron and arsenic during the EC process.

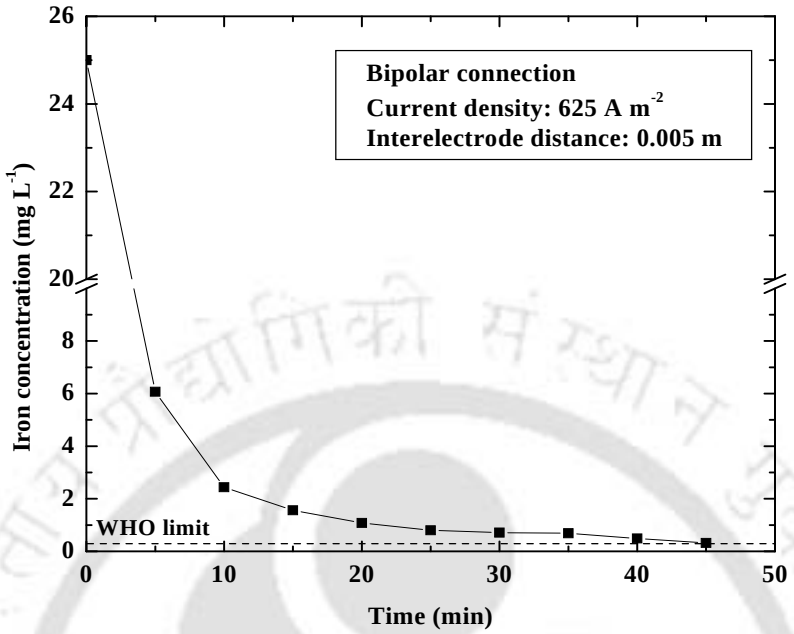

Fig.6.4b: Concentration of iron from the mixture of fluoride, iron and arsenic during the EC process.

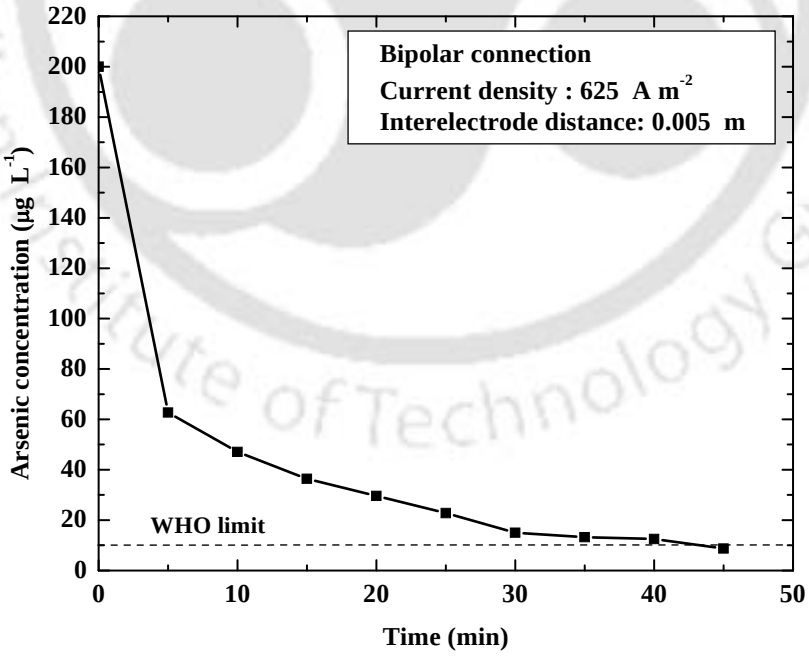

Fig.6.4c: Concentration of arsenic from the mixture of fluoride, iron and arsenic during the EC process.

6.3.3 Permeate flux profile after MF experiments

The electrocoagulated solution was subjected to microfiltration at conditions mentioned in section 6.2. Permeate flux and quality was measured and analyzed. Figure 6.5 shows the permeate flux profile during MF. It was observed that the permeate flux was declined with time for all the operating pressure differentials. For an example at 101.3 kPa the permeate flux was declined from 3.87 x 10^{-6} to 1.7 x 10^{-6} m^3 m^{-2} sec^{-1} at the end of 45 minutes of MF experiment. The similar trend was also noticed for the experiments operated at 41 and 202 kPa. In such cases the flux was declined from 2.95 x 10^{-5} to 1.52 x 10^{-5} m^3 m^{-2} sec^{-1} and from 4.79 x 10^{-6} to 1.93 x 10^{-6} m^3 m^{-2} sec^{-1}, for the transmembrane pressure differentials of 41 and 202 kPa, respectively. It can be found that at higher pressure differentials, the flux declination was more. The permeate flux were found to be declined 48.47% and 56.07% at the end of 45 minutes of MF at 41 and 101.3 kPa, respectively. The decline in flux with time is due to the fact that the deposition of suspended particles over the membrane surface restrict the permeate flux by blocking the active pores of the membranes. With time amount of sludge deposition becomes more which causes the lower permeate flux. Again, increase in permeate flux with pressure is due to the more driving force.

The quality of electrocoagulated solution and permeate after MF was measured in terms of conductivity, pH, total dissolve solids (TDS) and concentrations of fluoride, iron and arsenic and shown in Table 6.1. It may be seen that after electrocoagulation treatment, the final concentration of all the contaminants were at their respective safety limit recommended by WHO. However, the solution pH, TDS and conductivity were beyond

the recommendable limit. It was noticed that the pH was around 8.6 while conductivity and TDS were found 0.34 mS cm^{-1} and 1325 mg L^{-1}, respectively, after the EC treatment for 45 minutes. Hence, the treated water could not be used for drinking purpose after EC. Furthermore, the suspended particles generated during the treatment as discussed earlier also reflected the improper quality of treated water for drinking purpose.

Therefore, after the completion of EC, a further treatment was necessary to retain the drinking water quality in terms of pH, conductivity and TDS as specified in the Table 6. 1. In view to this, microfiltration was considered as an alternative in combination with the EC treatment to overcome the situation. It was observed that after the MF treatment, the pH, conductivity and TDS were found 7.9, 0.2 mS cm^{-1} and 580 mg L^{-1}, respectively.

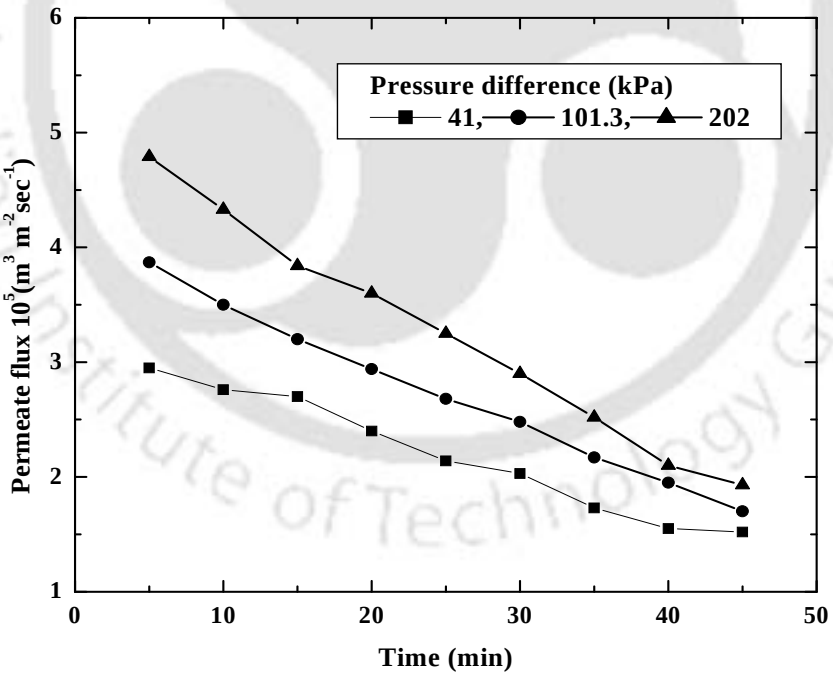

Fig 6.5 Flux declination of the treated drinking water with iron, fluoride and arsenic contamination by electrocoagulation followed by ceramic microfiltration membrane at different pressures

It was also observed that there were no noticeable changes in the final concentrations of fluoride, iron and arsenic in the permeate collected after the MF treatment. It was finally confirmed that electrocoagulation followed by microfiltration for the treatment of water with fluoride, iron and arsenic contamination could be an effective alternative to combat with the drinking water problem associated with such type of contamination in near future.

Table 6.1: Quality of electrocoagulated solution and permeate of MF

Parameters	**After electrocoagulation**	**After microfiltration**	**Drinking water specification [21]**
pH	8.6	7.8	6.5-8.2
Conductivity (mS cm^{-1})	0.34	0.2	0.2 -2.0
TDS (mg L^{-1})	1325	580	500-700
Concentration of fluoride (mg L^{-1})	0.8	0.8	1
Concentration of iron (mg L^{-1})	0.3	0.3	0.3
Concentration of arsenic (μg L^{-1})	8.7	8.7	10

6.4 Characterization of membranes and by-products

Characterization of MF membrane (before and after experiment)

In addition to this, SEM analysis of the membrane before and after the use for the specific purpose was taken at 2KX magnification which confirmed the successful retention of the electrocoagulated sludge by the ceramic microfiltration membrane

prepared by uni-axial cold pressing at 950 ^{o}C. Figure 6.6 (a) shows the SEM images of such membrane before use which had its morphological structure enough consolidated to retain the particles bigger than the pore sizes as can be visualized from the dimension of pores. Figure 6.6 (b) clearly shows the morphological outlook of the used membrane at the same magnification to clarify the successful retention of agglomerated sludge generated during the electrocoagulation treatment of contaminated drinking water. Apart from this, it was also clear from the image that almost all the agglomerates were trapped over the membrane surface and therefore hardly any active pores could be visible.

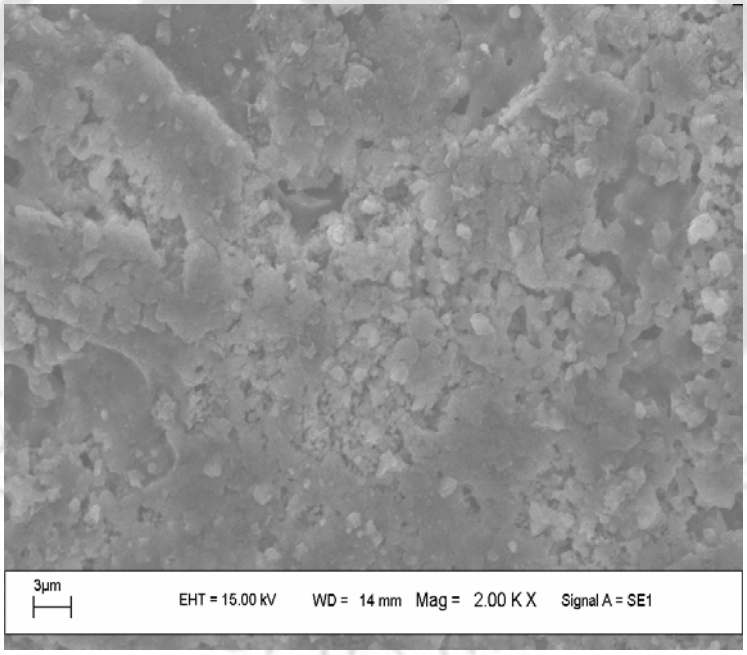

(a)

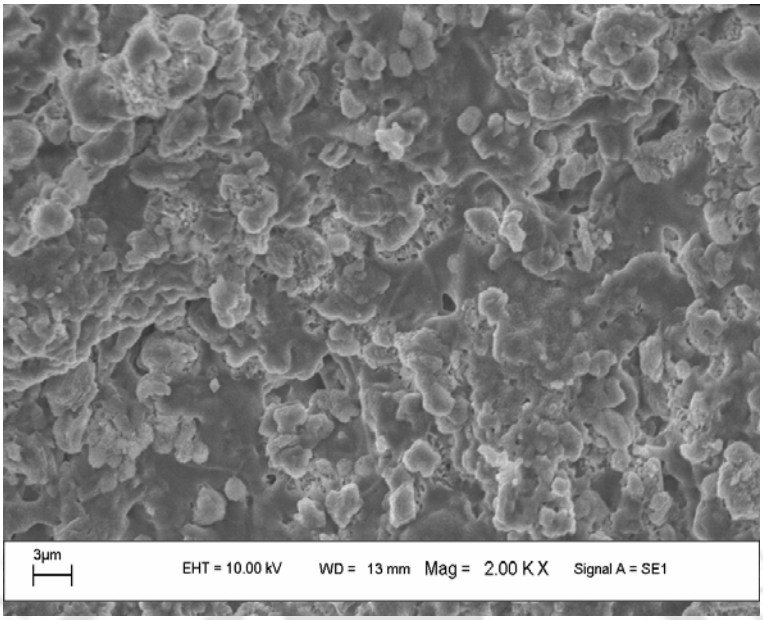

(b)

Fig 6.6 SEM images of the ceramic microfiltration membrane (a) before and (b) after the filtration of electrocoagulated sludge.

By-product characterization

The agglomerated sludge was successfully entrapped by the ceramic microfiltration membrane and taken out of the membrane surface after the filtration treatment by scrubbing for their characterization in order to ensure the removal of the contaminants from the drinking water efficiently. The collected sludge from the membrane surface was dried inside a hot air oven for 3 - 4 hours to remove mostly the unbounded moisture in it. After the completion of drying, it was observed that several lumps of dried solid were left. These lumps were grinded to powder and made ready for the XRD, SEM and EDX analyses for their characterization.

XRD analysis showed broad peaks with noise due to the interference of irregular reflection of the reflected monochromatic light beam throughout the prescribed 2θ (°)

range during the analysis and thus confirmed the amorphous nature of the sludge generated during the electrocoagulation treatment and retained by the ceramic microfiltration membrane thereafter. Figure 6.7 shows the XRD analysis of the sample as described above.

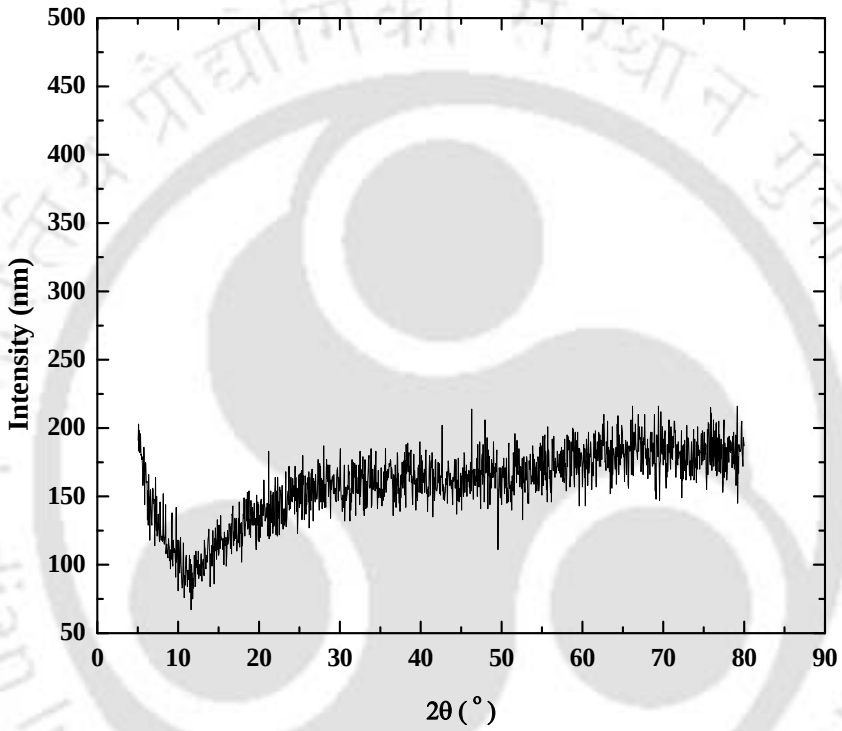

Fig 6.7: Characterization images of the electrocoagulated by-product retained by the ceramic microfiltration membrane by XRD

The sample was also subjected for the SEM analysis to get the confirmation about the amorphous nature of the product from its morphological overview. Figure 6.8 supported the amorphous nature that was observed during XRD that no definite shape and size of particles were noticed in the morphological view even at the 2KX magnification with

primary electrons hitting the sample at an energy level of 10 kV without charging of the main sample during the analysis.

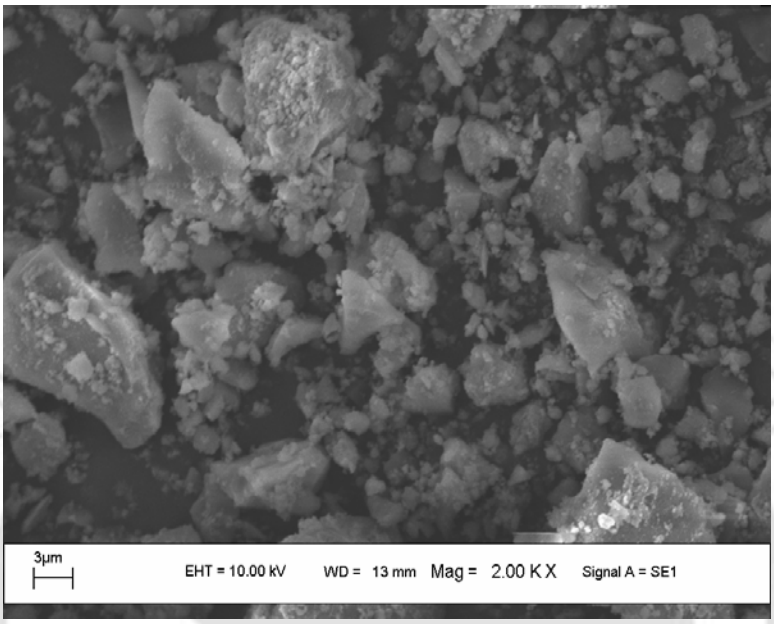

Fig 6.8 SEM images of the electrocoagulated by-product retained by the ceramic microfiltration membrane

Nevertheless, the EDX analysis of the same sample prominently provided a qualitative insight about the elements. Figure 6.9 clearly indicates the presence of elements like iron (Fe), aluminium (Al), fluoride (F) and arsenic (As) in particular of our interest along with carbon (C) that was mainly due to the carbon black tape used to hold the sample in position during the analysis. This observation undoubtedly justifies the successful entrapment of contaminants like iron, fluoride and arsenic from the drinking water treated by electrocoagulation followed by membrane filtration, thereby supports the potential of the hybrid process to remove such contaminants effectively from drinking water.

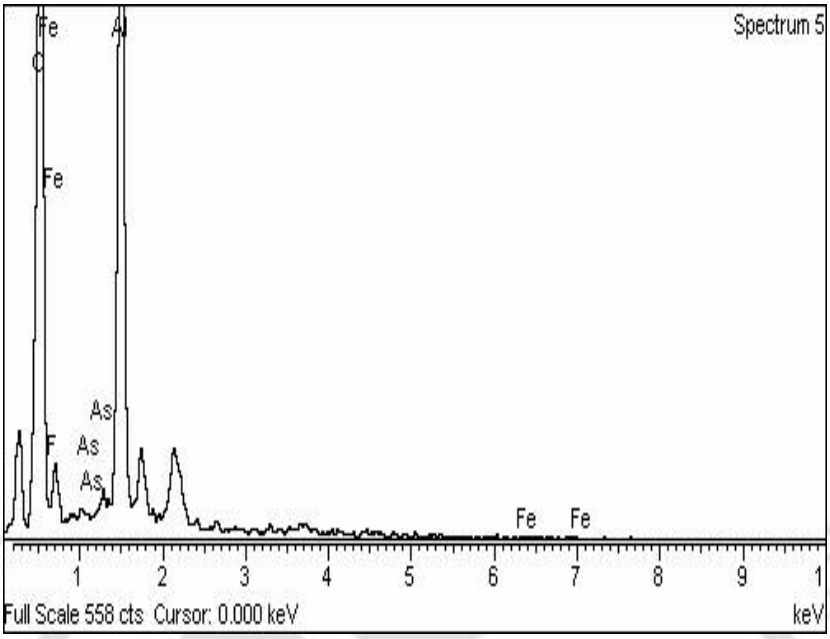

Fig 6.9: EDX analysis of the electrocoagulated by-product retained by the ceramic microfiltration membrane

6.5 Summary

The drinking water contaminated with significant amount of iron, fluoride and arsenic was treated by electrocoagulation followed by microfiltration technique. In this investigation, aluminium sheet electrodes with bipolar connection and ceramic microfiltration membrane prepared by uni-axial cold pressing were used in electrocoagulation and membrane filtration, respectively. The followings are the excerpts of the present investigation:

1) Drinking water contamination caused by the significant presence of iron, fluoride and arsenic was successfully monitored by the bi-polar electrocoagulation for 45 minutes at 625 A m^{-2}current density and at an interelectrode distance of 0.005 m.

2) Electrocoagulation performance was estimated in terms of the percentage removal of fluoride, iron and arsenic as 93.2%, 99.74% and 95.65%, respectively.

3) Electrocoagulated water solution was improper for drinking purpose unless was treated further combining with another technique such as microfiltration (MF). This combination process produced water of drinkable quality with pH 7.9 and conductivity of 0.2 mS cm^{-1}.

4) Ceramic microfiltration membrane prepared by uni-axial cold pressing method followed by sintering at 950 °C was beneficial for the MF treatment of the electrocoagulated water. .

5) SEM analysis of the ceramic microfiltration membrane used for the MF treatment of electrocoagulated water confirmed the successful retention of suspended agglomerates generated during EC treatment.

6) XRD, SEM and EDX analysis of the by-product taken out of the ceramic microfiltration membrane after the treatment clearly supported the successful removal of contaminants from the drinking water by electrocoagulation followed by ceramic microfiltration.

All the above mentioned findings might be useful for the further advancement of the hybrid technique to design a drinking water treatment system in continuous mode.

Chapter 7

Conclusions and scope of future works

Drinking water contamination due to the presence of fluoride, iron and arsenic threatens the current civilization from suffering incurable diseases such as skin cancer, fluorosis, hyper-pigmentation and many others in recent times. Different techniques were reported in the literatures along with their own benefits and limitations. This work presents electrocoagulation followed by microfiltration technique in order to improve the process performance as well as the output quality of drinking water. Furthermore, it was also claimed that such hybrid process with its cost-effective characteristic could be well directed towards designing a drinking water treatment plant in continuous mode. Therefore, this chapter is strongly advocated by the facts observed during the effective removal of fluoride, iron and arsenic contamination in drinking water by a hybrid technique (electrocoagulation followed by microfiltration). In addition, this section is also aimed at extending the ideas and initiatives for the future perspective of the work. The entire work was broadly divided into three parts. Firstly, electrocoagulation as well as the primary variables of the process such as electrocoagulation time, interelectrode distance, current density, pH, and feed concentration was investigated in detail along with the economical analysis for the removal of fluoride, iron and arsenic from drinking water. Secondly, preparation and characterization of ceramic microfiltration membranes in order to separate the electrocoagulated sludge in an effective manner. Finally, the work was stretched to build up a hybrid technique (electrocoagulation followed by microfiltration)

for the optimistic regulation of fluoride, iron and arsenic from drinking water. The first phase of the work was described in chapters 2 and 3. The second phase was elaborated in chapters 4 and 5 while the final phase of the work was explained well in the chapter 6. The whole work can be summarized on the basis of the following conclusions.

Electrocoagulation

1. Electrocoagulation (EC) technique was investigated in batch mode for the removal of fluoride, iron and arsenic from drinking water using monopolar and bipolar electrode connections.
2. Variation of different operating parameters such as, current density, inter electrode distance, time of EC and initial concentration of fluoride, iron and arsenic were investigated separately in detail.
3. Interelectrode distance of 0.005 m and current density of 625 A m^{-2} were found to be most effective variables for the removal of above mentioned contaminants.
4. The results showed that the performance of EC in terms of percentage removal of fluoride, iron and arsenic were increased with the increase in current density but decreased with inter electrode distance.
5. The results also confirmed that the bipolar connection can serve better removal than the monopolar connection. For example, the removal of arsenic were 78 % and 83 % for monopolar and bipolar, respectively for the initial arsenic concentration of 10 $\mu g\ L^{-1}$.
6. The operating cost for the removal of fluoride, iron and arsenic were calculated and presented well. The simplified cost equation was adopted to evaluate the operating cost. As for example, the total operating costs for monopolar and

bipolar connections were 0.38 and 0.62 US$ m^{-3}, respectively, for the initial fluoride concentration of 10 mg L^{-1}

7. Electrocoagulation was able to remove 93.2% fluoride, 98.74% iron and 95.65% arsenic from the mixture composed of 10 mg L^{-1} of fluoride, 25 mg L^{-1} of iron and 200 μg L^{-1} of arsenic, respectively from drinking water using bipolar electrode connection in 45 minutes. However, the solution pH (>8.5) was not recommended for drinking along with the presence of suspended agglomerates. Therefore, electrocoagulation is to be combined with other cost effective separation techniques to improve the water quality.

Membrane fabrication

1. Microfiltration was thought to be an effective measure in combination with the electrocoagulation to make electrocoagulated water drinkable. Hence, ceramic membranes were prepared by two well-known methods, viz. paste method and uni-axial cold pressing method. Membranes were sintered at 750 ^{o}C, 800 ^{o}C, 850 ^{o}C, 900 ^{o}C and 950 ^{o}C.
2. Prepared membranes were characterized by SEM, and XRD analysis. Pore size distribution and surface porosity were determined for all the membranes sintered at different temperatures. It was found that the membranes prepared by uni-axial cold pressing were less porous than the membranes prepared by the paste method. This observation was also supported by the porosity and surface pore density measurement.

3. The average pore diameter was 1.58 and 1.14 μm calculated from the pore size distribution of the ceramic microporous membranes prepared by paste and uni-axial cold pressing method, respectively at sintering temperature of 950 °C. Again, pore size distribution was found to be narrower with the increase in temperature for all the membranes.

4. The total estimated membrane cost including raw materials cost and energy consumption cost was found to be around 172.7 US$/m^2 and 197.82 US$/m^2 for ceramic microporous membranes prepared by paste and uni-axial cold pressing method, respectively. The higher membrane cost prepared by uni-axial method was due to the requirement of more amount of ceramic precursor than that required by paste method for the same size of membrane.

5. Although membrane cost was more in uni-axial method but this technique is recommended considering the ease of preparation methods, lower average pore diameter and narrower pore size distribution.

6. XRD, SEM and EDX analysis of the by-product taken out from the surface of the ceramic microfiltration membrane clearly supported the successful removal of contaminants as well as suspended particles from the drinking water. Hence, electrocoagulation followed by membrane filtration of another 45 minutes ensured the treated water to be used for drinking purpose.

Electrocoagulation followed by microfiltration

1. Fluoride, iron and arsenic contamination in drinking water was successfully treated by combination of electrocoagulation and microfiltration processes. The hybrid process removes fluoride, iron and arsenic to their respective acceptable limit. The pH, conductivity and TDS are also remained within the permissible limit.
2. Finally, the findings of the present study might be useful in order to treat the fluoride, iron and arsenic contaminated water for drinking purpose effectively and further advancement in designing a hybrid technique (electrocoagulation followed by microfiltration) for the treatment of fluoride, iron and arsenic rich ground water.

Future scope of the work

This work presents a hybrid technique for the removal of fluoride, iron and arsenic from drinking water using electrocoagulation followed by microfiltration. Details of electrocoagulation, microfiltration membrane preparation and microfiltration experiments along with all experimental findings are explained well. The future scopes of the work are as follows:

1. The proposed hybrid technique may be investigated to remove other contaminant of drinking water like heavy metals such as lead, mercury, cadmium.
2. Treatment of different industrial waste waters may be conducted using electrocoagulation followed by microfiltration technique.

3. A continuous system of the hybrid process for the treatment of waste waters may be a further scope of work.
4. Kinetic study for the EC and MF would be helpful for the prediction of performance of both the process.
5. Scaling up the existing process after investigating the process variables in wider range.
6. Preparation of cost effective ceramic microfiltration membrane either by changing compositions or by surface modification of the existing membrane through different coating techniques.
7. Detailed investigation of different combinations of other techniques like adsorption, precipitation, ion exchange, etc would be undoubtedly the furthermore realistic contribution to the advancement along with their comparative cost analysis.
8. By products obtained in the EC bath is really a problem from the environmental view point. Either a suitable treatment technology or proper utilization of the by products have to be developed. This would also be an additional scope of research.

References

[1] F. Anwar, Assessment and analysis of industrial liquid waste and sludge disposal at unlined landfill sites in arid climate, Waste Manage. 23 (9) (2003) 817–824.

[2] A. Liu, J. Ming, R.O. Ankumah, Nitrate contamination in private wells in rural Alabama, United States, Sci. Tot. Environ. 346 (1–3) (2005) 112–120.

[3] C.N. Mulligan, R.N.Yong, B.F. Gibbs, Remediation technologies for metal contaminated soils and groundwater: an evaluation, Eng. Geol. 60 (1–4) (2001) 193–200.

[4] R. Singh, R.C. Maheshwari, Defluoridation of drinking water–a review, Ind. J. Environ. Protec. 21 (11) (2001) 983–991.

[5] Meenakshi, V.K. Garg, Kavita, Renuka, A. Malik, Ground water quality in some villages of Haryana, India: focus on fluoride and fluorosis, J. Hazard. Mater. B 106 (2004) 85–97.

[6] S.R. Sengupta, B. Pal, Iodine and fluoride content of foodstuffs, Indian J. Nutr. Dicter. 8 (1971) 66–71.

[7] M.C. Bell, T.G. Ludwig, The supply of fluoride to man: ingestion from water, in: Fluorides and Human Health,WHOMonograph Series 59,World Health Organization, Geneva, 1970.

[8] N. Mameri, A.R. Yeddou, H. Lounici, H. Grib, D. Belhocine, B. Bariou, Defluoridation of septentrional Sahara water of North Africa by electrocoagulation process using bipolar aluminium electrodes, Water Res. 32 (5) (1998) 1604–1610.

[9] W.E. Shortt, Endemic fluorosis in Nellore District, South India, Ind. Med. Gazette (1937) 72–396.

[10] A.K. Susheela, Fluorosis management programme in India, Curr. Sci. 77 (10) (1999) 1250–1256.

[11] D. Ghosh, H. Solanki, M. K. Purkait, Removal of Fe (II) from tap water by electrocoagulation technique, J. Hazard. Mater.155 (2008) 135–143

[12] National Research Council. Recommended dietary allowances, 10th Ed. Washington, DC,National Academy Press, 1989.

[13] B. Das, J. Talukdar, S. Sarma, B. Gohain, R. K. Dutta, H. B. Das, S. C. Das, Fluoride and other inorganic constituents in groundwater of Guwahati, Assam, India, Current Science, 85 (5) (2003) 657 - 661

[14] C.F. Harvey, C.H. Swartz, A.B.M. Badruzzaman, N. Keon-Blute, W. Yu, M.A. Ali, J. Jay, R. Beckie, V. Niedan, D. Brabander, P.M. Oates, K.N. Ashfaque, S. Islam, H.F. Hemond and M.F. Ahmed, Arsenic mobility and groundwater extraction in Bangladesh, Science 298 (2002) 1602–1606

[15] R. S. Oremland, J.F. Stolz, Ecology of arsenic, Science 300 (2003) 939–944.

[16] L.C.D. Anderson and K.D. Bruland, Biochemistry of arsenic in natural waters: the importance of methylated species, Environ. Sci. Technol. 25 (1991) 420–429.

[17] M. Leist, R.J. Casey and D. Caridi, The management of arsenic wastes: problems and prospects, J. Hazard. Mater. 76 (2000) 125–138.

[18] L.S. McNeill and M. Edwards, Predicting arsenate removal during metal hydroxide precipitation, J. AWWA 89 (1997) 75–86

[19] D.K. Nordstrom and C.N. Alpers, Negative pH, efflorescent mineralogy, and consequences for environmental restoration at the Iron Mountain Superfund Site, California, Proc. Natl. Acad. Sci. U.S.A. 96 (1999) 3455–3462.

[20] S. Banga, M.D. Johnson, G.P. Korfiatisa and X. Meng, Chemical reactions between arsenic and zero-valent iron in water, Water Res. 39 (2005) 763–770.

[21] WHO (World Health Organization), Guidelines for Drinking Water Quality (vol. II): Health Criteria and Supporting Information, World Health Organization, Geneva, Switzerland, (1984).

[22] US Public Health Service DrinkingWater Standards,USGovernment Printing Office, Department of Health Education andWelfare,Washington, DC, (1962).

[23] S.L. Choubisa, K. Sompura, Dental fluorosis in tribal villages of Dungerpur district (Rajasthan), Poll. Res. 15 (1) (1996) 45–47.

[24] R. Green, R. Charlton, H. Seftel, T. Bothwell, F. Mayet, Body iron excretion in man. A collaborative study. American J. of medicine, 45 (1968) 336-353.

[25] C. A. Finch, E. R. Monsen, Iron nutrition and the fortification of food with iron, J. of the American Medical Asso., 219 (1972)1462-1465.

[26] S. Bhattacharjee, S. Chakravarty, S. Maity, V. Dureja and K.K. Gupta, Metal contents in the ground water of Sahebgunj district, Jharkhand, India, with special reference to arsenic, Chemosphere 58 (2005) 1203–1217.

[27] R.T. Nickson, J.M. McArthur, B. Shrestha, T.O. Kyaw-Myint and D. Lowry, Arsenic and other drinking water quality issues, Muzaffargarh District, Pakistan, Appl. Geochem. 20 (2005) 55–68.

[28] M. Berg, H.C. Tran, T.C. Nguyen, H.V. Pham, R. Schertenleib and W. Giger, Arsenic contamination of ground water and drinking water in Vietnam: a human health threat, Environ. Sci. Technol. 35 (2001) 2621–2626.

[29] T. Yoshida, H. Yamanchi and G.F. Jun, Chronic health effect in people exposed to arsenic via the drinking water: dose–response relationship in review, Toxicol. Appl. Pharmacol. 198 (2004) 243–252.

[30] X. Wu, Y. Zhang, X. Dou, M. Yang, Fluoride removal performance of a novel Fe-Al-Ce trimetal oxide adsorbent, Chemosphere 69 (2007) 1758-1764.

[31] V.K. Gupta, I. Ali, V.K. Saini, Defluoridation of waste waters using waste carbon slurry, Water Res. 41 (2007) 3307-3316.

[32] M. Srimurali, A. Pragathi, J. Karthikeyan, A study on removal of fluorides from drinking water by adsorption onto low-cost materials, Env. Pollution 99 (1998) 285-289.

[33] Z. Amor, B. Bariou, N. Mameri, M. Taky, S. Nicolas, A. Elmidaoui, Fluoride removal from brakish water by electrodialysis, Desalination 133 (2001) 215-223.

[34] M. Hichour, F. Persin, J. Sandeaux, C. Gavach, Fluoride removal from waters by Donnan dialysis, Sep. Purif. Technol. 18 (2000) 1-11.

[35] K. Hu, J.M. Dickson, Nanofiltration membrane performance on fluoride removal from water, J. Membr. Sci. 279 (2006) 529-538.

[36] A. Tor, Removal of fluoride from water using anion-exchange membrane under Donnan dialysis condition, J. Hazard. Mater. 141 (2007) 814-818.

[37] H. Garmes,F. Persin, J. Sandeaux, G. Pourcelly, M. Mountadar, Defluoridation of groundwater by a hybrid process combining adsorption and Donnan dialysis, Desalination 145 (2002) 287-291.

[38] J. Zhu, H. Zhao, J. Ni, Fluoride distribution in electrocoagulation defluoridation process, Sep. Purif. Technol. 56 (2007) 184-191.

[39] M.M. Emamjomeh, M. Sivakumar, An empirical model for defluoridation by batch monopolar electrocoagulation/flotation (ECF) process, J. Hazard. Mater. 131 (2006) 118-125.

[40] K. Vaaramaa, J. Lehto, Removal of metals and anions from drinking water by ion exchange, Desalination. 155 (2003) 157-170.

[41] R. Munter, H. Ojaste, J. Sutt, Complexed iron removal from ground water, J. Env. Eng. 131 (2005) 1014-1020.

[42] W. C. Andersen, T. J. Bruno, Application of gas–liquid entraining rotor to supercritical fluid extraction: removal of iron(III) from water, Anal. Chim. Acta 485 (2003) 1–8.

[43] P. Berbenni, A. Pollice, R. Canziani, L. Stabile, F. Nobili, Removal of iron and manganese from hydrocarbon-contaminated groundwaters, Bioresour. Technol. 74 (2000) 109–114.

[44] H. A. Aziz, M. S. Yusoff, M. N. Adlan, N. H. Adnan, S. Alias, Physicochemicalremoval of iron from semiaerobic landfill leachate by limestone filter, Water Manage. 24 (2004) 353–358.

[45] D. Ellis, C. Bouchard, G. Lantagne, Removal of iron and manganese from groundwater by oxidation and microfiltration, Desalination 130 (2000) 255-264.

[46] B. Das, P. Hazarika, G. Saikia, H. Kalita, D. C. Goswami, H. B. Das, S. N. Dube, R. K. Dutta, Removal of iron by groundwater by ash: a systematic study of a traditional method, J. Hazard. Mater. 141 (2007) 834-841.

[47] B. Y. Cho, Iron removal using aerated granular filter, Process Biochem. 40 (2005) 3314-3320.

[48] S. S. Tahir, N. Rauf, Removal of Fe^{2+} from the waste water of a galvanized pipe manufacturing industry by adsorption onto bentonite clay, J. of Env. Manage. 73 (2004) 285-292.

[49] J.G. Hering, P.Y. Chen, J.A. Wilkie, M. Elimelech, Arsenic removal by ferric chloride. J. Am. Water Works Assoc. 88 (1996) 155–167.

[50] S.K. Gupta, K.Y. Chen, Arsenic removal by adsorption. J. Water Pollut. Control Fed. 50 (1978) 493–506.

[51] D.A. Clifford, Ion-exchange and inorganic adsorption. Water Quality and Treatment: A Handbook of Community Water Supplies (5^{th} Ed.), American Water Works Association, McGraw-Hill, New York (1999).

[52] K. Christen, Cleaning technologies can remove arsenic, but at cost. Environ. Sci. Technol. 34 (2000) 75–79.

[53] A. Joshi, M. Chaudhuri, Removal of arsenic from ground water by iron-oxide coated sand. J. Environ. Eng. 122 (1996). 769–776.

[54] S. Bajpai, M. Chaudhuri, Removal of arsenic from ground water by manganese dioxide-coated sand., J. Environ. Eng. 125 (1999) 782–784.

[55] S. Chakravarty, V. Dureja, G. Bhattacharyya, S. Maity, S. Bhattacharjee, Removal of arsenic from ground water using low cost ferruginous manganese ore. Water Res. 36 (2002) 625–632.

[56] A. Jain, K.P. Ravene, R.H. Loeppert, Arsenite and arsenate adsorption on ferrichydrite: surface charge reduction and net OH^- release stoichiometry. Environ. Sci. Technol. 33 (1999) 1179–1184.

[57] A. Manning, S. Goldberg, Adsorption and stability of arsenic(III) at the clay mineral–water interface. Environ. Sci. Technol. 31 (1997) 2005–2011.

[58] S. Fendorf, M. Eick, P. Grossl, D.L. Sparks, Arsenate and chromate reduction mechanisms on goethite. 1. Surface structure. Environ. Sci. Technol. 31 (1997) 315–320.

[59] B. Krishna, K. Chadrasekaran, D. Karunasagar, J. Arunachalam, A combined treatment approach using Fenton's reagent and zero-valent iron for the removal of arsenic from drinking water. J. Hazard. Mater. 84 (2001) 229–240.

[60] M. Edwards, Chemistry of arsenic removal during coagulation and Fe–Mn oxidation. J. Am. Water Works Assoc. 86 (1994) 64–78.

[61] W.J. Farrell, O.D. Peggy, M. Colklin, Electrochemical and spectroscopic study of arsenate removal from water using zero-valent ion media. Environ. Sci. Technol. 35 (2001) 2026–2032.

[62] E. Kartinen, J.C.J. Martin, An overview of arsenic removal processes, Desalination 103 (1995) 79–88.

[63] N.S. Abuzaid, A.A. Bukhari, Z.M. Al-Hamouz, Removal of bentonite causing turbidity by electrocoagulation. J. of Env. Sci. and Health Part A: 33 (7) (1998) 1341-1358.

[64] B.M. Belongia, P.D. Haworth, J.C. Baygents, S. Raghavan, Treatment of alumina and silica chemical mechanical polishing waste by electrodecantation and electrocoagulation. J. of the Electrochemical Society 146 (11) (1999) 4124 - 4130.

[65] M.J. Matteson, R.L. Dobson, R.W.J. Glenn, N.S. Kukunoor, W.H.I Waits, E.J. Clayfield, Electrocoagulation and separation of aqueous suspensions of ultrafine particles. Colloids and Surf. A: Physicochemical and Engineering Aspects 104 (1995) 101-109.

[66] J.S. Do, M.L. Chen, Decolourization of dye-containing solutions by electrocoagulation. Journal of Applied Electrochemistry 24 (8) (1994) 785-790.

[67] J.G. Ibanez, M.M. Singh, Z. Szafran, Laboratory Experiments on Electrochemical remediation of the environment. Part 4: color removal of simulated wastewater by electrocoagulation-electroflotation. J. of Chem. Edu. 75 (1998), 1040-1041.

[68] M. Kashefialasl, M. Khosravi, M. Seyyedi, Treatment of dye solution containing colored index acid yellow 36 by electrocoagulation using iron electrodes, Int. J. Environ. Sci. Tech., 2 (2005) 365-371.

[69] A.K. Golder, N. Hridaya, A.N. Samanta, S. Ray, Electrocoagulation of methylene blue and eosin yellowish using mild steel electrodes, J. Hazard. Mater., 127 (2005) 134–140.

[70] N. Daneshwar, A. Oladegarazope, N. Djafarzadeh, Decolorization of basic dye solutions by Electrocoagulation: An investigation of the effect of operational parameters, J. Hazard. Mater., 129 (2006)116-122.

[71] V.Y. Baklan, I. Kolesnikova, Influence of electrode material on the electrocoagulation. J. of Aerosol Sci., 27 (1996) S209-S210.

[72] M.F. Pouet, A. Grasmick, Urban wastewater treatment by electrocoagulation and flotation. Water Sci.and Technol., 31 (3-4) (1995) 275- 283.

[73] M.F. Pouet, A Grasmick, A. Electrocoagulation and Flotation: Applications in crossflow microfiltration. Filtration and Separation 31 (1994) 269-272.

[74] E.A. Vik, D.A. Carlson, A.S. Eikun, E.T. Gjessing, Electrocoagulation of potable water. Water Res., 18 (11) (1984) 1355-1360.

[75] M. Kobya, E. Senturk, M. Bayramoglu, Treatment of poultry slaughterhouse waste waters by Electrocoagulation, J. Hazard. Mater, 123 (2006) 172-176.

[76] L.M. Balmer, A.W. Foulds, Separating oil from oil-in-water emulsions by electroflocculation / electroflotation, Filtration and Sep., 23 (6)(1986) 366-370.

[77] S. Rubach, I.F. Saur, Onshore testing of produced water by electroflocculation, Filtration and Sep., 34 (8) (1997) 877-882.

[78] D.L. Woytowich, C.W. Dalrymple, F.W. Gilmore, M.G. Britton, Electrocoagulation (CURE) Treatment of Ship Bilge water for the U.S. coast guards in Alaska, Marine Technol. Society J., 27 (1) (1993) 62-67.

[79] N. Mameri, H. Lounici, D. Belhocine, H. Grib, D.L. Piron, Y. Yahiat, Defluoridation of Sahara water by small plant electrocoagulation using bipolar aluminium electrodes, Sep. and Purif. Technol., 24 (1-2) (2001) 113-119.

[80] N. Mameri, A.R. Yeddou, H. Lounici, D. Belhocine, H. Grib, B. Bariou, Defluoridation of septentrional Sahara water of North Africa by electrocoagulation process using bipolar aluminium electrodes, Water Res. 32 (5) (1998) 1604-1612.

[81] P.R. Kumar, S. Chaudhuri, K.C. Khilar, S.P. Mahajani, Removal of arsenic from water by electrocoagulation, Chemosphere, 55 (2004) 1245 – 1252.

[82] R.D. Letterman, A. Amirtharajah, C.R. O'Melia, Coagulation and Flocculation. In Water Quality and Treatment, A Handbook of community water supplies (Eds, Letterman, R. D. and American Water Works Association) McGraw-Hill, New York.(1999)

[83] J.C. Donini, J. Kan, J. Szynkarczuk, T.A. Hassan, K.L. Kar, Operating cost of electrocoagulation. Canadian Journal of Chemical Engineering 72 (6) (1994) 1007-1012.

[84] D. Ghosh, C. R. Medhi, M. K. Purkait, Treatment of fluoride contaminated drinking water by electrocoagulation using monopolar and bipolar electrode connection, Chemosphere, 73 (2008) 1393 – 1400.

[85] C.F. Baes, R.E. Mesmer, The Hydrolysis of Cations, Krieger Publishing Company, Malabar, Florida, (1976).

[86] N. Daneshwar, A. Oladegarazope, N. Djafarzadeh, Decolorization of basic dye solutions by Electrocoagulation: An investigation of the effect of operational parameters, J. Hazard. Mater. 129 (2006) 116-122.

[87] M.J. Matteson, R.L. Dobson, R.W.J Glenn, N.S. Kukunoor, W.H.I. Waits, E.J. Clayfield, Electrocoagulation and separation of aqueous suspensions of ultrafine

particles. Colloids and Surf. A: Physicochemical and Engineering Aspects 104 (1995) 101-109.

[88] R.J. Petersen, Composite reverse osmosis and nanofiltration membranes, J. Membr. Sci. 83 (1993) 81–150.

[89] I.C. Escobar, S. Hong, A. Randall, Removal of assimilable and biodegradable dissolved organic carbon by reverse osmosis and nanofiltration membranes, J. Membr. Sci. 175 (2000) 1–17.

[90] D.E. Potts, R.C. Ahlert, S.S. Wang, A critical review of fouling of reverse osmosis membranes, Desalination 36 (1981) 235–264.

[91] Q. Li, M. Elimelech, Synergistic effects in combined fouling of a loose nanofiltration membrane by colloidal materials and natural organic matter, J. Membr. Sci. 278 (2006) 72–82.

[92] P. H¨orsch, A. Gorenflo, C. Fuder, A. Deleage, F.H. Frimmel, Biofouling of ultra- and nanofiltration membranes for drinking water treatment characterized by fluorescence *in situ* hybridization (FISH), Desalination 172 (2005) 41–52.

[93] T.F. Speth, A.M. Gusses, R.S. Summers, Evaluation of nanofiltration pretreatments for flux loss control, Desalination 130 (2000) 31–44.

[94] B. Van der Bruggen, J.H. Kim, F.A. DiGiano, J. Geens, C. Vandecasteele, Influence of MF pretreatment on NF performance for aqueous solutions containing particles and an organic foulant, Sep. Purif. Technol. 36 (2004) 203–213.

[95] D. Babra, P. Caputi, D.S. Cifoni, Drinking water supply in Italy, Desalination 113 (1997) 111–117.

[96] Meenakshi, R.C. Maheshwari, S.K. Jain, A. Gupta, Use of membrane technique for potable water production, Desalination 170 (2) (2004) 105–112.

[97] K. A. DeFriend, M. R. Wiesner, A. R. Barron, Alumina and aluminate ultra-filtration membranes derived from alumina nanoparticles, J. Membr. Sci., 224 (2003) 11 - 28.

[98] T. V. Gestel, C. Vandecasteele, A. Buekenhoudt , C. Dotremont, J. Luyten , R. Leysen , B. V. Bruggen , G. Maesc, Alumina and titania multilayer membranes for nanofiltration: preparation, characterization and chemical stability. J. Membr. Sci., 207 (2002) 73 - 89.

[99] C. Falamaki, M. S. Afarani, A. Aghaie, Initial sintering stage pore growth mechanism applied to the manufacture of ceramic membrane supports, J.Europ. Cer. Soci., 24 (2004) 2285 - 2292.

[100] Y. H. Wang, T. F. Tian, X. Q.Liu, G. Y. Meng, Titania membrane preparation with chemical stability for very hash environments applications, J. Membr. Sci., 280 (2006) 261 - 269.

[101] Y. Yoshino, T. Suzuki, , B. N. Nair, H. Taguchi, N. Itoh, Development of tubular substrates, silica based membranes and membrane modules for hydrogen separation at high temperature, J. Membr. Sci., 267 (2005) 8 - 17.

[102] S. Sourirajan, Reverse Osmosis, Logos Press, London, (1970).

[103] S. Masmoudia, A. Larbot, H. El Feki, R. Ben Amara, Elaboration and characterisation of apatite based mineral supports for microfiltration and ultrafiltration membranes, Cer. Inter., 33 (2007) 337 - 344.

[104] N. Saffaj , S. A. Younssi , A. Albizane, A. Messouadi, M. Bouhria, M. Persin, M. Cretin, A. Larbot, Preparation and characterization of ultra-filtration membranes for toxic removal from wastewater, Desalination, 168 (2004) 259 - 263.

[105] N. Saffaj, M. Persin, S. A. Younsi, A. Albizane , M. Cretin , A. Larbot, Elaboration and characterization of micro-filtration and ultra-filtration membranes deposited on raw support prepared from natural Moroccan clay: Application to filtration of solution containing dyes and salts, Appl. Clay Sci., 31 (2006) 110 - 119.

[106] F. Bouzerara, A. Harabi, S. Achour, A. Larbot, Porous ceramic supports for membranes prepared from kaolin and doloma mixtures, J.Eur. Ceram. Soc., 26 (2006) 1663 - 1671.

[107] A. Belouatek, N. Benderdouche, A. Addou, A. Ouagued, N. Bettahar, Preparation of inorganic supports for liquid waste treatment, Micropor. and Mesopor. Mater., 85 (2005) 163 - 168.

[108] M. C. Almandoza, J. Marchese, P. Prádanos , L. Palacio , A. Hernández, Preparation and characterization of non-supported micro-filtration membranes from aluminosilicates, J. Membr. Sci., 241 (2004) 95 - 103.

[109] S. Workneh, A. Shukla, Synthesis of sodalite octahydrate zeolite-clay composite membrane and its use in separation of SDS, J. Membr. Sci., 309 (2008) 189 - 195.

[110] A Potdar, A sukla, A. Kumar, Effect of gas phase modification of analcime zeolite composite membrane on separation of surfactant by ultra-filtration, J. Membr. Sci., 210 (2002) 209 - 225.

[111] R. Das, B. K. Dutta, Permeation and Separation Characteristics of Supported Alumina and Titania Membranes, Sep. Sci. Technol., 34 (1999) 609 - 625.

[112] S. Vivanpatarakij, N. Laosiripojana, A. Arpornwichanop, S. Assabumrungrat, Performance improvement of solid oxide fuel cell system using palladium membrane reactor with different operation modes, Chem. Eng. J., 146 (2009) 112 - 119.

[113] S. Luque, D. Gómez, J. R. Álvarez, Industrial Applications of Porous Ceramic Membranes (Pressure-Driven Processes), Membr. Sci. Technol., 13 (2008)177 - 216.

[114] H.P. Hsieh, Enorganic Membranes for separation and reaction, Membrane science technology series - 3, Elsevier, 1996

[115] A.D. Dhale, V.V. Mahajani, Studies on treatment of disperse dye waste: membrane-wet oxidation process, Waste Manage. 20 (2000) 85-92.

[116] D. Abdessemed, G. Nezzal, Treatment of primary effluent by coagulation-adsorption- ultrafiltration for reuse, Desalination 152 (2002) 367-373.

[117] S.H. Lin, C.S. Wang, Treatment of high-strength phenolic wastewater by a new two-step method, J. Hazard. Mater. B90 (2002) 205-216.

[118] S.M. Ghoreishi, R. Haghighi, Chemical catalytic reaction and biological oxidation for treatment of non-biodegradable textile effluent, Chem. Eng. J. 95, (2003)163-169.

[119] I. Baudin, M. R. Chevalier, C. Anselme, S. Cornu and J. M. Laine, L'Apie and Vigneux case studies: First months of operation, Desalination 113 (1997) 273-275.

[120] J. Meier, T. Melin, L.H. Eilers, Nanofiltration and adsorption on powdered adsorbent as process combination for the treatment of severely contaminated wastewater, Desalination 146 (2002) 361-366.

[121] H.M. Pigmon, C.F. Brasquet, P.L. Cloiree, Adsorption of dyes onto activated carbon cloths: approach of adsorption mechanisms and coupling of ACC with ultrafiltration to treat colored wastewaters, Sep. and Puri,. Technol. 31 (2003) 3-11.

[122] Q. Zuoa, X. Chena,Wei Li, Guohua Chen. Combined electrocoagulation and electroflotation for removal of fluoride from drinking water J. of Hazard. Mater.159 (2008) 452–457.

[123] A. Aouni, C. Fersi, Mourad Ben Sik Ali, Mahmoud Dhahbi, Treatment of textile wastewater by a hybrid electrocoagulation/nanofiltration process. J. Hazard. Mater. (2009), doi:10.1016/j.jhazmat.2009.02.112.

[124] W. Den, C. Wang, Removal of silica from brackish water by electrocoagulation pretreatment to prevent fouling of reverse osmosis membranes. Sep. and Purif. Technol. 59 (2008) 318–325.

[125] A. Alverez-Gallegos, D. Pletcher, The removal of low level organics via hydrogen peroxide formed in a reticulated vitreous carbon cathode cell. Part 2: The removal of phenols and related compounds from aqueous effluents. Electrochim. Acta 44 (1999) 2483–2492.

[126] Y.S. Yildiz, A.S. Koparal, S. Irdemdez, B. Keskinler, Electrocoagulation of synthetically prepared waters containing high concentration of NOM using iron cast electrodes. J. Hazard. Mater. B139 (2007) 373–380.

[127] I. Linares-Hernández, C. Barrera-Díaz, G. Roa-Morales, B. Bilyeu, F. Ureña-Núñez, A combined electrocoagulation–sorption process applied to mixed industrial wastewater. J. Hazard. Mater. 144 (2007) 240–248.

[128] Bi, S., Wang, C., Cao, Q., Zhang, C., 2004. Studies on the mechanism of hydrolysis and polymerization of aluminium salts in aqueous solution: Correlations between the Core-links model and Cage-like Keggin-Al13 model. Coord. Chem. Rev. 248, 441–455.

[129] W.J. Weber, Physicochemical Processes for Water Quality Control. Wiley-Interscience, New York, (1972).

[130] W. Sung, J.J. Morgan, Kinetics and product of ferrous iron oxygenation in aqueous systems, Environ. Sci. Technol.,14(1980) 561–568.

[131] A. Gures, M. Yalcin, C. Dogar, Electrocoagulation of some reactive dyes: a statistical investigation of some electrochemical variables, Waste Manage. 22(2002) 491-499.

[132] J.M. Duan, J. Gregory, Coagulation by hydrolyzing metal salts, Adv. Colloid Interf. Sci. 10 (2003) 475-502.

[133] U. Gross, S. R*ü*diger, E. Kemnitz, K.W. Brzezinka, S. Mukhopadhyay, C. Bailey, A. Wander, N. Harrison, Vibrational analysis study of aluminium trifluoride phases, J. Phy. Chem. A 111 (2007) 5813-5819.

[134] J.A.G. Gomes, P. Daida, M. Kesmez, M. Weir, H. Moreno, J.R. Parga, G. Irwin, H. McWhinney, T. Grady, E. Peterson, D.L. Cocke, Arsenic removal by electrocoagulation using combined Al–Fe electrode system and characterization of products, J. Hazard. Mater. B139 (2007) 220-231.

[135] W. Sung, J.J. Morgan, Kinetics and product of ferrous iron oxygenation in aqueous systems, Environ. Sci. Technol. 14 (1980) 561–568.

[136] W. Stumm, G.F. Lee, Oxygenation of ferrous iron, Ind. Eng. Chem. Res. 53 (1961) 143–146.

[137] D.W. Sundstrom, H.E. Klei, Wastewater treatment, Prentice-Hall inc., Englewood Cliffs, NJ, (1979).

[138] C. Escobar, C. Soto-Salazar, M. Ines Toral, Optimization of the Electrocoagulation process for the removal of copper, lead and cadmium in natural water and simulated waste waters, J. of Environ. Manage. 81 (2006) 381-391.

[139] A. Gures, M. Yalcin, C. Dogar, Electrocoagulation of some reactive dyes: a statistical investigation of some electrochemical variables, Waste Manage. 22 (2002) 491-499.

[140] H. József, P. Klára, 'Determination of surface properties of iron hydroxide-coated alumina adsorbent prepared for removal of arsenic from drinking water', J. Colloid. Interf. Sci., Vol. 284 (1)(2005) 71-77.

[141] M.M. Jordan , M.A. Montero , S. Meseguer , T. Sanfeliu, Influence of firing temperature and mineralogical composition on bending strength and porosity of ceramic tile bodies, Appl. Clay Sci. 42 (2008) 266–271.

[142] K. Okada , H. Yoshizaki , Y. Kameshima, A. Nakajima, Effect of the crystallinity of kaolinite precursors on the properties of mesoporous silicas, Appl. Clay Sci. 41 (2008) 10–16.

[143] E. Levänen, T. Mäntylä, Effect of sintering temperature on functional properties of alumina membranes, Jr. of the Eur. Ceram. Soc. 22 (2002) 613–623.

[144] B.D. Bhide, S.A. Stern, S.A.,. A new evaluation of membrane processes enrichment of air. II. Effects of economic membrane properties. J. Membr. Sci. 62, (1991) 37–58.

[145] S.P. Nunes, K.V.Peinemann, Membrane Technology in the Chemical Industry, 1st Ed, Wiley-New York, (2001).

Error Analysis

The errors in experimentally measured quantities and in parameters calculated from those measurements are important in that they determine the accuracy of calculation and predictions using those quantities. There are two types of errors viz. systematic error and random error. Systematic errors are the results of faulty assumptions or improper experimental measuring techniques. In this work, care was taken in eliminating systematic errors by appropriately designing the experiments and adopting qualified methods for analysis of the data. On the other hand, random errors result from variation in the precision of measuring parameters and the slight variations that occur in successive measurements made by the same observer under nearly identical conditions. Random errors cannot be eliminated. The focus of the error analysis presented in this section is on the random errors.

In most of the experiments performed in this work, the quantities that are measured directly are concentrations and permeate flow rates that are used to determine the rejection (%R) and permeate flux respectively.

Error in the measurement of concentration

Concentration of fluoride in aqueous medium is determined using fluoride ion meter and that of for iron and arsenic is determined using AAS as discussed in Chapter 2. Calibration curves were prepared by taking known values of concentrations of fluoride, iron and arsenic. From the calibration curves of fluoride, iron and arsenic it is seen that the standard deviation of the predicted value from actual value of concentration is more

than 0.9917 for three different cases. Thus, every measurement of concentration in synthetic is associated with an error of 0.83 % whose effect on removal values can be ignored.

Error in the measurement of permeate flux

The errors in the values of permeate flux are related to the errors in the measurements used to calculate those values. In this section, statistical analysis is used for estimation of the uncertainty associated with the values of permeate flux. Determination of standard deviation is generally considered to be one of the best methods to estimate the uncertainty which is based on the following method:

If u_1, u_2, ..., u_N are the N results of the measurements of a particular quantity u, then the mean value of u (i.e. $\bar{u}$), is defined by

$$\bar{u} = \frac{u_1 + u_2 + ... + u_N}{N} = \frac{1}{N}\sum_{i=1}^{N} u_i \qquad \text{(III.1)}$$

The uncertainty in the result is usually expressed as "root-mean-squared-deviation", which is denoted as Δu, which is computed using the following Eq. (III.2):

$$\Delta u = \sqrt{\frac{(u_1 - \bar{u})^2 + (u_2 - \bar{u})^2 + ... + (u_N - \bar{u})^2}{N - 1}} \qquad \text{(III.2)}$$

Since in the present work, all the membranes were cleaned thoroughly after each experiment and before each experiment, the performance of all the membranes were checked through pure water flux (PWF) measurement, hence uncertainties involved in the PWF measurements are reported here.

The uncertainties involved in different experimental measurements for (PWF) for different membranes are estimated and shown in Table ER1.

Table ER1: Values of uncertainties estimated in PWF measurements for membranes prepared at 950 ^{o}C and operated at 202.65 kPa of transmembrane pressure

Membrane used	**Run 1** **WPF ($m^3m^{-2}sec^{-1}$) $\times 10^5$**	**Run 2** **WPF ($m^3m^{-2}sec^{-1}$) $\times 10^5$**	**Run 3** **WPF ($m^3m^{-2}sec^{-1}$) $\times 10^5$**	**ū** **WPF ($m^3m^{-2}sec^{-1}$) $\times 10^5$**	Δu	**Uncertainties (%)**
Paste method	34.1	34.7	33.8	34.2	0.458	1.34
Uni-axial cold pressing method	13.2	13.3	13.6	13.37	0.826	1.55

List of publications

Journal

1. **D. Ghosh**, C. R. Medhi, M. K. Purkait, Treatment of fluoride contaminated drinking water by electrocoagulation using monopolar and bipolar electrode connection, ***Chemosphere***, 73 (2008) 1393 – 1400.

2. **D. Ghosh**, H. Solanki, M. K. Purkait**,** Removal of Fe (II) from tap water by electrocoagulation technique, ***J. Haz. Mat***, 155 (2008) 135–143

3. **D. Ghosh**, M. K. Purkait**,** Treatment of Drinking Water Containing Iron Using Electrocoagulation, (Accepted, ***Int. J. Env. Waste Manage***, 2008)

4. **D. Ghosh,** C.R Medhi, M.K. Purkait, Techno economic analysis for the electrocoagulation of fluoride contaminated drinking water, (Submitted, Sep. Sci. Technol, 2009)J.

5. **D. Ghosh**, M.K. Purkait, Effect of sintering temperature on the morphological characteristic of porous ceramic membrane. (*Manuscript under preparation*).

6. **D. Ghosh**, M.K. Purkait, Treatment of fluoride, iron and srsenic containing drinking water using a hybrid technique, (*Manuscript under preparation***)**

Conference:

1 **D. Ghosh**, C.R. Medhi, M.K.Purkait, "Regulation of arsenic contamination in water by electrocoagulation" International Congress of Environmental Research 18-20 December, 2008, Goa (India).